Technical Report Documentation Page

1. Report No.	2. Government Accession No.	3. Recipient's Catalog No.
FHWA/TX-94/1335-1		

4. Title and Subtitle	5. Report Date
VICTORIA SUPERHEAVY LOAD MOVE: REPORT ON ROUTE ASSESSMENT AND PAVEMENT MODELING	October 1994
	6. Performing Organization Code

7. Author(s)	8. Performing Organization Report No.
F.J. Jooste and E.G. Fernando	Research Report 1335-1

9. Performing Organization Name and Address	10. Work Unit No. (TRAIS)
Texas Transportation Institute The Texas A&M University System College Station, Texas 77843-3135	11. Contract or Grant No. Study No. 0-1335

12. Sponsoring Agency Name and Address	13. Type of Report and Period Covered
Texas Department of Transportation Research and Technology Transfer Office P. O. Box 5080 Austin, Texas 78763-5080	Interim: September 1992 - August 1993
	14. Sponsoring Agency Code

15. Supplementary Notes

Research Performed in cooperation with the Texas Department of Transportation and the U.S. Department of Transportation, Federal Highway Administration.
Research Study Title: Movement of Superheavy Loads Over the State Highway System.

16. Abstract

The Texas Department of Transportation (TxDOT) has been issuing an increasing number of permits for movement of superheavy loads. The effect of superheavy loads on pavements is not well established at the present time. To address this problem, TxDOT has funded a research project with the Texas Transportation Institute (TTI) with the objective of developing a procedure to evaluate the potential for pavement damage on a proposed superheavy load route, as well as to determine whether temporary strengthening measures are needed.

During the study a number of superheavy loads will be monitored. This report describes the data collection and analysis results for a superheavy load move which took place in Victoria during December, 1992. The move involved the transport of two superheavy loads. A Multi-Depth Deflectometer measured pavement deflection under the superheavy loads. This study used the deflection data to evaluate the applicability of linear elastic layered theory to predict pavement response under the loading. Predicted displacement from the theory compared favorably with corresponding measurements.

To evaluate the effects of multiple wheel loads, an analysis was done to establish how predicted pavement response varies with distance from a given load and with different load configurations. The results indicate that stresses based on a single-axle model yield conservative estimates of the potential for pavement damage. This analysis showed that the road had adequate structural capacity to sustain the superheavy loads without developing visible distress.

17. Key Words	18. Distribution Statement
Superheavy Loads, Pavement Analysis, Load Modeling, Pavement Evaluation, Pavement Damage	No Restrictions. This document is available to the public through NTIS: National Technical Information Service 5285 Port Royal Road Springfield, Virginia 22161

19. Security Classif.(of this report)	20. Security Classif.(of this page)	21. No. of Pages	22. Price
Unclassified	Unclassified	86	

VICTORIA SUPERHEAVY LOAD MOVE: REPORT ON ROUTE ASSESSMENT AND PAVEMENT MODELING

by

Fritz J. Jooste
Graduate Research Assistant
Texas Transportation Institute

and

Emmanuel G. Fernando
Assistant Research Engineer
Texas Transportation Institute

Research Report 1335-1
Research Study Number 0-1335
Research Study Title: Movement of Superheavy Loads over the State Highway System

Sponsored by the
Texas Department of Transportation
In Cooperation with
U.S. Department of Transportation
Federal Highway Administration

October 1994

TEXAS TRANSPORTATION INSTITUTE
The Texas A&M University System
College Station, TX 77843-3135

METRIC (SI*) CONVERSION FACTORS

APPROXIMATE CONVERSIONS TO SI UNITS

Symbol	When You Know	Multiply By	To Find	Symbol
		LENGTH		
in	inches	2.54	centimeters	cm
ft	feet	0.3048	meters	m
yd	yards	0.914	meters	m
mi	miles	1.61	kilometers	km
		AREA		
in^2	square inches	6.452	centimeters squared	cm^2
ft^2	square feet	0.0929	meters squared	m^2
yd^2	square yards	0.836	meters squared	m^2
mi^2	square miles	2.59	kilometers squared	km^2
ac	acres	0.395	hectares	ha
		MASS (weight)		
oz	ounces	28.35	grams	g
lb	pounds	0.454	kilograms	kg
T	short tons (2000 lb)	0.907	megagrams	Mg
		VOLUME		
fl oz	fluid ounces	29.57	milliliters	mL
gal	gallons	3.785	liters	L
ft^3	cubic feet	0.0328	meters cubed	m^3
yd^3	cubic yards	0.765	meters cubed	m^3

Note: Volumes greater than 1000 L shall be shown in m^3.

		TEMPERATURE (exact)		
°F	Fahrenheit temperature	5/9 (after subtracting 32)	Celsius temperature	°C

APPROXIMATE CONVERSIONS TO SI UNITS

Symbol	When You Know	Multiply By	To Find	Symbol
		LENGTH		
mm	millimeters	0.039	inches	in
m	meters	3.28	feet	ft
yd	meters	1.09	yards	yd
km	kilometers	0.621	miles	mi
		AREA		
mm^2	millimeters squared	0.0016	square inches	in^2
m^2	meters squared	10.764	square feet	ft^2
yd^2	kilometers squared	0.39	square miles	mi^2
ha	hectares (10,000 m^2)	2.53	acres	ac
		MASS (weight)		
g	grams	0.0353	ounces	oz
kg	kilograms	2.205	pounds	lb
Mg	megagrams (1000 kg)	1.103	short tons	T
		VOLUME		
mL	milliliters	0.034	fluid ounces	fl oz
L	liters	0.264	gallons	gal
m^3	meters cubed	35.315	cubic feet	ft^3
m^3	meters cubed	1.308	cubic yards	yd^3

		TEMPERATURE (exact)		
°C	Celsius temperature	9/5 (then add 32)	Fahrenheit temperature	°F

These factors conform to the requirement of FHWA Order 5190.1A

*SI is the symbol for the International System of Measurements

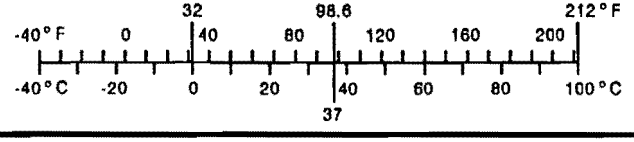

IMPLEMENTATION STATEMENT

The methodology presented to evaluate the structural capacity of proposed superheavy load routes uses existing capabilities within the Texas Department of Transportation (TxDOT). This should facilitate implementation once the methodology is fully developed. It is noted that the analysis of Ground Penetrating Radar and Falling Weight Deflectometer data will require training of TxDOT personnel. TTI can provide this training to assist in the initial implementation of the comprehensive methodology presented herein. To further facilitate implementation, the study is developing simpler procedures for evaluating superheavy load routes. These simpler procedures will be incorporated into a multi-level framework that will include the comprehensive and detailed methodology included in this report. Guidelines will be established in the appropriate use of the procedures developed.

DISCLAIMER

The contents of this report reflect the views of the authors who are responsible for the facts and the accuracy of the data presented herein. The contents do not necessarily reflect the official views or the policies of the Federal Highway Administration (FHWA) or the Texas Department of Transportation (TxDOT). This report does not constitute a standard, specification, or regulation. It is not intended for construction, bidding, or permit purposes. The engineer in charge of the project is Emmanuel Fernando, P.E. # 69614.

TABLE OF CONTENTS

LIST OF TABLES

LIST OF FIGURES

SUMMARY

This report forms part of the work done under Texas Department of Transport (TxDOT) Study 1335 which is aimed at investigating the movement of superheavy loads over the state highway system. During the course of this project, a number of superheavy load moves will be monitored. This report describes the superheavy load move which took place in Victoria in December 1992, and presents the analysis of the data gathered during the move. A detailed route evaluation is presented, together with some of the results of the superheavy load and pavement modeling.

The route consisted of three sections of road, namely Loop 175, State Highway 185 and Farm-to-Market road 1432. The route evaluation included a radar survey, coring, Falling Weight Deflection measurements, Dynamic Cone Penetrometer tests, and an ARAN survey. Based on the analysis of the data from these tests, it appears that all three sections have a good-to-very-good structural capacity. All sections showed very little rutting and good riding quality. No cracking was observed. An analysis of the ARAN survey data taken before and after the superheavy load move showed that no visible damage took place as a result of the move.

The superheavy loads and pavement structure were modeled using the backcalculated pavement moduli, the predicted layer thicknesses from the radar survey, and linear elastic layered theory. The pavement model was shown to correlate well with the measured response of the pavement under the superheavy load obtained with a multi-depth deflectometer. The shear strength of one of the pavement sections along FM 1432 was obtained through Texas triaxial class tests. Based on the Mohr-Coulomb failure theory, the pavement section was found to have adequate structural capacity against subgrade shear failure.

The load and pavement modeling results obtained to date are encouraging. However, there are still several assumptions in the model that need to be verified before a first stage evaluation procedure can be finalized. Work in this area is still in an early phase and further work is required to model more accurately the pavement response under superheavy loads.

CHAPTER 1. BACKGROUND AND INTRODUCTION

GENERAL

In September 1992 the Texas Transportation Institute (TTI) was commissioned by the Texas Department of Transportation (TxDOT) to execute a research project in order to investigate the movement of superheavy loads over the state highway system. During this project, a number of superheavy load moves will be monitored. This report describes the data collection and the analysis results pertaining to the first of these superheavy load moves, which took place in Victoria during December 1992. A detailed route evaluation is presented, based on the results of field testing and analysis. Some preliminary notes on the load and structure modeling are also included.

DESCRIPTION OF THE ROUTE AND LOAD MOVEMENT

General Description of the Superheavy Load Route

The route on which the load movement took place can be subdivided into three different sections, namely Loop 175, State Highway 185, and FM 1432. Figure 1 shows a schematic layout of the total route. The move started at reference marker 13.562 on Loop 175, where the load was moved from a private field owned by the Victoria Machine Works where it was manufactured. It was then moved along State Highway 185 and FM 1432 to the Victoria barge canal.

Details of the Superheavy Load

In total, four pieces of equipment were moved along the route described in the previous section. Two of these loads fell below the 250 kip. (1112 kN) gross vehicle weight limit and were therefore not classified as superheavy loads. Of the two superheavy loads, one weighed just 4 kip. (17.8 kN) over the 250 kip. limit. The other superheavy load was well over the 250 kip. limit at 534.3 kip. (2378 kN). Pavement deflections under three of these loads were obtained from an instrumented section of FM 1432. All the equipment that was moved formed part of an offshore pipe layer. The heaviest load was

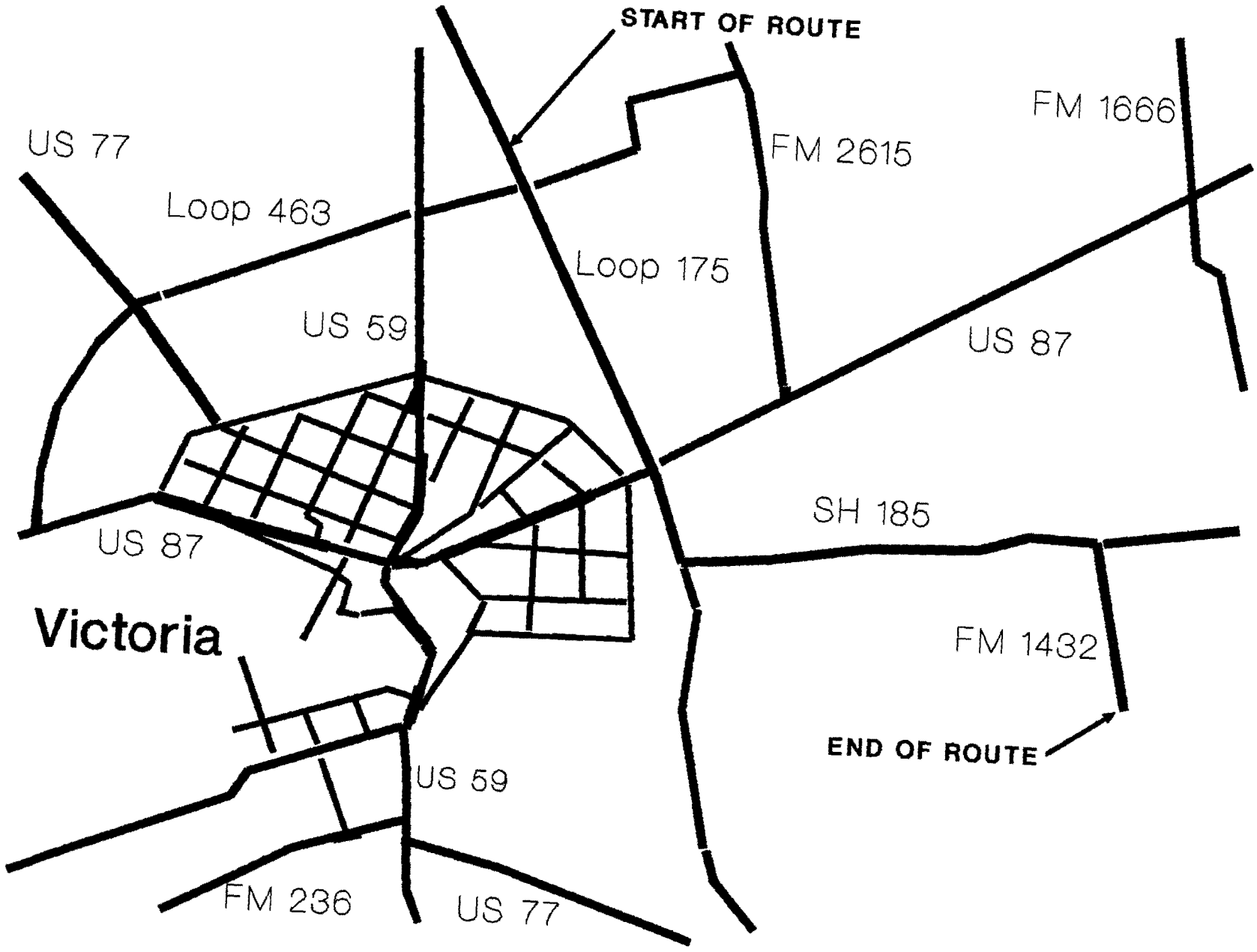

Figure 1. Schematic layout of the superheavy move route.

called the tower. The three lighter units were called the base support, stinger, and strongback units. The heaviest of the superheavy loads was moved on December 10, 1992. This load was transported on a self-propelled trailer which consisted of three units. Each unit had six steerable lines, with four wheels per line. The superheavy load weights and dimensions are summarized as follows.

load weight	347.3 kip. (1545 kN)
front vehicle unit weight	53.9 kip. (240 kN)
middle vehicle unit weight	49.5 kip. (220 kN)
rear vehicle unit weight	53.9 kip. (240 kN)
vehicle cabin	3.3 kip. (15 kN)
engine	26.4 kip. (118 kN)
total vehicle weight	187.0 kip. (832 kN)
gross vehicle weight	**534.3 kip. (2378 kN)**
average weight/axle	29.7 kip. (132 kN)
average weight/tire	**7421 lb. (33 kN)**

A photograph of the tower load is shown in Figure 2. Table 1 provides pertinent information on the three lighter loads.

Table 1. Loads Moved at Victoria

UNIT	DATE OF MOVEMENT	GROSS VEHICLE WEIGHT (kip)	NUMBER OF LINES
Base support	12-8-92	254	12
Stinger	12-8-92	108	6
Strongback	12-9-92	168	8

Note: 1 kip. = 4.45 kN

Figure 2. Photograph of the tower load moved at Victoria.

CHAPTER 2. FIELD TESTING AND DATA ANALYSIS

TESTING CONDUCTED

A number of tests were conducted during the fall of 1992 to assist in the route evaluation. The test program consisted of the following:

1) a thickness survey using the TTI Ground Penetrating Radar (1,2), supplemented with cores;
2) a subgrade evaluation using the Dynamic Cone Penetrometer (3);
3) a structural evaluation using the Falling Weight Deflectometer; and
4) a pavement condition survey using the ARAN system (4).

In addition to the tests noted above, a Multi-Depth Deflectometer (MDD) (5,6) was installed on FM 1432 in order to monitor the effects of the superheavy load on the pavement structure. These results are discussed in Chapter 3.

DISCUSSION OF TEST DATA ANALYSIS AND RESULTS

General

The basic analysis procedure can be divided roughly into two phases:

1) identification of subsections based on layer thicknesses, and
2) modeling of pavement structure through backcalculation using Falling Weight Deflectometer (FWD) (7) results and specific subsection thicknesses as identified in 1) above.

The ultimate aim of the procedure is to model the stress and strain conditions under superheavy loading conditions to evaluate the potential for pavement damage. In addition to the structural evaluation, a condition survey of the route was also conducted before and after the load movement using the TxDOT's Automated Road Analyzer (ARAN) unit (4). Data derived from the field measurements, with the subsectioning and backcalculation results, are presented in the following sections.

Layer Thickness Determination and Subsectioning

Ground penetrating radar (GPR) measurements (1,2) were taken at 10-ft. (3.05 m) intervals on each of the three road sections. Each road section was divided into subsections by applying the method of cumulative differences (8) to the layer thicknesses determined by the ground penetrating radar. In order to verify the GPR results, a number of cores were also taken on each section. The thicknesses obtained from the coring are shown in Table 2, together with the radar results obtained at the core positions. The layer thicknesses reported in Table 2 are those which were measured on the lane on which the superheavy load move took place. Figures 3 through 7 show the subsectioning as made by the cumulative difference method as well as the layer thicknesses as determined by the cores.

The following should be noted:

1) The distances shown in Table 2 and Figures 3 through 7 refer to the following:
   a) For Loop 175, distance is from Reference Marker (RM) 13.562, which is the starting point of the move.
   b) For SH 185, distance is from RM 8.161, just past the bridge crossing Loop 175.
   c) For FM 1432, distance is from the intersection of FM 1432 and SH 185.
2) The core which was taken at a distance of 3062 feet on Loop 175 is not shown with the other cores taken on Loop 175 in Figures 3 and 4. This core was taken in an area of localized thickening where the asphalt thickness increased substantially while the thickness of the concrete layer diminished to virtually nothing, as indicated in Figures 3 and 4.
3) The radar trace reflection from the bottom of the base course on FM 1432 was not clear enough to predict base layer thicknesses. For this reason the average thicknesses recorded from the cores were used in subsequent calculations.

Table 2. Layer Thicknesses as Determined by Radar and Coring

a) Loop 175

DMI (ft.)	Layer 1 Thickness (in.)		Material Type	Layer 2 Thickness (in.)		Material Type
	Cores	Radar		Cores	Radar	
1357	1.81	2.20	AC	8.38	7.85	CRC
3062	13.75	-	AC	-	-	-
10644	2.75	2.16	AC	8.5	7.74	CRC

Note: 1 in. = 25.4 mm, 1 mile = 1.6 km

b) State Highway 185

DMI (ft.)	Layer 1 Thickness (in.)		Material Type	Layer 2 Thickness (in.)		Material Type
	Cores	Radar		Cores	Radar	
2740	5.69	5.59	AC	8.31	7.04	River Gravel
9097	6.75	3.97	AC	8.0	7.12	River Gravel
14272	6.5	4.70	AC	8.0	6.47	River Gravel
20433	5.0	3.65	AC	10.5	9.20	River Gravel

Note: 1 in. = 25.4 mm, 1 mile = 1.6 km

c) State Highway FM 1432

DMI (ft.)	Layer 1 Thickness (in.)		Material Type	Layer 2 Thickness (in.)		Material Type
	Cores	Radar		Cores	Radar	
1172	4.25	3.74	AC	6.0	-	Stab. Shell
5312	2.75	4.24	AC	13.5	-	Stab. Shell
9536	3.75	3.80	AC	11.25	-	Stab. Shell

Note: 1 in. = 25.4 mm, 1 mile = 1.6 km

FWD Tests

a) Backcalculation Modulus

The elastic modulus of each pavement layer was calculated using the Modulus 4.1 backcalculation program developed at TTI (7,9). For these calculations the layer thicknesses obtained from the GPR results were used. The calculations were done as accurately as possible by using, for each test point, the average thicknesses of the subsection on which the test was done. The backcalculated layer moduli were used to evaluate the potential for failure under the superheavy load. Figures 8 through 10 show the results of the backcalculation procedures.

b) Calculation of SSI

In addition to the backcalculation of layer moduli, the FWD results were also used to calculate the Structural Strength Index (SSI) for each deflection bowl. The SSI is basically an index value which is indicative of the pavement structural capacity with respect to 18-kip ESAL values and climatic zone (10). The SSI value used in this analysis is the statistically-based SSI developed by TTI and incorporated into TxDOT's Pavement Evaluation System database (10). The calculated SSI values are shown in Figures 11 through 13.

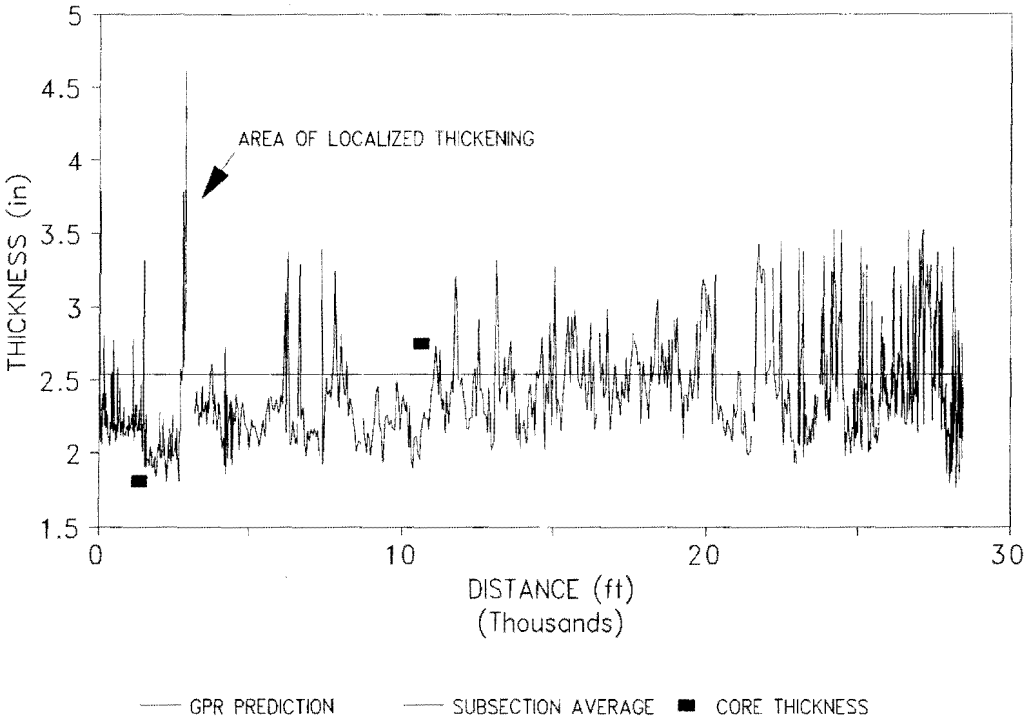

Figure 3. Loop 175 surfacing thickness (1 ft.= 0.30 m, 1 in.= 25.4 mm).

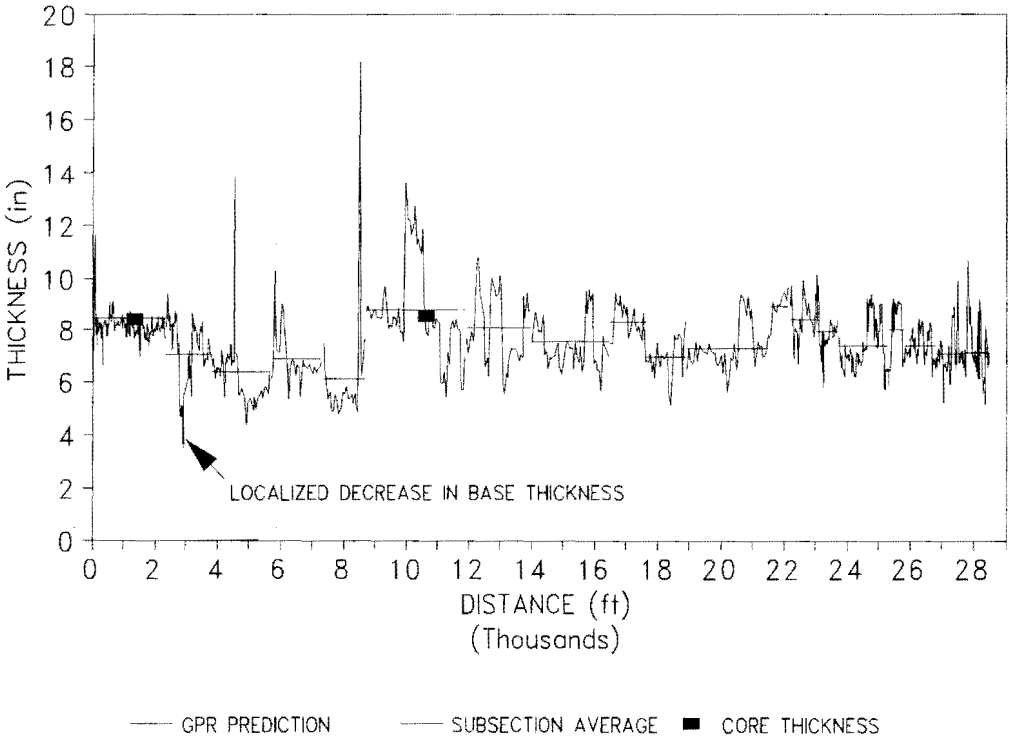

Figure 4. Loop 175 base thickness (1 in.= 25.4 mm, 1 ft.= 0.30 m).

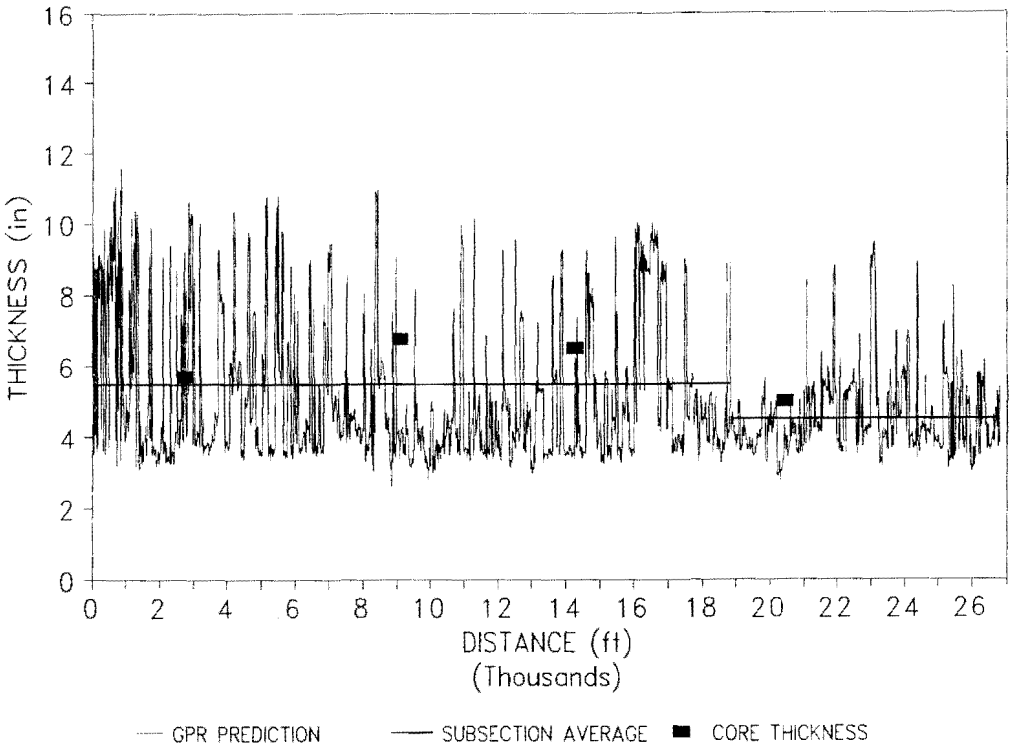

Figure 5. State Highway 185 surfacing thickness (1 in.= 25.4 mm, 1 ft.= 0.30 m).

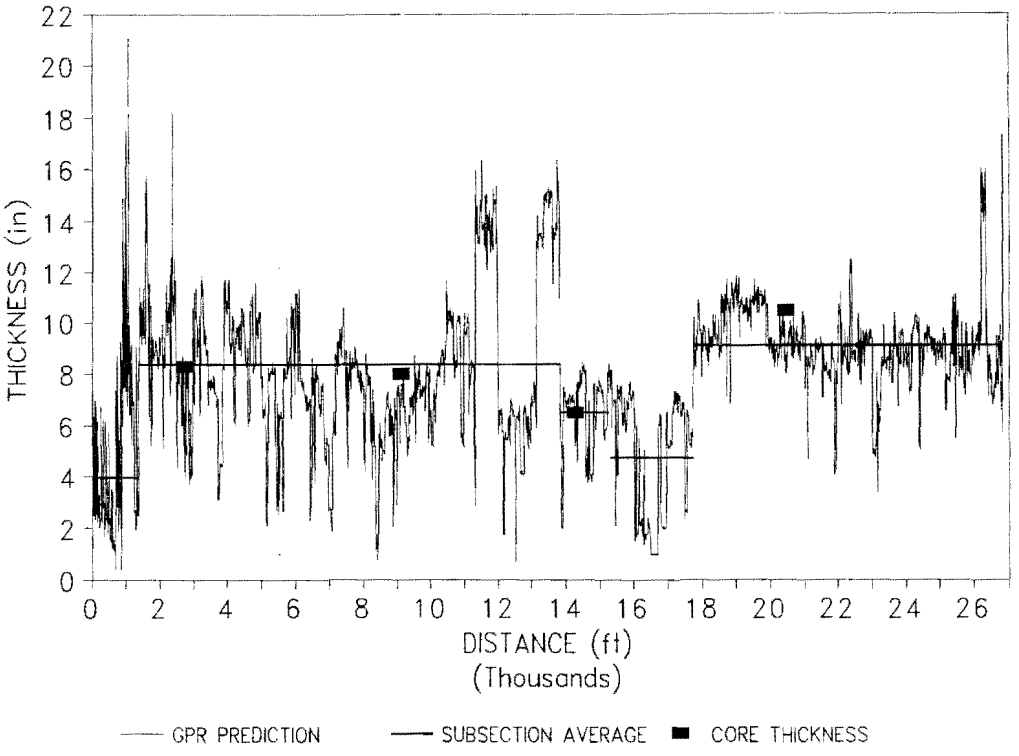

Figure 6. State Highway 185 base thickness (1 in.=25.4 mm, 1 ft.= 0.30 m).

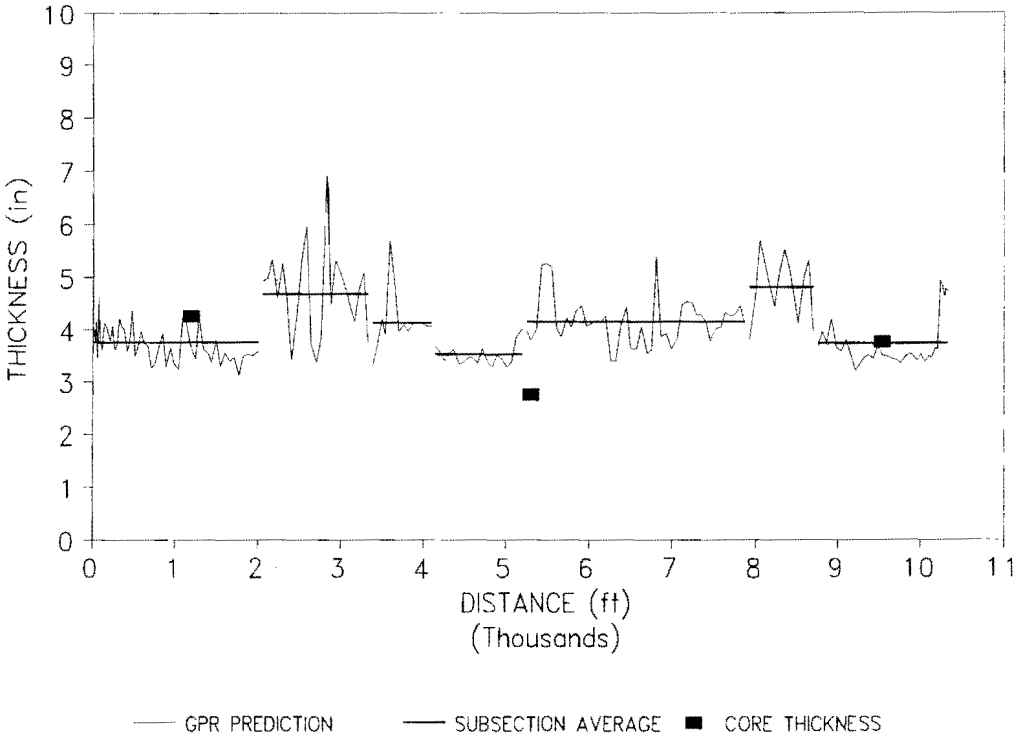

Figure 7. FM 1432 surfacing thickness (1 in.= 25.4 mm,1ft.= 0.30 m).

In general, the roadways which comprised the superheavy route have reasonably good structural capacity, with the exception of two unacceptably low SSI values on FM 1432.

Dynamic Cone Penetrometer Results

Dynamic Cone Penetrometer (DCP) tests were conducted in order to assist in the subgrade assessment (3). DCP testing was done only on the subgrade. The DCP rod was inserted into the core hole, after which the rate of penetration into the subgrade was measured. No DCP data could be collected on Loop 175, because of the presence of a cement-stabilized subbase. Figures 14 and 15 show the results of the DCP testing. The figures show that the rate of penetration is fairly constant, which indicates that the subgrade is, in general, fairly uniform throughout the penetrated depth, without any visibly layered substructure.

ARAN Survey

The results of the ARAN survey are summarized in Figures 16 through 23. These figures show that all roadways comprising the superheavy load route are in good condition. The rutting, in general, is very low (maximum of 0.14 in. (3.55 mm)), both before and after the superheavy load move. No rutting was recorded in the right wheel path of FM 1432. A visual survey of the road confirmed the ARAN results.

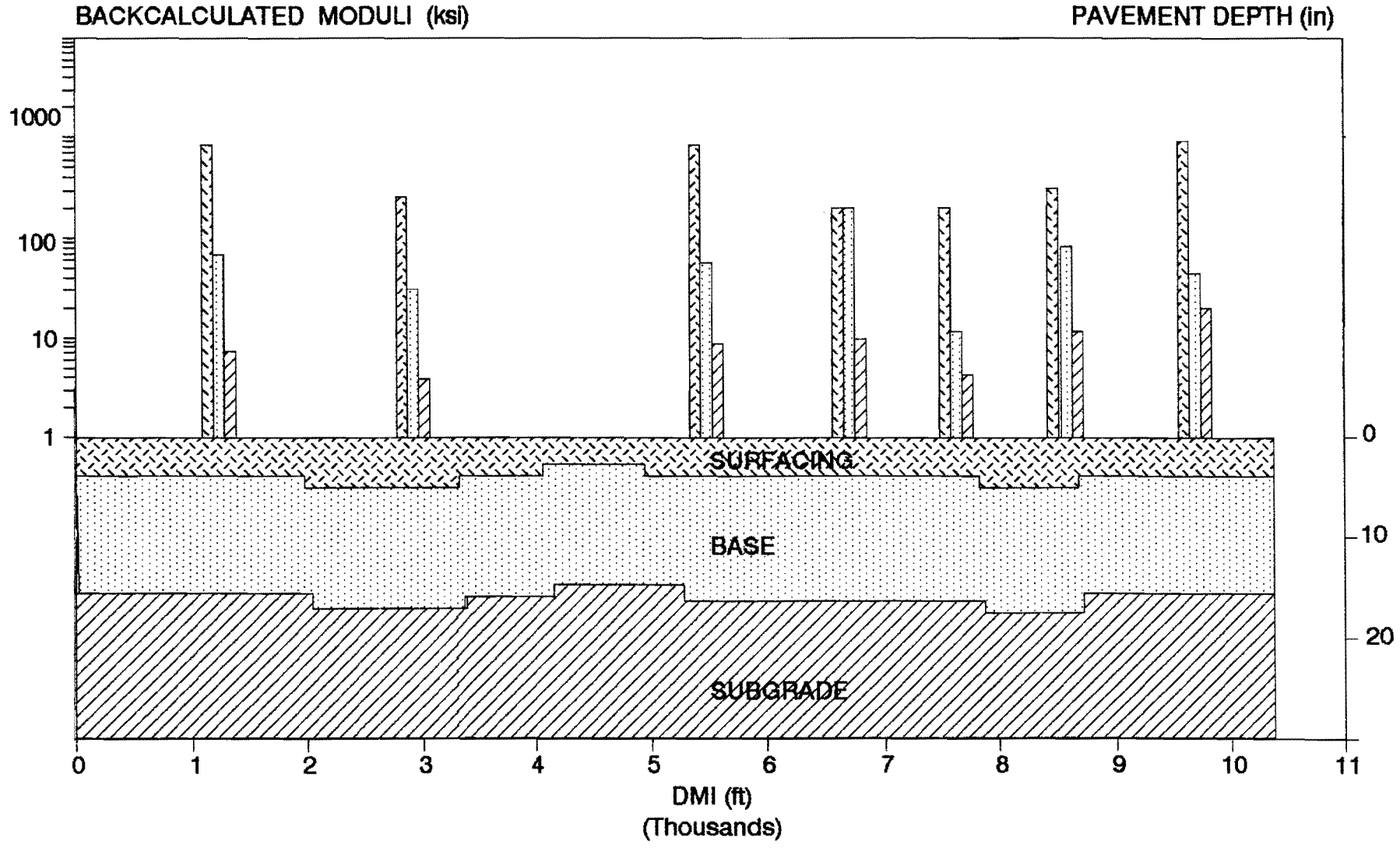

Figure 8. FM 1432 outer lane structural evaluation.

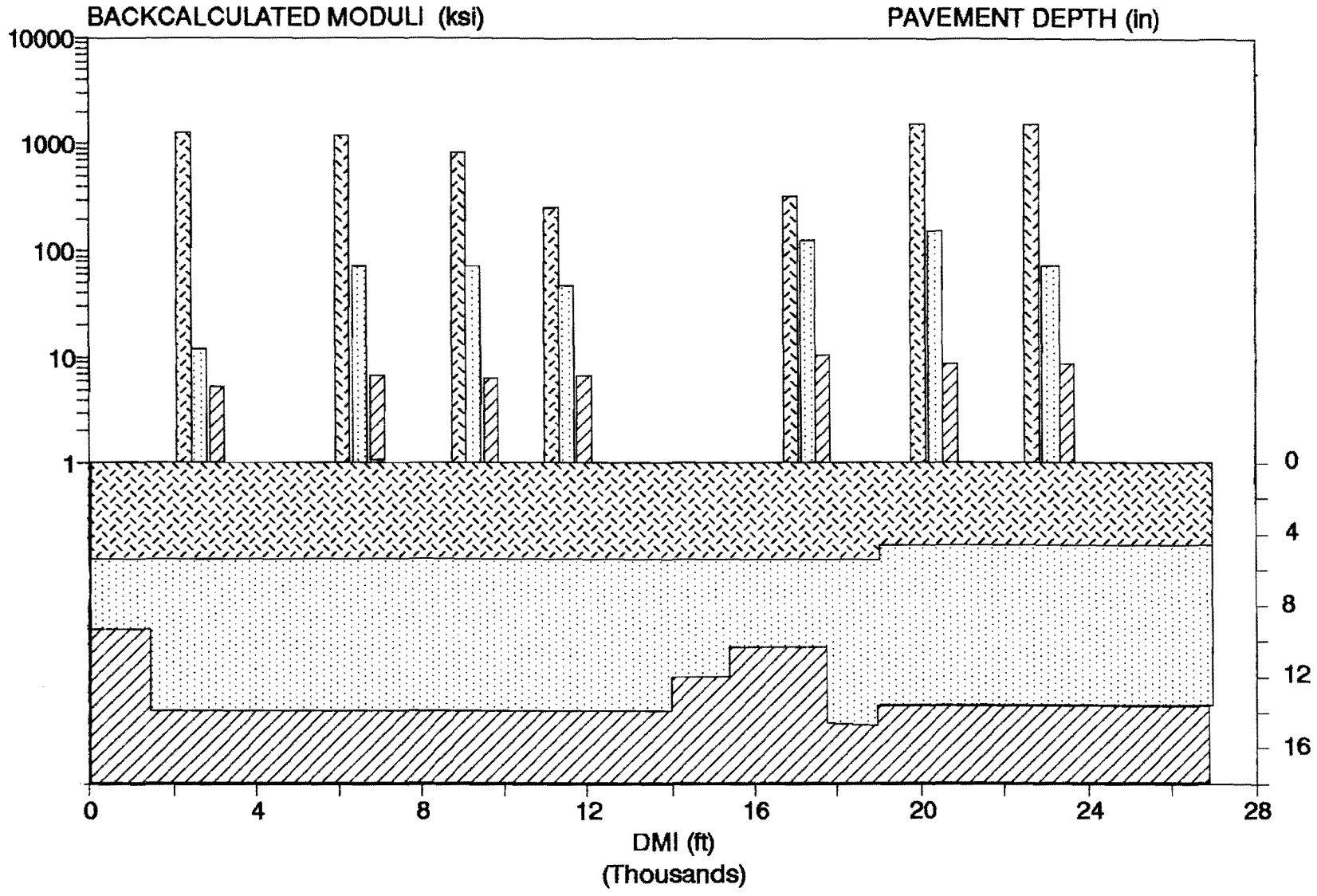

Figure 9. SH 185 outer lane structural evaluation.

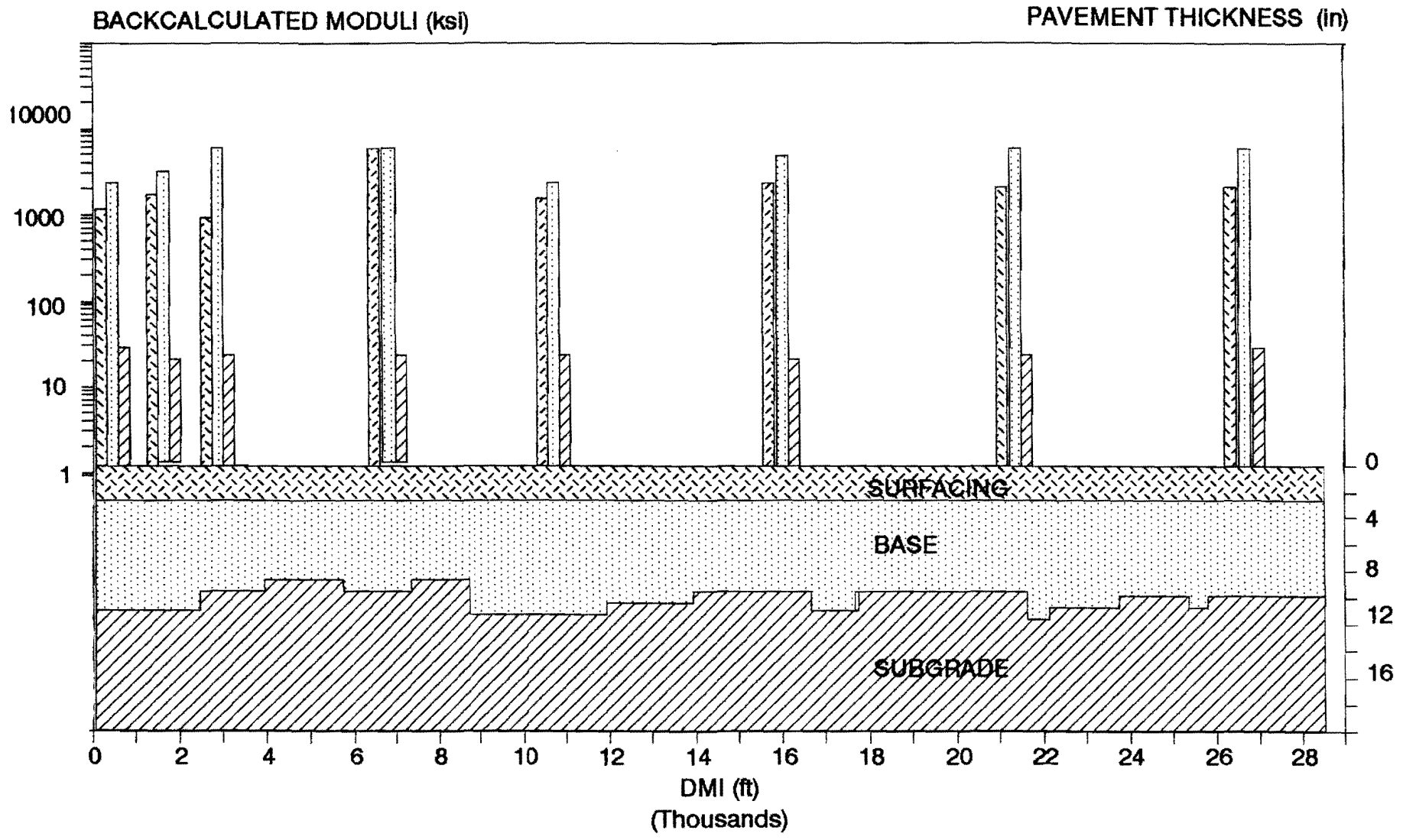

Figure 10. Loop 175 Outer lane structural evaluation.

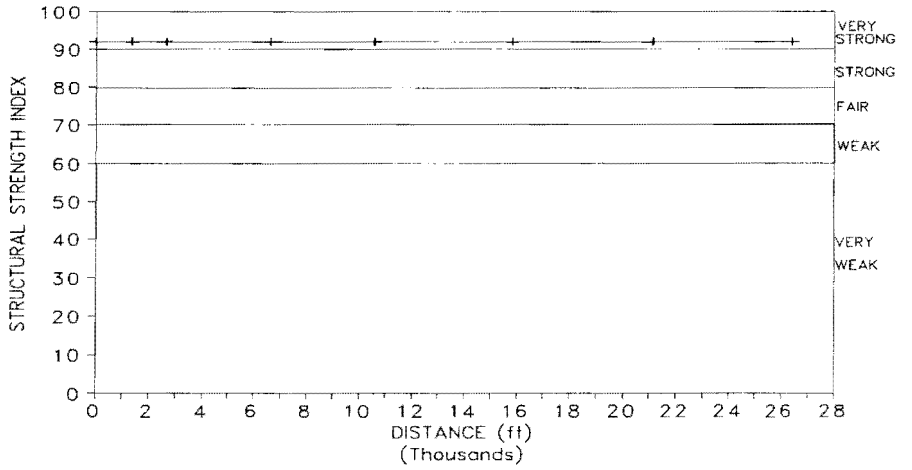

Figure 11. SSI for Loop 175 (1 ft.= 0.30 m).

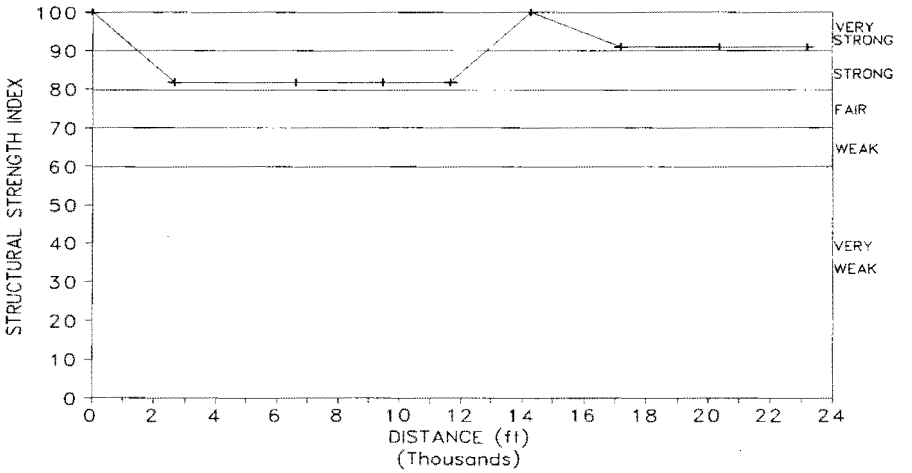

Figure 12. SSI for State Highway 185 (1 ft.= 0.30 m).

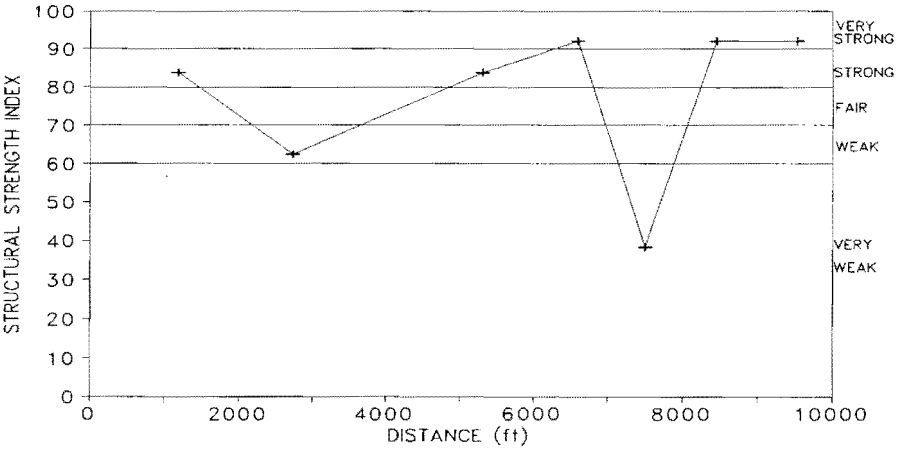

Figure 13. SSI for FM 1432 (1 ft.= 0.30 m).

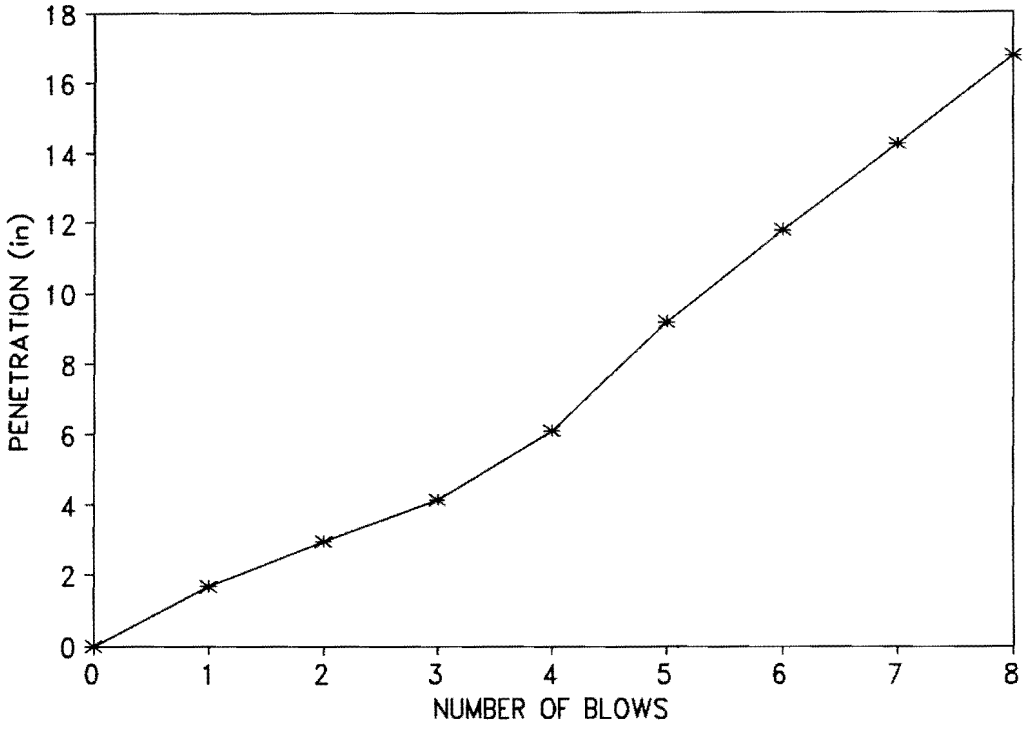

Figure 14. DCP results for State Highway 185 (1 in.= 25.4 mm).

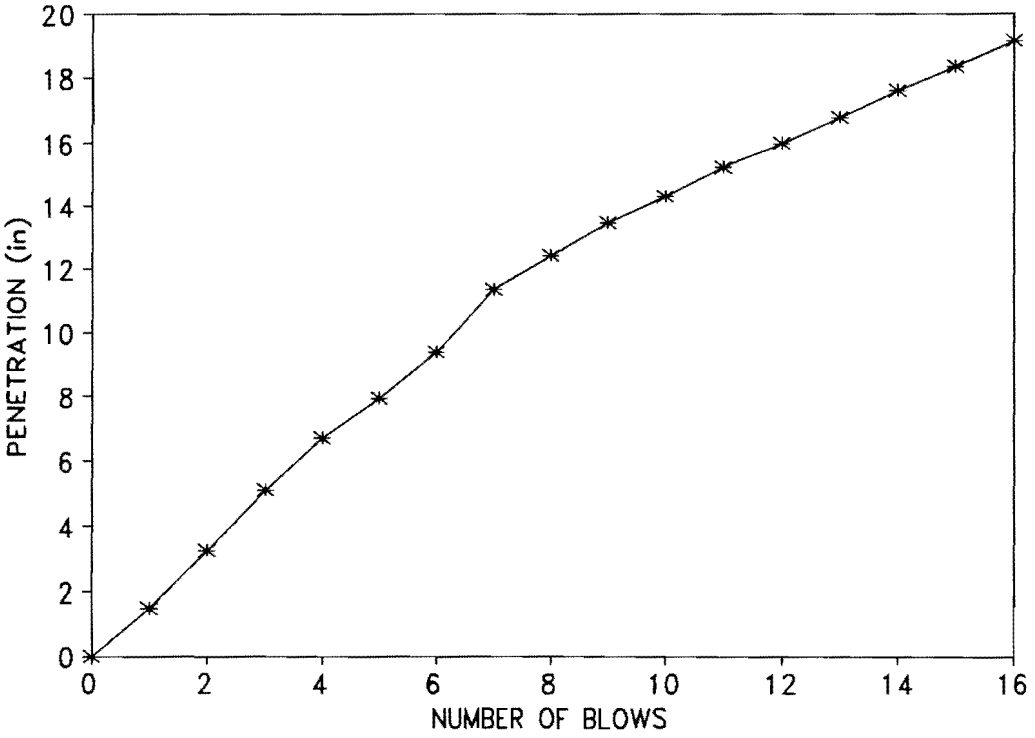

Figure 15. DCP results for FM 1432 (1 in.= 25.4 mm).

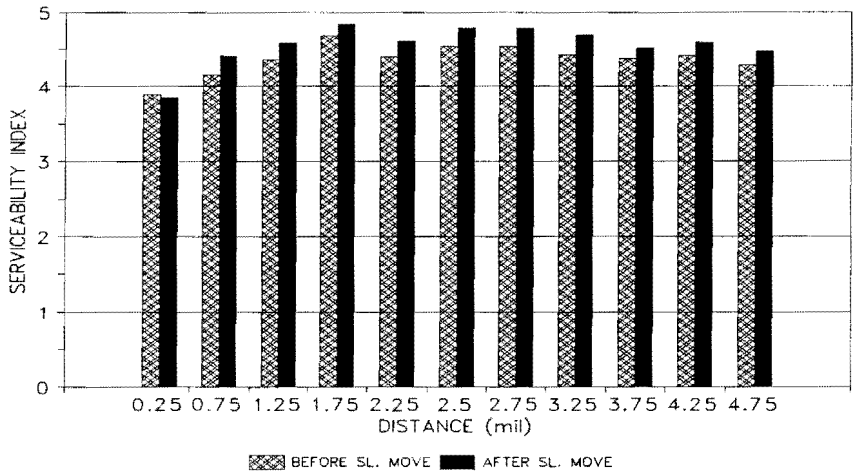

Figure 16. Riding quality on Loop 175 (1 mile = 1.6 km).

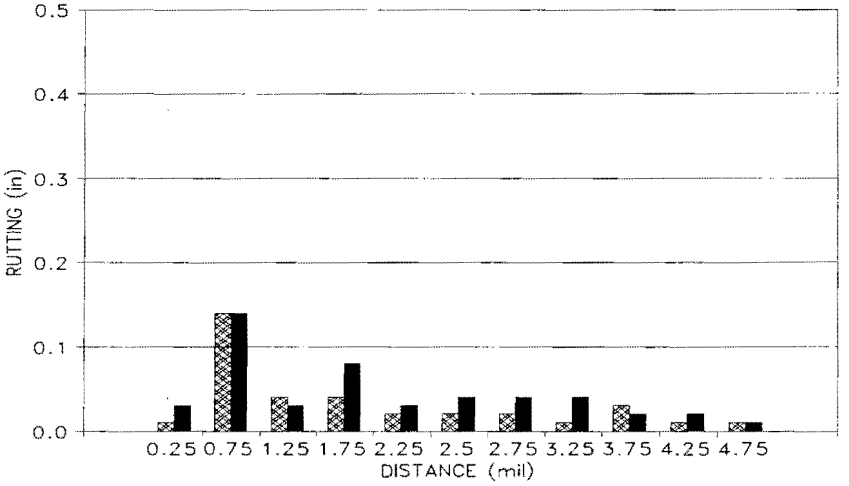

Figure 17. Rutting in right wheelpath on Loop 175 (1 mile = 1.6 km).

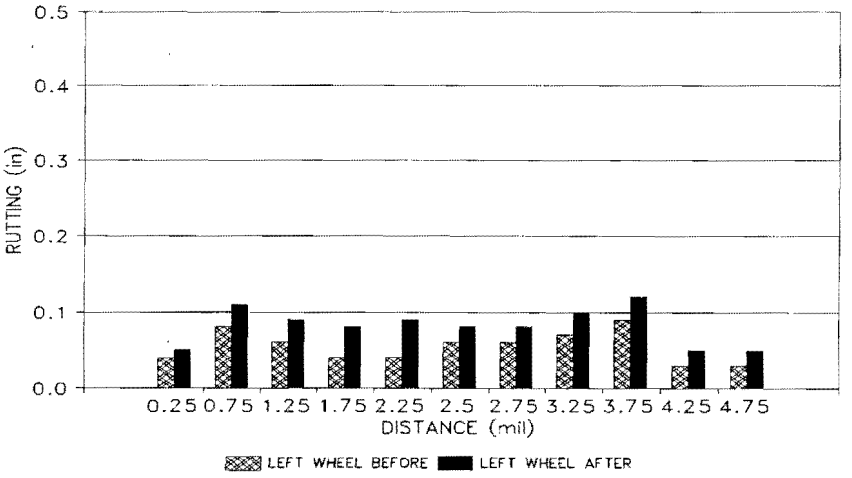

Figure 18. Rutting in left wheelpath on Loop 175 (1 mile = 1.6 km).

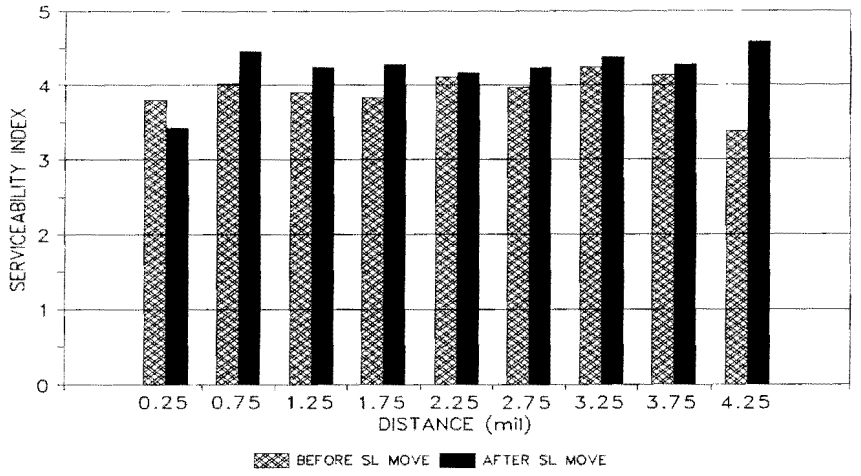

Figure 19. Riding quality on State Highway 185 (1 mile = 1.6 km).

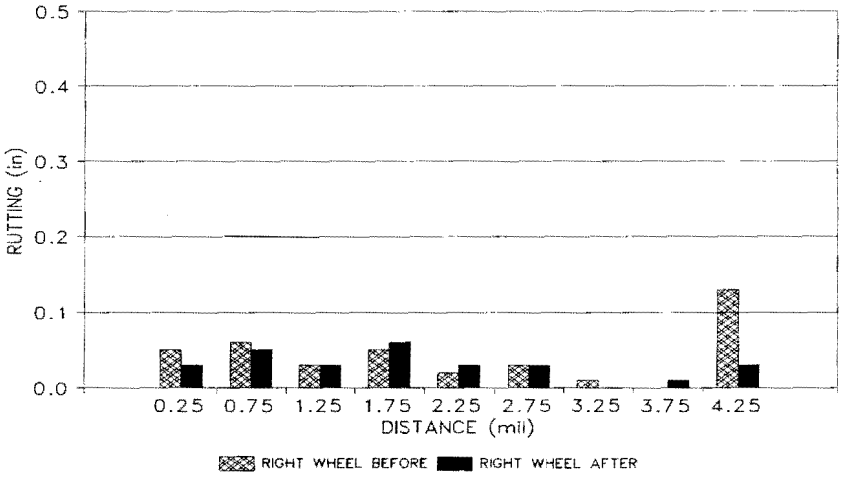

Figure 20. Rutting in right wheelpath on State Highway 185 (1 mile = 1.6 km).

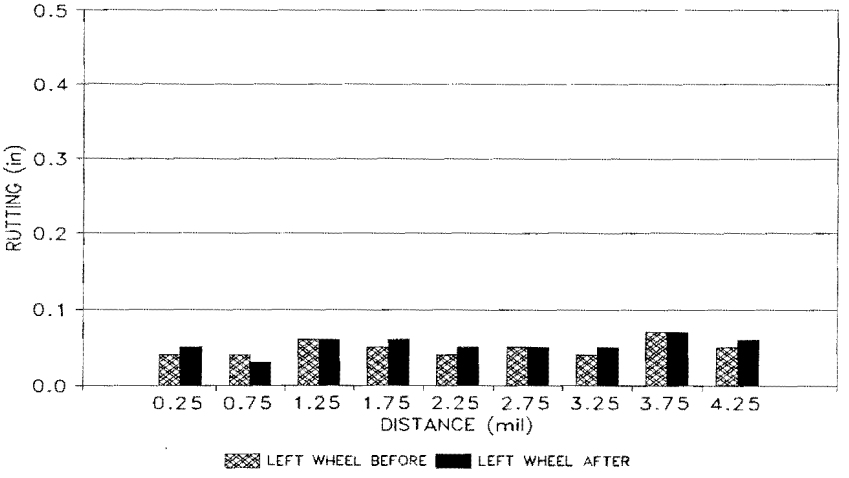

Figure 21. Rutting in left wheelpath on State Highway 185 (1 mile = 1.6 km).

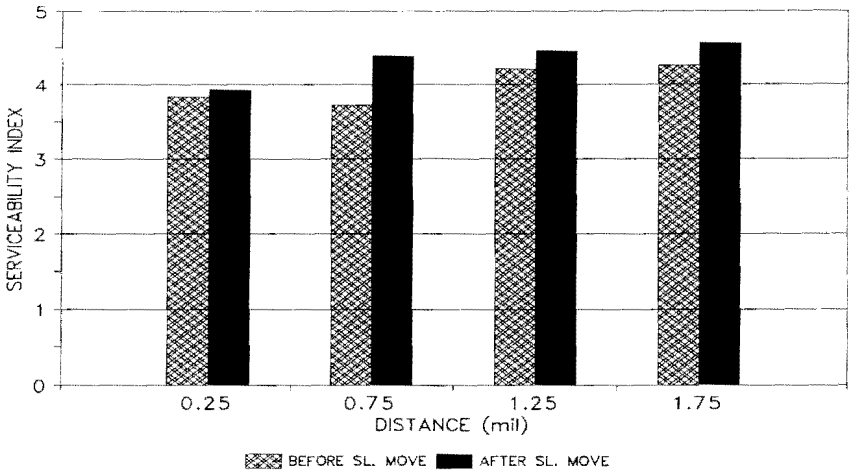

Figure 22. Riding quality on FM 1432 (1 mile = 1.6 km).

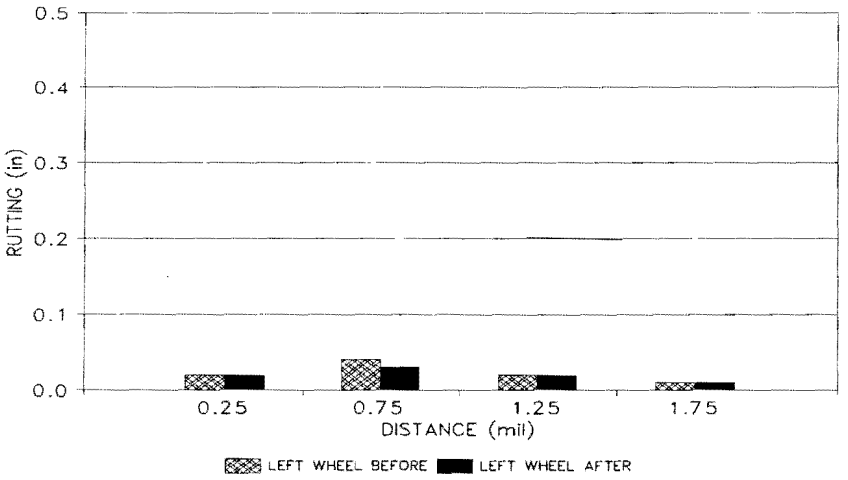

Figure 23. Rutting in left wheelpath on FM 1432 (1 mile = 1.6 km).

CHAPTER 3: LOAD AND PAVEMENT MODELING

GENERAL

A multi-depth deflectometer (MDD) was installed at Reference Marker 1.421 on FM 1432, which corresponds to a distance of 7500 ft. (2286 m) from the intersection of SH 185 and FM 1432. MDD sensors were placed at three different depths, viz. 3.7 in. (9.4 cm), 13.3 in. (33.8 cm) and 25 in. (63.5 cm) from the pavement surface. The MDD sensors were used primarily to measure the pavement response under the superheavy load. Also, the MDD response was measured under an FWD load. Because the MDD measures the actual displacement within the pavement structure at different depths, it is an excellent tool for checking the accuracy of the pavement model used in the analysis of the FWD data (5,6). The MDD response measured under the actual superheavy load can similarly be used to establish the model for calculating stresses and strains. The procedure and results presented in this section form part of the first steps toward establishing a Level 1 version of a superheavy load analysis procedure.

MDD RESPONSE UNDER FWD LOADING

The MDD response was measured under the influence of an FWD load. The FWD load was applied at a 9-in. (22.86 cm) offset from the MDD sensor position, at four different drop heights. Figures 24 and 25 show the MDD response under FWD loads applied at the third and fourth drop heights. The MDD measurements under FWD loading were used to verify the pavement model used in the analysis of the FWD data. This was done in the following way.

1) Pavement layer moduli were backcalculated using the Modulus 4.1 program and the FWD deflection bowl measured at the MDD location.
2) The backcalculated moduli and layer thicknesses were then used with the WESLEA linear elastic layered program (11) to calculate the displacements at the same depths as the actual MDD sensors, under a simulated FWD load. The FWD load simulated here was of exactly the same magnitude as that of the fourth drop

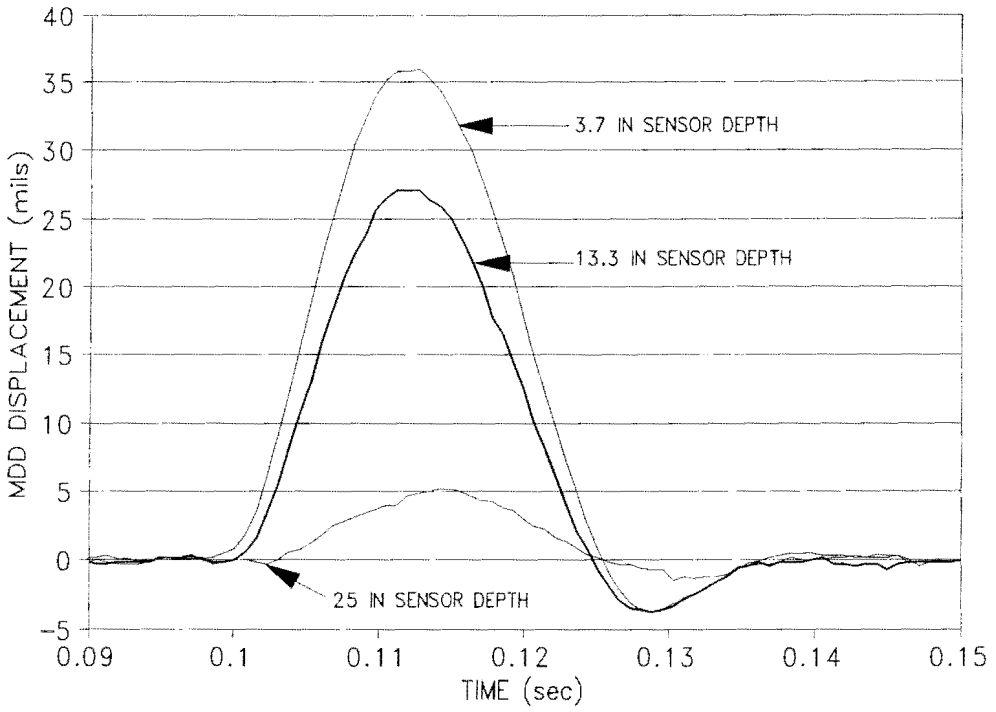

Figure 24. MDD response under FWD load, third drop height (1 mil = 25.4 μm).

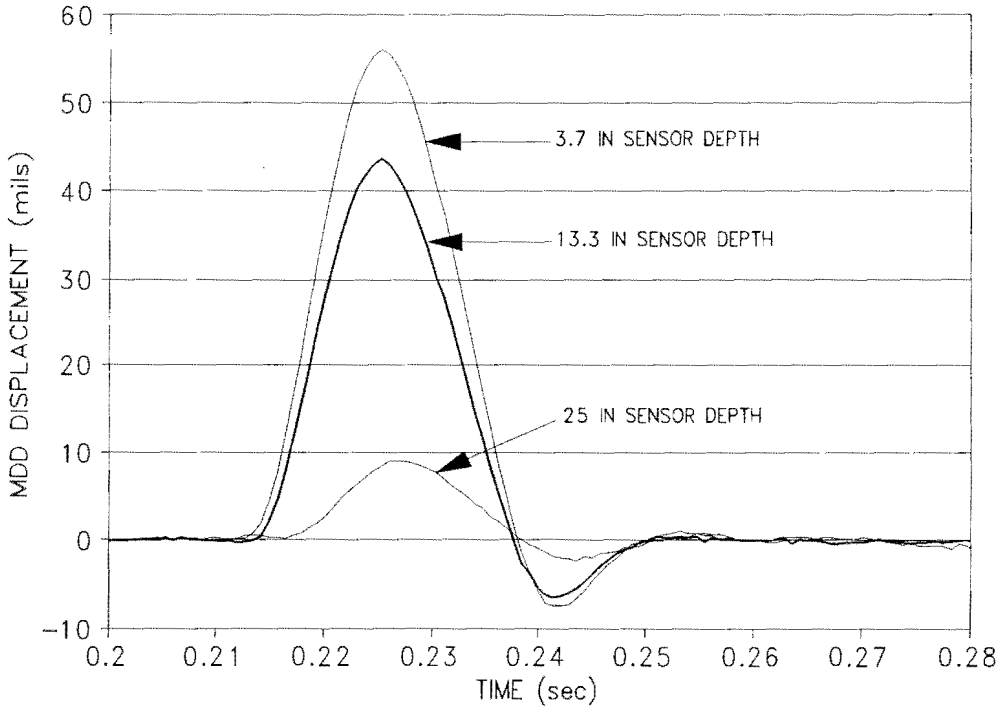

Figure 25. MDD response under FWD load, fourth drop height (1 mil = 25.4 μm).

height under which the MDD response was measured (i.e. the load response shown in Figure 25). The fourth drop height was chosen because it was considered to be the best simulation of the superheavy load.

3) Finally, the measured MDD displacements were compared with the displacements calculated at the same depth. All calculations were done using the WESLEA linear elastic layered program (11).

The results of this comparison (Figure 26) show good agreement between measured and calculated displacements for the first and second sensor depths. There is, however, a substantial error between the measured and calculated displacements at the third sensor depth. It should be noted that the measured ratios between the third MDD displacement and the first and second sensor displacements are somewhat unusual. Typical MDD measurements show that the ratio between the first and second MDD sensor output is similar to that of the second and third sensor output. This is clearly not the case with the output shown in Figures 24 and 25, where the third sensor output is substantially less than the second. Displacements measured in the upper pavement layers consist of two parts, viz. (i) the displacements measured in the pavement layers, and (ii) the displacement measured in the subgrade. Research has shown that approximately 70 percent of the displacement measured in the upper pavement layers can be attributed to the subgrade (12). This is clearly not the case with the MDD displacements measured at Victoria. For instance, the maximum displacement measured under the FWD load at a depth of 13.3 inches is 43.56 mils. At the 25 inch sensor, a displacement of only 8.94 mils was measured. This means that only 20 percent of the displacement measured at a 13.3 inch depth can be attributed to the material below the 25 inch depth. The remaining displacement (i.e. 43.56 minus 8.94 = 34.62 mils) could only have originated in the material between the depths of 13.3 and 25.5 inches. Although this in itself is highly inconsistent with the authors' previous experience, there are two possible reasons for this observation:

1) The third sensor may be founded on quite stiff subgrade material. At the same time there may be an extremely soft interlayer between the third sensor and the sensors placed at lesser depths.

2) The low displacement of the third sensor may be due to some electrical or mechanical problem with the MDD sensor, such as slipping.

The first of the possibilities noted above was tested in several ways. This included recalculating the layer moduli with the inclusion of a soft interlayer in the pavement system. Also, the pavement moduli were backcalculated by using the PENMOD program, which backcalculates moduli from MDD data (13).

None of the results obtained indicated that the low displacement measured on the third sensor was due to a soft interlayer. This conclusion is supported by the DCP evaluation of the subgrade, shown in Figure 15. The DCP evaluation indicated a fairly

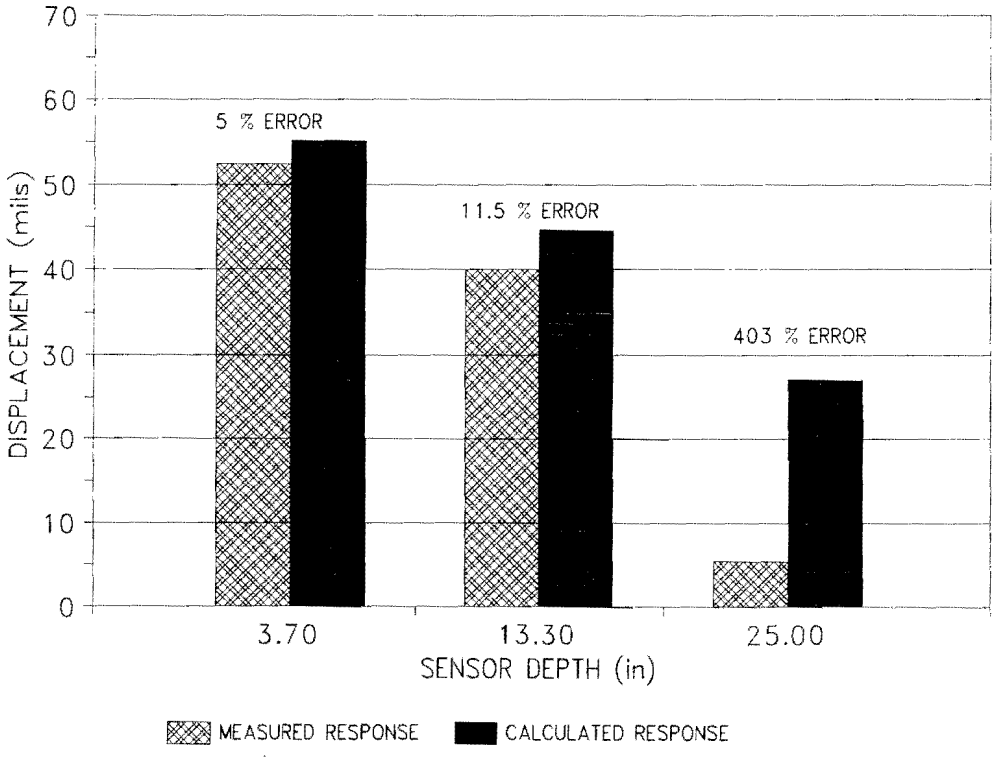

Figure 26. Measured vs. calculated MDD displacements under FWD load (1 mil = 25.4 μm).

uniform rate of penetration (given by the slope of the curve in Figure 15), with no apparent sublayering. It can be assumed, then, that the third MDD sensor was faulty, and the displacement measured at this sensor is, therefore, not representative of the actual pavement condition. If this assumption is correct, the good agreement between the calculated and measured deflections at the first two sensors indicates that the linear elastic pavement model is appropriate and can be used in a first-stage evaluation procedure.

MODELING OF THE 534.3 KIP. SUPERHEAVY LOAD (TOWER)

A schematic representation of the tower is shown in Figure 27. The MDD response under this superheavy load is shown in Figure 28. As part of the development of the first-stage evaluation procedure, an attempt was made to simulate pavement response under loading using linear elastic layered theory. This procedure employs a simplified approach in that it does not take into account material characteristics such as viscoelasticity, the response of which will depend on the speed at which the load passes. This approach attempts to take account of non-linearity by using a pavement structure that was backcalculated at load levels that are similar to those of the superheavy load wheels. The load modeling consisted mainly of the following:

1) a sensitivity analysis to determine the number of loads which need to be included in the analysis, and
2) simulation of the MDD response under the superheavy load using the results from the sensitivity analysis.

The sensitivity analysis was done using multiple runs of the BISAR linear elastic layered program (14). This sensitivity analysis is presented in detail in the Appendix. By calculating the stresses and strains at different distances from the load, the load influence at different offset positions could be established. The analysis was done with different pavement structures and different load magnitudes. The sensitivity analysis indicated that only about 5 percent of the maximum displacement is calculated at distances greater than 9 ft. (2.74 m) from the load. This seems to indicate that, for the purpose of modeling multiple wheel loads, a zone of influence having a radius of approximately 9-to-10 ft.

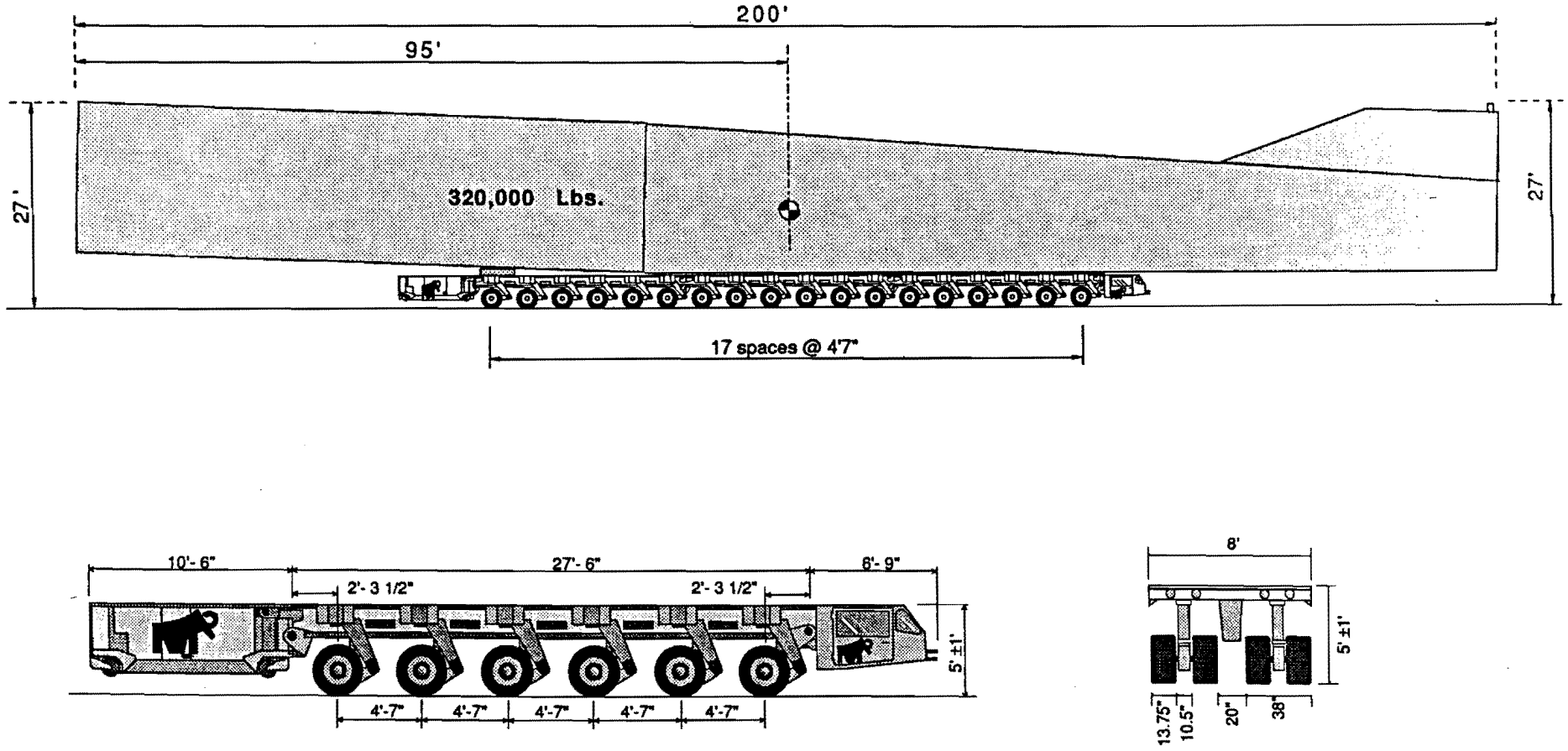

Figure 27. Schematic illustration of tower load-carrying vehicle (courtesy of Davenport Mammoet).

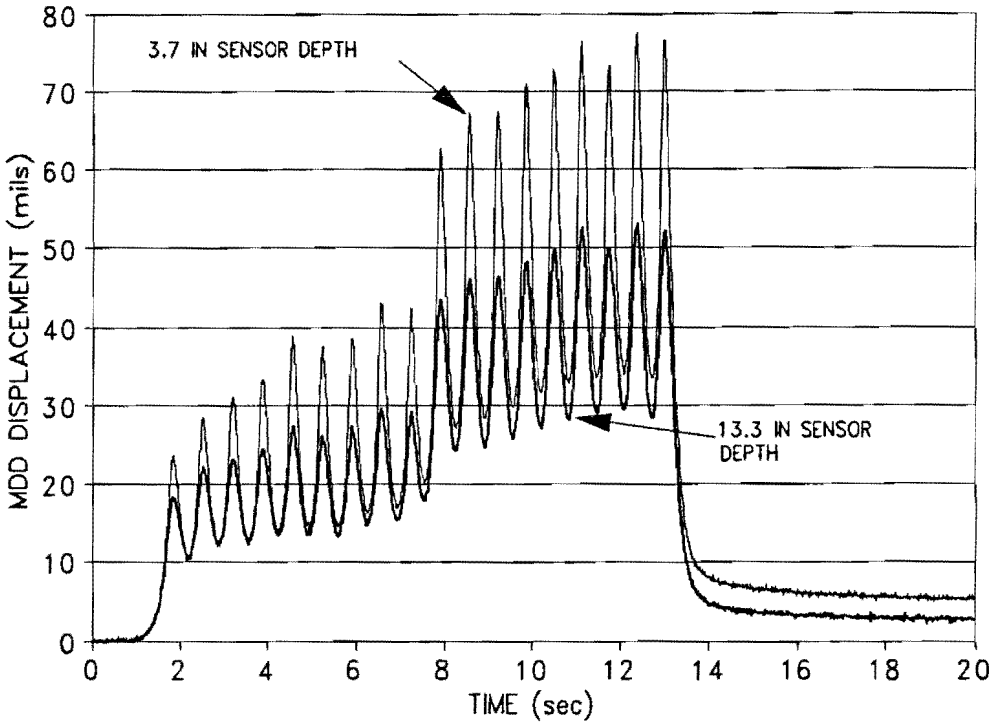

Figure 28. Measured MDD response under superheavy load (1 mil = 25.4 μm, 1 in.= 25.4 mm).

(2.74-to-3.05 m) should be established around the point where stresses and strains are to be calculated. Wheel loads which fall within this zone of influence should then be considered in the pavement-response computations.

The superheavy load was modeled by using a load configuration which resembles the actual line and wheel spacing of the superheavy load vehicle. By varying the evaluation positions, the effect of a moving load could be simulated. Also, by detailed inspection of the video which was taken during the move, the lateral distance between the outside wheel and the MDD sensor at different times could be established with reasonable accuracy. Therefore, similar lateral offset positions were used to simulate the load as accurately as possible.

The calculated and measured displacements of the top two MDD sensors are plotted in Figures 29 and 30. This simulation was done using the average load per tire of 7421 lb. (3369 kg). Figures 29 and 30 show that the calculated response is approximately

halfway between the lower and higher portions of the measured response. There are several encouraging points to note from the figure. It can be seen that the difference between the displacements measured by the top and middle sensors is similar in the calculated response. Also, the tendency of the measured top and middle displacements to fall together between axles (that is, in the trough of the waveform shown in Figure 28) is accurately reflected in the calculated response. In order to show this aspect more clearly, the calculated responses for the first and second sensors are shown on the same set of axes in Figure 31.

As noted before, there are two distinct phases in the measured response. One possible explanation for this observation may be an uneven load distribution, causing some axles to carry a heavier load than others. If the load was indeed unevenly distributed, it would also explain why the calculated response using a constant wheel load falls approximately halfway between the higher and lower phases of the measured response. In order to test this hypothesis, it was necessary to determine first whether the MDD response is an accurate reflection of the load magnitude, and second, whether the assumed mechanistic model can also accurately reflect a change in load magnitude. This verification was done by considering the MDD response under a dump truck for which the exact axle weights were known. The MDD response measured under the dump truck is shown in Figure 32. The axle weights of the dump truck were as follows:

Front axle: 7720 lb. (34.4 kN)

Rear axle (single axle, dual tires): 18720 lb. (83.3 kN).

These wheel loads were used to simulate the pavement response under the front and rear wheels of the dump truck. The calculated response was then compared with the measured response. The results of this comparison are shown in Figures 33 and 34. The figures indicate the following.

1) **The MDD response is proportional to the axle weight.**

This can be seen from the lower and higher peaks in Figure 32, representing the front and rear axles of the dump truck, respectively. The ratio between the lower and higher displacements is 19.5/40.4 = 0.48. This ratio is relatively close to that of the ratio between the lower (front) and higher (rear) axle weights of 0.41. This

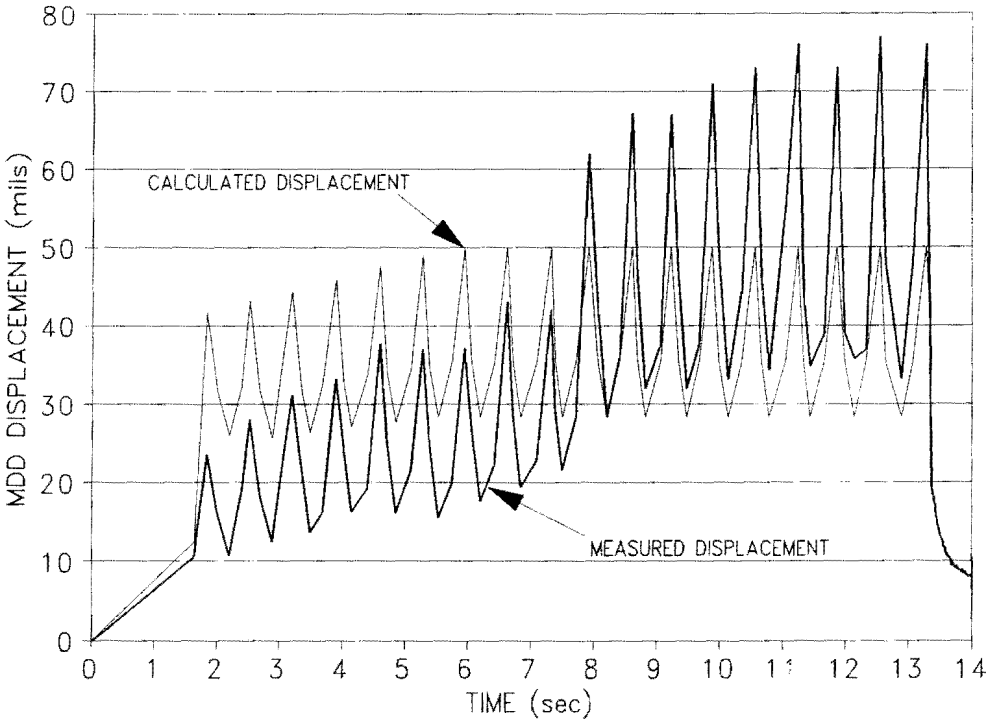

Figure 29. Measured vs. calculated response for sensor 1, 3.7 in. depth (1 mil = 25.4 μm, 1 in.= 25.4 mm).

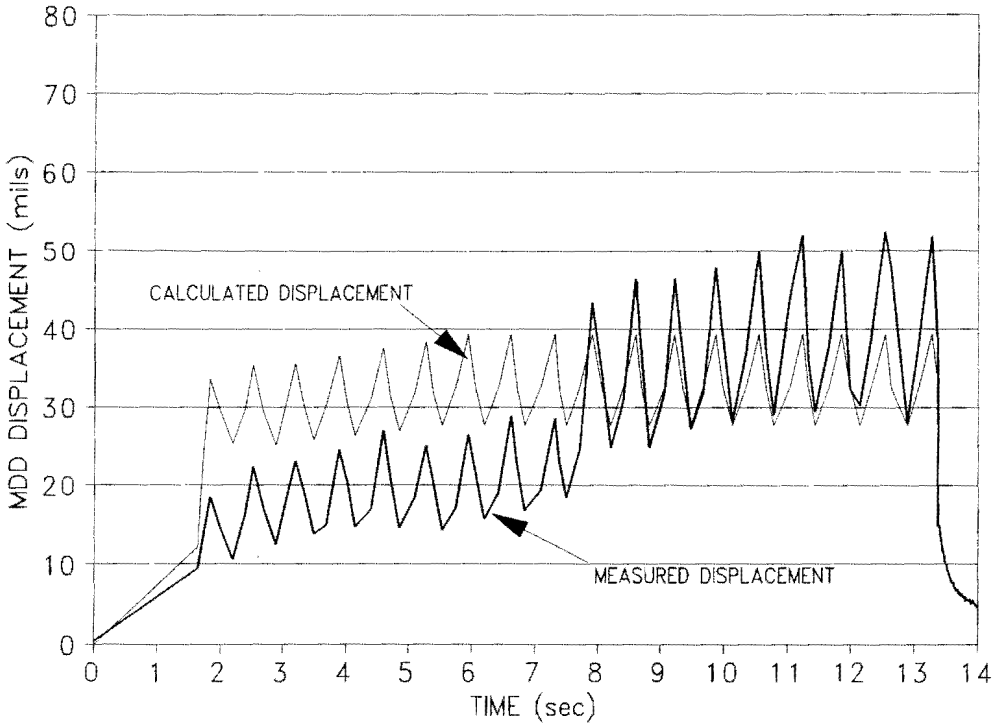

Figure 30. Measured vs. calculated response for sensor 2, 13.3 in. depth (1 mil = 25.4 μm, 1 in.= 25.4 mm).

indicates that the MDD displacements are proportional to the axle loads under which they were measured.

2) **The calculated response shows acceptable agreement with the measured response under variable loads.**

This conclusion follows from the relatively low percentage error between the calculated and measured responses. For both the front and rear axle weights of the dump truck, the linear elastic layered analysis resulted in absolute displacements that agreed very well with the measured displacements.

Following the conclusions drawn from the analysis of the MDD response under the dump truck, the simulation of the superheavy load was redone. However, for this analysis, the total load was divided in proportion to the measured displacements, instead of assuming a uniform load distribution as before. This was done by considering the average displacement measured for the lower portion of the total response (first nine lines) as well as the average displacement measured for the higher part of the response (lines ten to eighteen). The total load was then divided according to these averages. The resulting loads were as follows:

1) lines one to ten: 5195 lb./tire (23.1 kN/tire) (30 percent less than the theoretical average load-per-tire of 7421 lb. (33 kN) mentioned in Chapter 1);
2) lines ten to eighteen: 9647 lb./tire (42.9 kN/tire) (30 percent higher than the theoretical average load-per-tire).

The results of the simulation using the loads given above are summarized in Figures 35 and 36. These figures show a much improved correlation between the calculated and the measured response. The results of this analysis therefore strongly suggest that there could have been an uneven load distribution.

A meeting was subsequently held with the hauling company in order to discuss the possibility of an uneven load distribution. The representatives of the hauling company pointed out that the trailers used to haul heavy loads cannot equalize grossly eccentric loads. The only load that can be equalized among all lines is one that is symmetrically

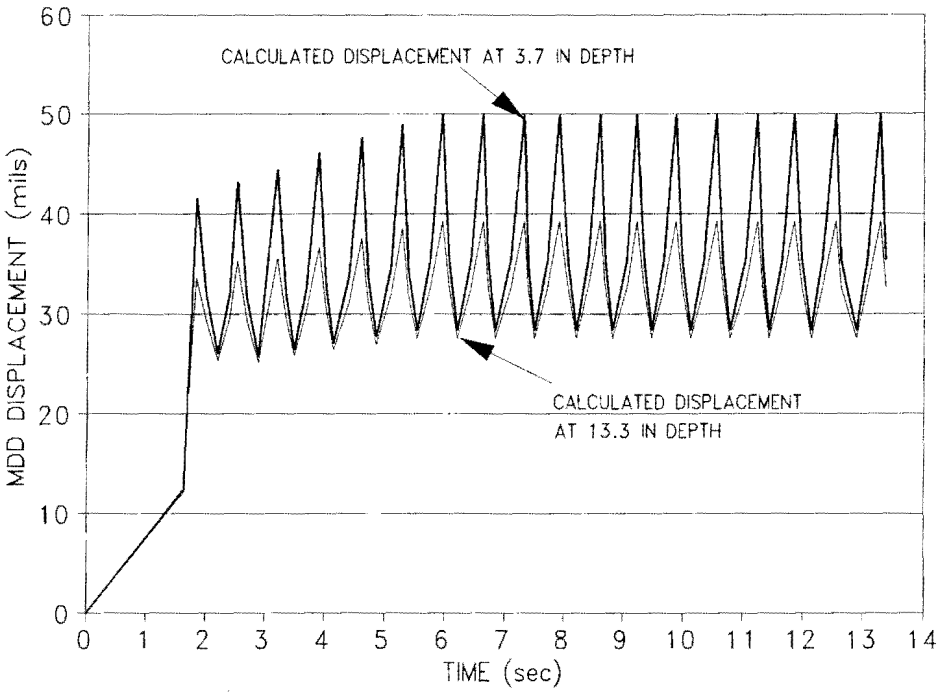

Figure 31. Calculated displacements under 3.7 and 13.3 in. sensor depths (1 mil = 25.4 μm, 1 in.= 25.4 mm).

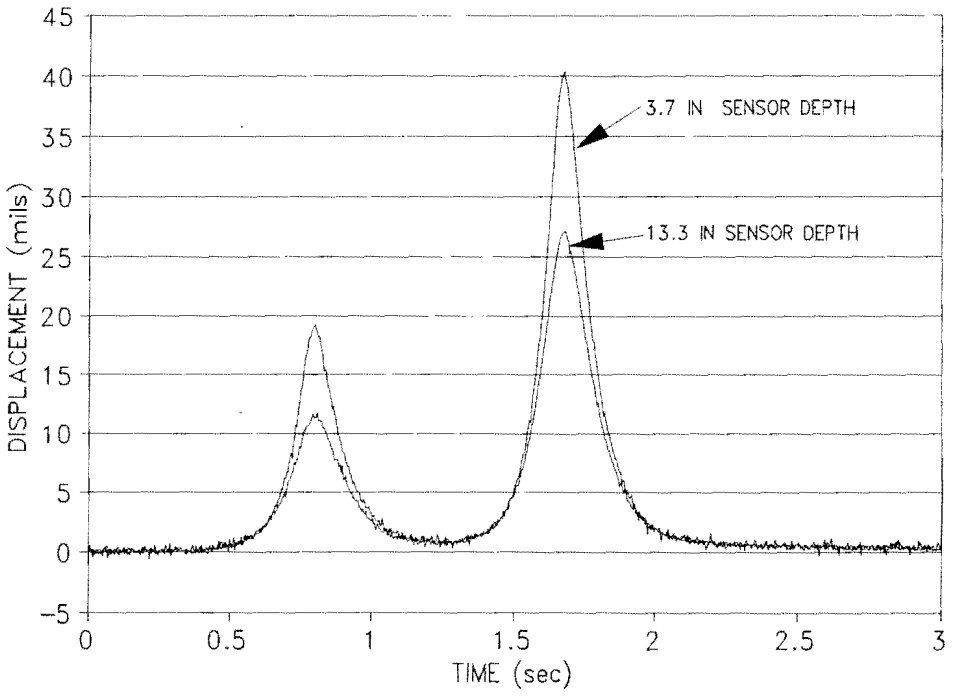

Figure 32. MDD response under dump truck (1 mil = 25.4 μm, 1 in.= 25.4 mm)

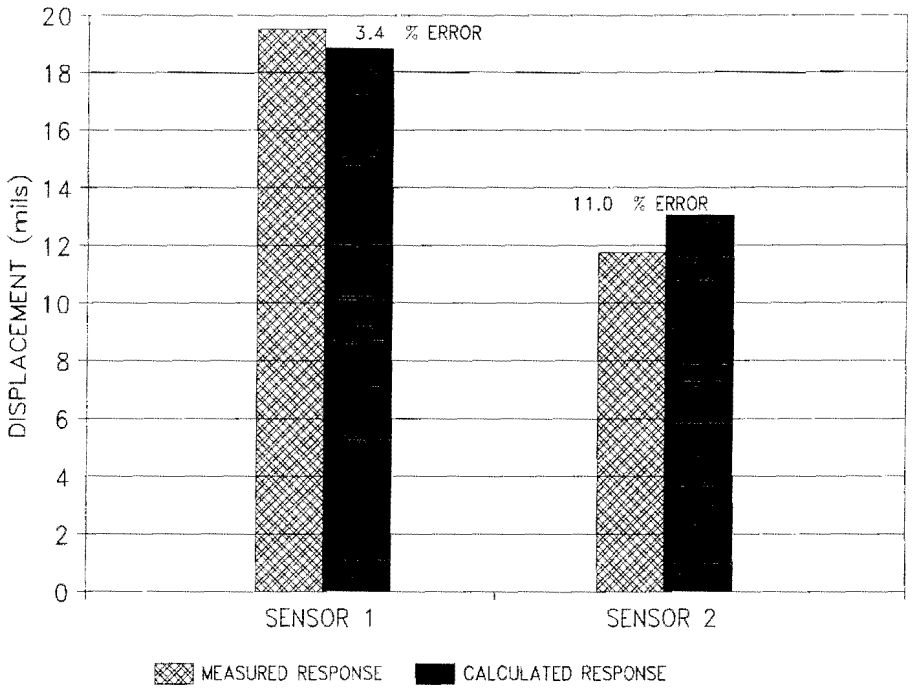

Figure 33. Calculated vs. measured response: dump truck front axle (1 mil = 25.4 μm).

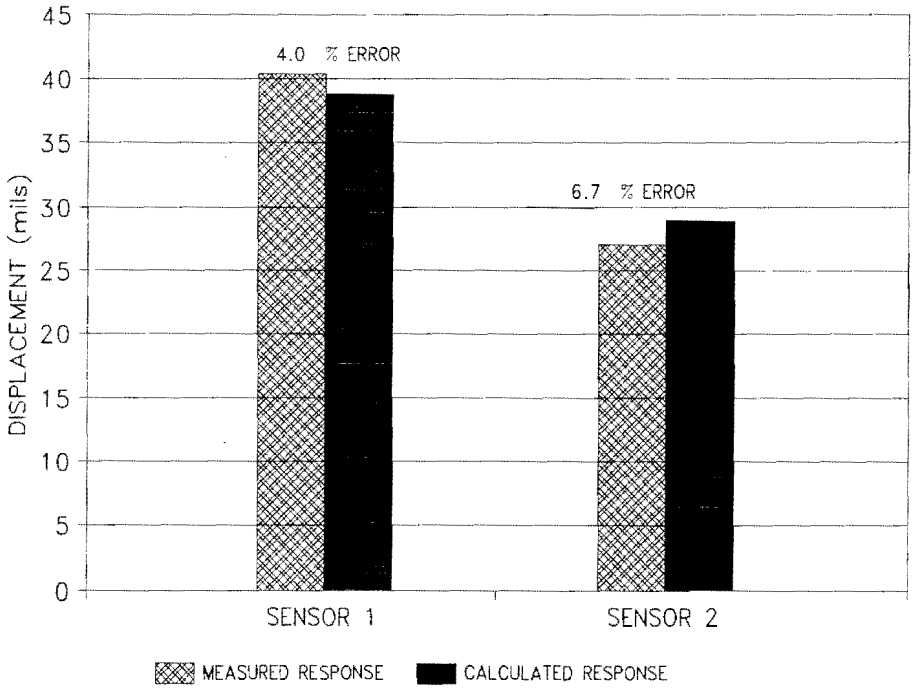

Figure 34. Calculated vs. measured response: dump truck rear axle (1 mil = 25.4 μm).

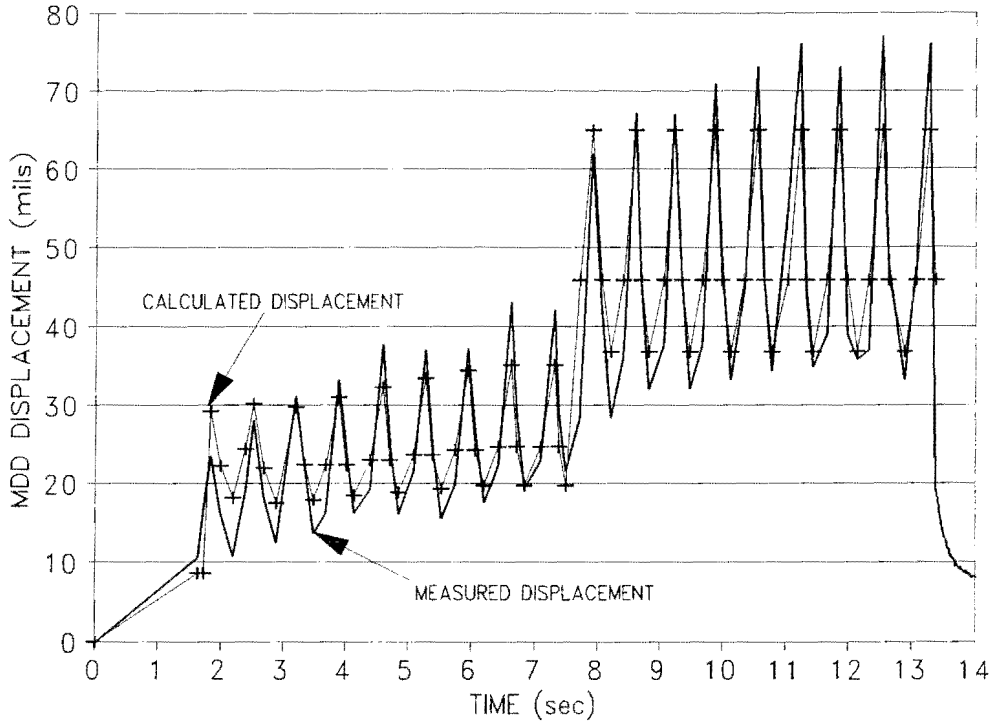

Figure 35. Measured vs. calculated response: top sensor, 3.7 in. depth (1 mil = 25.4 μm, 1 in.= 25.4 mm).

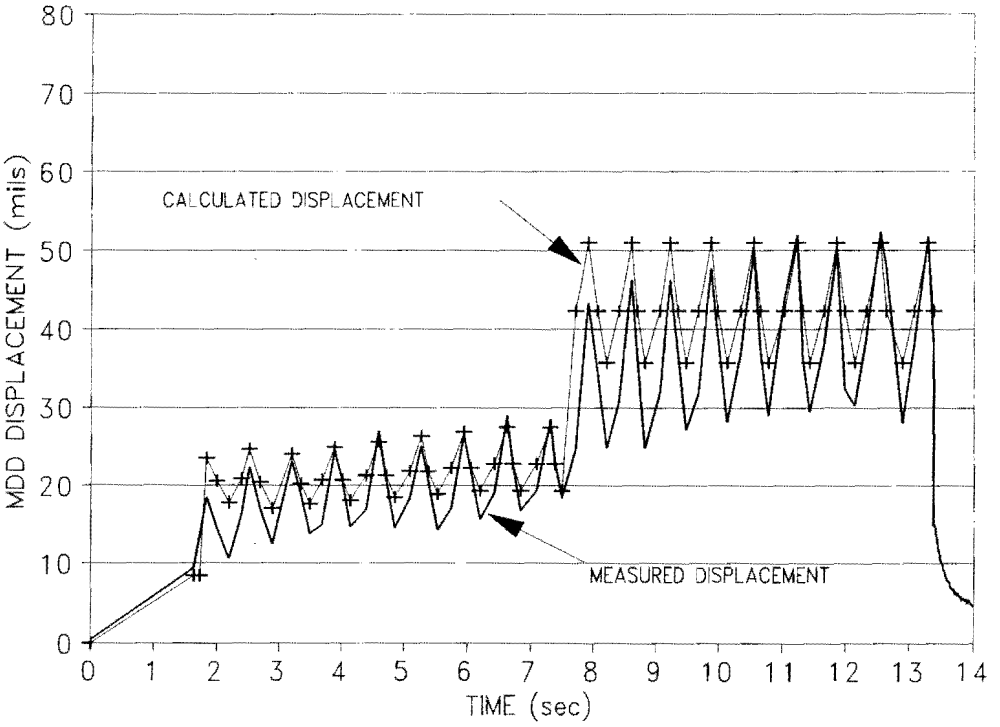

Figure 36. Measured vs. calculated response: second sensor, 13.3 in. depth (1 mil = 25.4 μm, 1 in. = 25.4 mm).

placed on the trailer with a center of gravity that approximately coincides with the geometric center of the trailer.

MODELING OF THE 254 KIP. SUPERHEAVY LOAD (BASE SUPPORT)

The lighter of the two superheavy loads was modeled in the same way as that described in the previous section, i.e., by using the backcalculated pavement structure and simulating the superheavy load in order to obtain displacements. A good correlation between measured and calculated responses would mean that the pavement and vehicle models are valid and can be used for further evaluation of stresses and strains in order to determine the possibility of subgrade failure. The MDD response measured under the lighter superheavy load is shown in Figure 37. A schematic diagram of the loading configuration is given in Figure 38.

In modeling this load, the gross vehicle weight was divided according to the measured displacements, similar to the method used in the analysis of the pavement response under the tower load. This resulted in the following weights per axle.

Axle group one	11,800 lb. (52.5 kN)
Axle group two	29,730 lb. (132.3 kN)
Axle group three	61,580 lb. (275.2 kN)
Axle group four	75,430 lb. (335.6 kN)
Axle group five	75,430 lb. (335.6 kN)
Gross Vehicle Weight	253,970 lb. (1130.1 kN)

It should be noted that, although the drive-axle assembly of the tractor has three axles, as shown in Figure 38, one of these three axles was raised when the move took place. This means that the total weight was distributed between twelve axles and not thirteen, as seen from the MDD trace shown in Figure 37.

The measured and calculated responses for the top and middle sensors are shown in Figures 39 and 40, respectively. Both these figures indicate relatively good agreement between the measured and calculated responses. The agreement between the measured and calculated displacements under loading are slightly better for the top sensor. However, the calculated responses for both sensors show close agreement with the field-measured

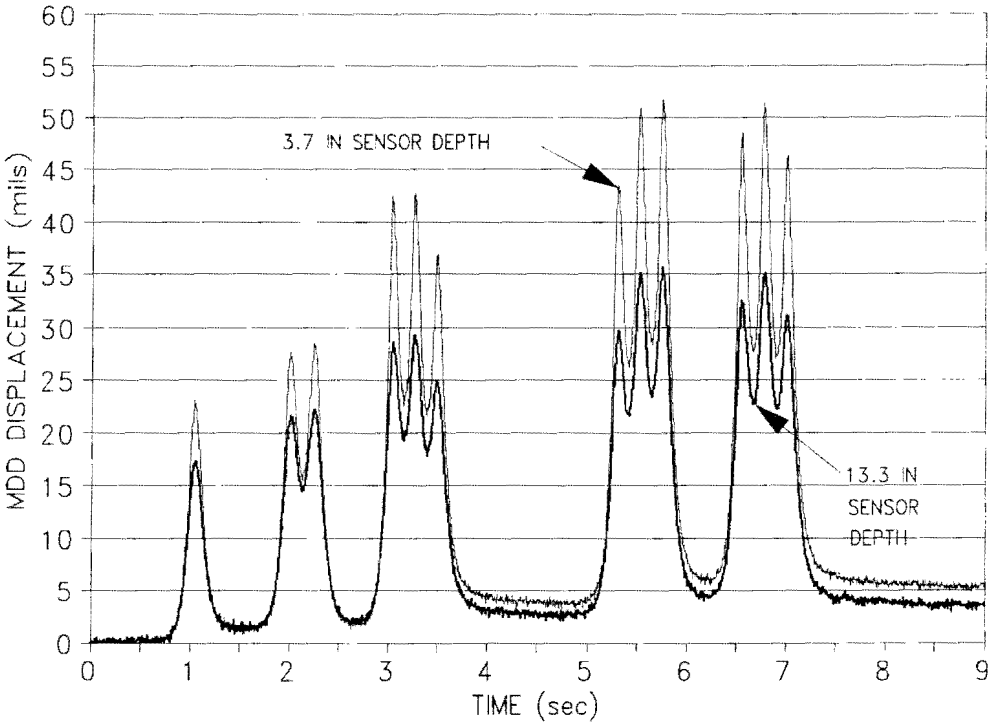

Figure 37. MDD response under 254 kip. superheavy load (base support) (1 mil = 25.4 μm, 1 in.= 25.4 mm).

response as far as the relative displacement at the top and bottom of the waveform is concerned. That is, for both sensors the ratio between the maximum displacement and the minimum displacement between axles of a given assembly is similar for the measured and calculated responses. The results thus seem to indicate that, for the pavement structure considered, layered linear elastic theory provides a reasonable estimate of the pavement response, based on comparisons between the predicted and measured displacements under loading. This theory is used in the subsequent section to predict the stress state under loading for the purpose of evaluating the potential for pavement damage.

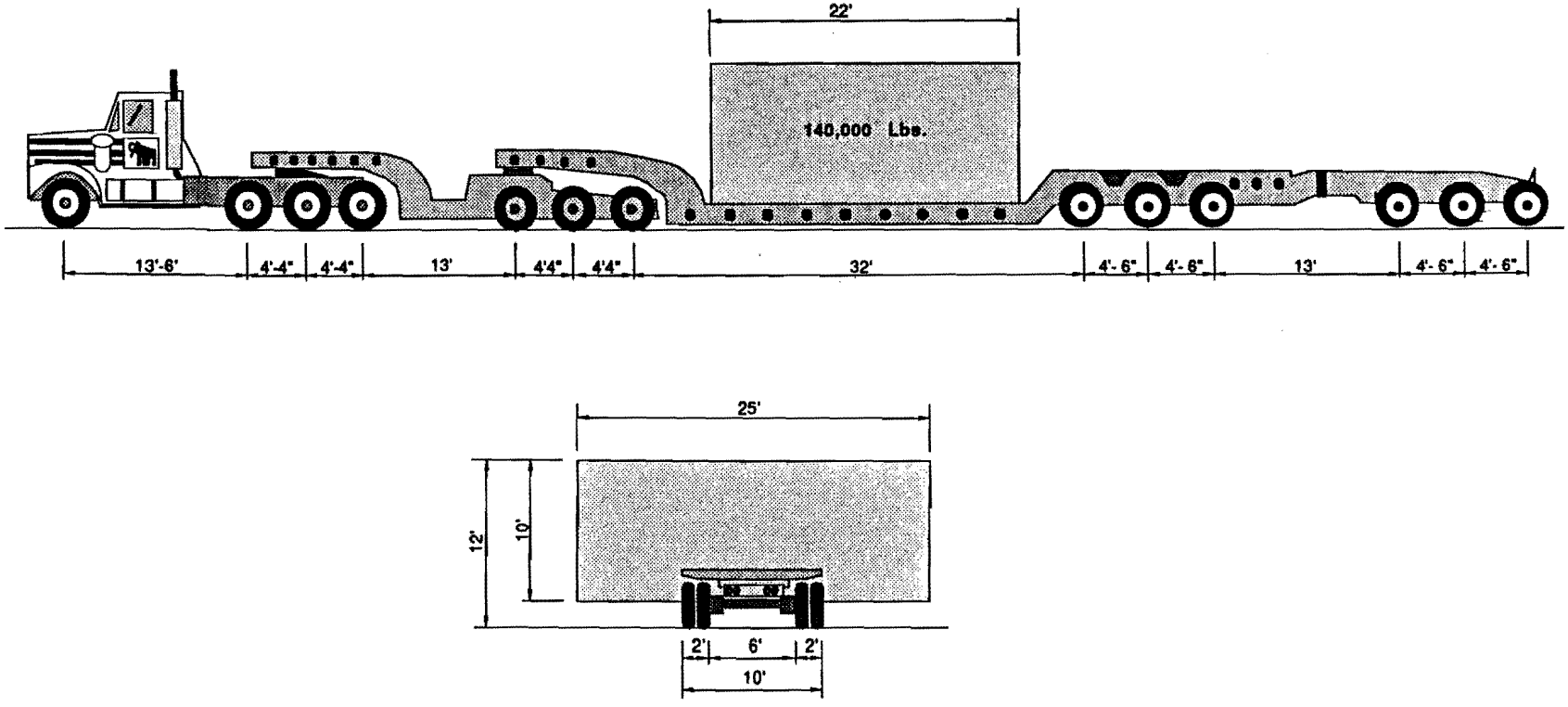

Figure 38. Schematic illustration of base support load-carrying vehicle (courtesy of Davenport Mammoet).

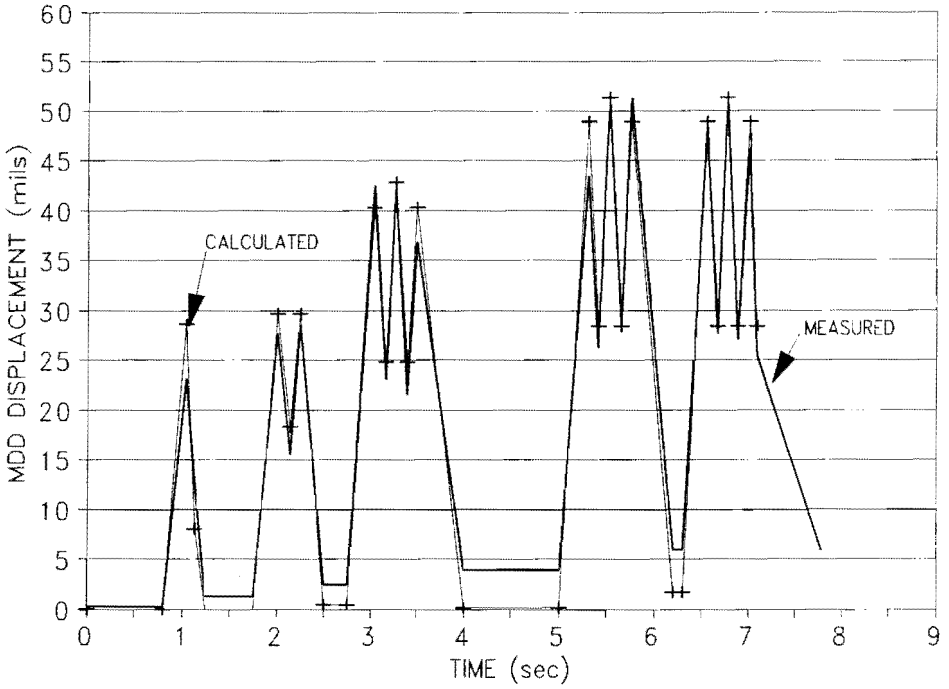

Figure 39. Measured vs. calculated response: 3.7 in. sensor depth (1 mil = 25.4 μm, 1 in. = 25.4 mm).

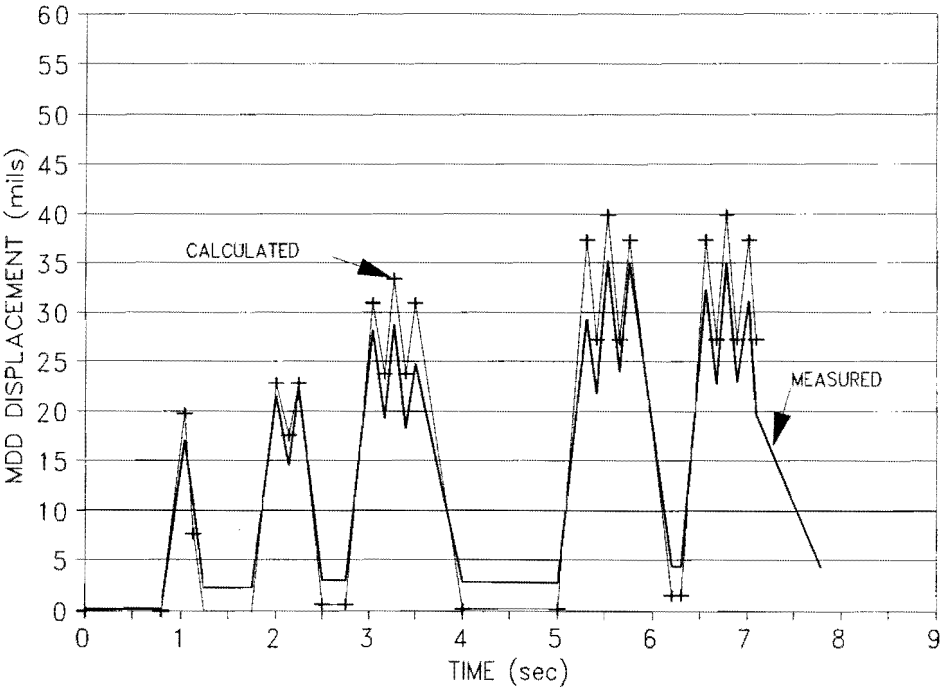

Figure 40. Measured vs. calculated response: 13.3 in. sensor depth (1 mil = 25.4 μm, 1 in.= 25.4 mm).

CHAPTER 4. EVALUATION OF POTENTIAL FOR PAVEMENT DAMAGE

EVALUATION OF POTENTIAL FOR SUBGRADE FAILURE

Texas triaxial class tests (15) were performed on soil samples taken from the subgrade at the site of the MDD installation on FM 1432. The results of these tests are summarized in Table 3, and the Mohr's circles are plotted in Figure 41. Also shown in Figure 41 is the fitted failure envelope with the derived values for cohesion, c, and angle of internal friction, ϕ.

Table 3. Results of Texas Triaxial Class Test

Sample #	Confining Pressure (psi)	Failure Load (lb.)	Strength (psi)
1	0	442.3	33.75
2	3	580.0	43.82
3	5	627.0	48.5
4	10	982.9	74.63
5	15	1063.0	82.11

Note 1 psi = 6.9 kPa, 1 lb. = 0.454 kg

The cohesion and friction parameters were used to determine the shear strength of the subgrade and thus evaluate the possibility of subgrade shear failure under the superheavy loads. The possibility of subgrade failure was evaluated through the use of the three-dimensional Mohr-Coulomb yield criterion. In three-dimensional stress space, the Mohr-Coulomb yield criterion is given, in terms of stress invariants, by the following equation (16):

$$\frac{1}{3}I_1\sin\phi + \sqrt{J_2}\sin\left(\theta + \frac{\Pi}{3}\right) + \frac{\sqrt{J_2}}{\sqrt{3}}\cos\left(\theta + \frac{\Pi}{3}\right)\sin\phi - c\cos\phi = 0 \qquad (1)$$

where,

I_1 = bulk stress

J_2 = second invariant of the deviatoric stress tensor

c = cohesion

ϕ = friction angle

and the angle of similarity, θ, is given by the following expression:

$$\cos 3\theta = \frac{\sqrt{2}\,J_3}{\tau^3_{oct}} \tag{2}$$

where,

J_3 = third invariant of the deviatoric stress tensor

τ_{oct} = octahedral shear stress

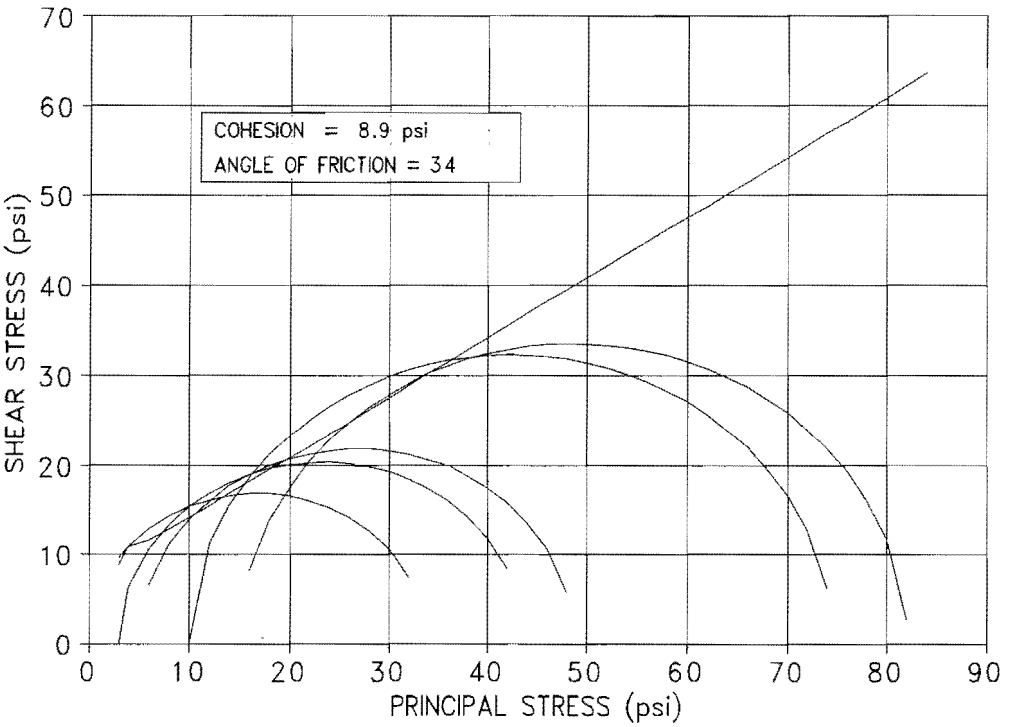

Figure 41. Mohr's circles and fitted failure envelope from laboratory test data (1 psi = 6.9 kPa).

Equations (1) and (2) were used to evaluate the potential for subgrade failure under the tower load. A negative value of the yield function given by Equation (1) would indicate elastic soil behavior, i.e., no failure, at the given point where stresses were evaluated. In the analysis, three different cases were considered, as illustrated in Figure 42. In two of these cases, five lines of the superheavy load transport vehicle were modeled. In one instance, the stresses were evaluated around the center line (Figure 42a). In another, the stresses were calculated around the lead line (Figure 42b). In the third case, only a single line was considered (Figure 42c).

Although the two cases involving the five-line model represent the actual load situation more closely, the single-line model is much easier to use in practice, and it would be of interest to evaluate the differences in the results between the five-line and single-line models. For each case, the yield function was evaluated at various offsets from the origins of the coordinate systems shown in Figure 42. All stress calculations were done with the WESLEA program (11) using the tire loads associated with the last nine lines of the transport vehicle. The Mohr-Coulomb failure parameters, c and ϕ, for the subgrade soil, were determined from laboratory triaxial tests. Results of the calculations are summarized in Figure 43. The following observations are made:

1) For the superheavy load and pavement structure considered, the values of the yield function are all negative, indicating that the subgrade had adequate cover and shear strength to accommodate the tower load without failure or plastic deformations taking place. It is noted that no visible distress was observed after the superheavy load move.
2) For the five-line model, yield function values are more critical under the lead line than the middle line. However, the single-line model resulted in the most conservative predictions, with yield function values about nine percent higher (on average) than the corresponding values for the lead line of the five-line model. This difference is not considered to be significant.

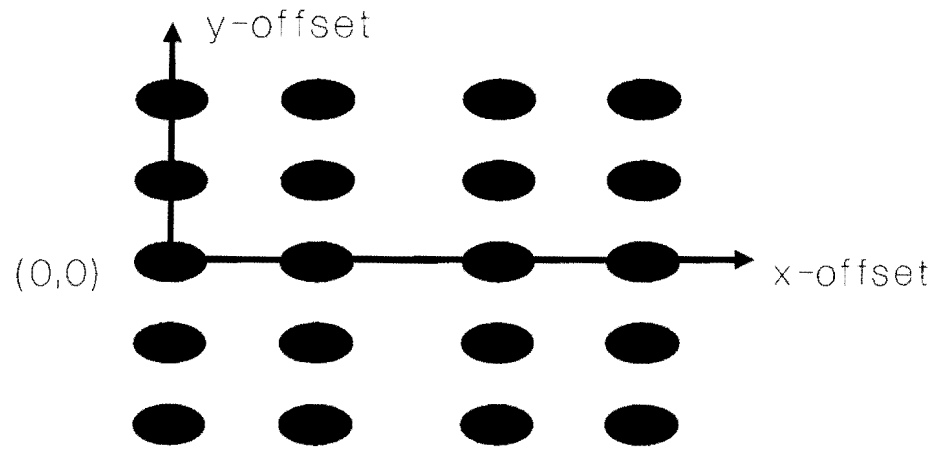

a) Five line model. Evaluation around center line

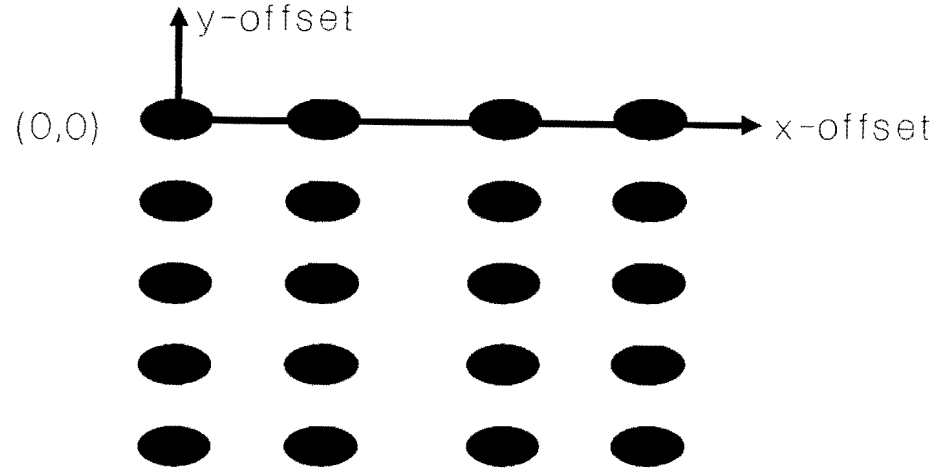

b) Five line model. Evaluation around lead line

c) Single line model

Figure 42. Different load models used for superheavy load simulation.

For practical purposes, a single-line model is easier to use for evaluating the potential for pavement damage under superheavy loads and the results obtained are expected to be more conservative (i.e higher potential for pavement damage will be predicted). The effect of multiple lines is considered in terms of repeated applications of the single-line load.

The more conservative factors of safety from the single-line model can be explained by examining the induced stresses under the single- and five-line models given in Table 4. The stress invariants I_1 and J_2 at the point where the maximum yield function is obtained, are given in the table for the single- and five-line models. It is observed that while the predicted bulk stress, I_1, for the single-line model is slightly higher than that of the five-line model, the higher value of J_2 for the single-line model offsets the slightly higher confinement (i.e. higher I_1) predicted using this load configuration. Consequently, a higher yield function is calculated for the single-line model. However, for the pavement considered, all computed yield functions are negative, indicating that no failure is expected under the superheavy load.

Table 4. Calculated Stresses for Single- and Five-line Models

Model	Bulk Stress, I_1 (psi)	Second deviatoric stress invariant, J_2 (psi)	Yield Function
Single-line	-11.5	3.8	-6.3
Five-line*	-11.0	3.1	-7.5

* Stresses and yield function evaluated around lead line

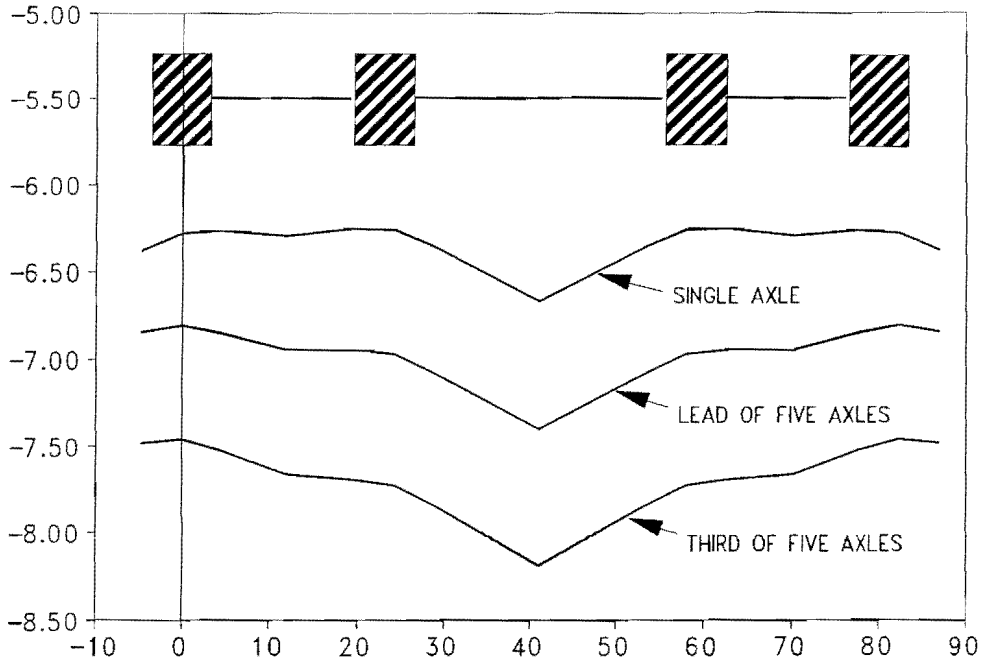

Figure 43. Calculated yield function values for different load cases.

CHAPTER 5. SUMMARY OF FINDINGS

A framework for evaluating the structural adequacy of proposed superheavy load routes was demonstrated using test data collected on superheavy load moves monitored in Victoria, Texas. The significant findings of the study are:

1) From the analysis of test data, it is clear that the potential for subgrade shear failure was very minimal for the pavement structure and superheavy loads considered. No visible distress was observed after the superheavy load moves.
2) Test data from MDD measurements indicate that reasonable predictions of pavement response under loading can be obtained using elastic layered theory. The data suggest that non-linear effects are not very significant for the pavement structure analyzed.
3) On the basis of the yield function values computed for single- and five-line models, the use of a single-line model led to a slightly more conservative prediction of the potential for subgrade failure. For practical purposes, the use of a single-line model is easier to implement. The effect of multiple lines may be considered in terms of repeated applications of the single-line load.

The procedure for evaluating superheavy load routes based on the framework demonstrated herein is still under development. While non-linear effects were not significant for the pavement structure analyzed herein, conditions may be encountered where such effects are pronounced. Consequently, development of the procedure must consider non-linear pavement behavior. The effects of non-linearity on predicted stresses under loading and the onset of yielding need to be investigated.

REFERENCES

1. T. Scullion, C.L. Lau, and Y. Chen. Implementation of the Texas Ground Penetrating Radar System. Research Report 1233-1. Texas Transportation Institute, College Station, Texas, 1992.
2. E.G. Fernando. Highway Speed Pavement Thickness Surveys using Radar. FHWA Contract DTFH 78-92-P-F281. Texas Transportation Institute, College Station, Texas, 1992.
3. E.G. Klein, J.H. Maree, P.F. Savage. The Application of a Portable Pavement Dynamic Cone Penetrometer to Determine In-Situ Bearing Properties of Road Pavement Layers and Subgrades in South Africa. Proceedings of the 2nd European Symposium on Penetration Testing, Amsterdam, May 1982, pp. 277-283.
4. J. Lu, C. Bertrand, and W.R. Hudson. Evaluation and Implementation of the Automated Road Analyzer (ARAN). Research Report 1223-2F, Center for Transportation Research, Austin, Texas, 1991.
5. T. Scullion, J. Uzan, I. Yazdani, and P. Chan. Field Evaluation of the Multi-Depth Deflectometer. Research Report 1123-2. Texas Transportation Institute, College Station, Texas, 1988.
6. Y.R. Kim, N.P. Khosla, S. Satish, and T. Scullion. Validation of Moduli Backcalculation Procedures Using Multidepth Deflectometers Installed in Various Flexible Pavement Structures. In Transportation Research Record 1377, National Research Council, Washington D.C.,1991, pp. 128-142.
7. R.L. Lytton. Backcalculation of Pavement Layer Properties. Nondestructive Testing of Pavements and Backcalculation of Moduli, Special Technical Publication 1026, American Society for Testing and Materials, 1989, pp. 7-38.
8. E.G. Fernando, and T. Chua. Development of a Procedure for Route Segmentation Using Predicted Layer Thicknesses from Radar Measurements, Florida DOT State Project 99700-7550, Phase 2A Report. Texas Transportation Institute, College Station, Texas, 1993.

9. MODULUS: Preliminary User's Manual-Version 4.0.. Texas Transportation Institute, College Station, Texas, 1990.

10. T. Scullion. Incorporating a Structural Strength Index into the Texas Pavement Evaluation System, Research Report 409-3F. Texas Transportation Institute, College Station, Texas, 1988.

11. F.J. Van Cauwelaert, D.R. Alexander, T.D. White, and W.R. Barker. Multilayer Elastic Program for Backcalculating Layer Moduli in Pavement Evaluation, Special Technical Publication 1026, American Society for Testing and Materials, 1989.

12. P. Ullidtz. Pavement Analysis, Elsevier, New York, 1987.

13. P. Sebaaly, N. Tabatabaee, B. Kulakowski, and T. Scullion. Instrumentation for Flexible Pavements - Field Performance of Selected Models, Volume I. Research Report FHWA-RD-91-094, Pennsylvania Transportation Institute, University Park, Pennsylvania, 16802, 1991.

14. D.L. De Jong, M.G.F. Pentz, and A.R. Korswagen. Computer Program BISAR. Extended Report, Koninklijke/ Shell Laboratorium, The Netherlands, 1973.

15. Test Method TEX-117-E. Triaxial Compression Test For Disturbed Soils and Base Material. Manual of Testing Procedures. Texas Department of Transportation, Austin, Texas, 1993.

16. W.F. Chen, and G.Y. Baladi. Soil Plasticity: Theory and Implementation. *Developments in Geotechnical Engineering, No 38*, Elsevier, New York, 1985.

APPENDIX:

EVALUATION OF EFFECTS OF MULTIPLE WHEEL LOADS

BACKGROUND

Superheavy vehicles are equipped with multiple axles, each having multiple tires per axle. It is important to evaluate the contributions of different wheel loads to predicted pavement response at a given point to determine a zone of influence outside of which the wheel load contributions become negligible. This is necessary to establish a reference multiple-tire-axle assembly for appropriately modeling the multiple wheels of a superheavy vehicle, which can number in the hundreds. By establishing guidelines for modeling pavement response due to multiple wheel loads, the analysis of superheavy load effects may be significantly simplified and done more efficiently.

OBJECTIVE

The objective of this exercise is to analyze pavement response under superheavy tire loads for different pavement systems and loadings in order to establish guidelines for modeling the multiple wheels of a superheavy vehicle. The linear elastic layered computer program, BISAR, was used to accomplish this objective.

MODELING OF ONE AXLE OF SUPERHEAVY TRAILER

In this analysis, pavement response under the multiple tire loads of the superheavy trailer axle illustrated in Figure A1 was evaluated. The configuration shown is commonly used in superheavy load moves. The following pavement response parameters were predicted:

1) the horizontal strain, ε_{ac}, at the bottom of the asphalt concrete layer, and
2) the vertical strain, ε_{sg}, at the top of the subgrade.

The strain, ε_{ac}, is a predictor of fatigue cracking in the asphalt layer, while ε_{sg} is a predictor of pavement rutting. Both of these parameters are used as failure criteria in several existing pavement performance models. The pavement system shown in Figure A2 was assumed in the analysis. Figures A3 and A4 show, respectively, the predicted asphalt horizontal strains and subgrade vertical strains at the different wheel positions of the superheavy trailer axle.

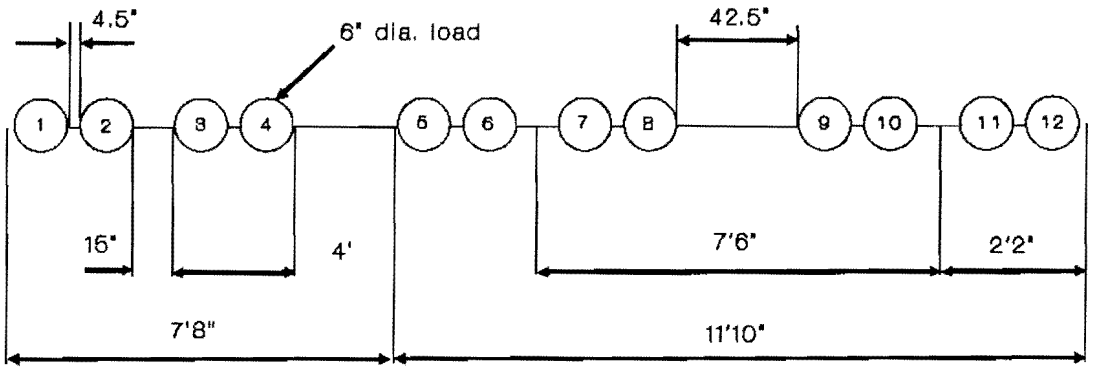

Figure A1. Dimensions for Goldhofer 20 axle, 1.5 wide hydraulic trailer (1032 ton capacity).

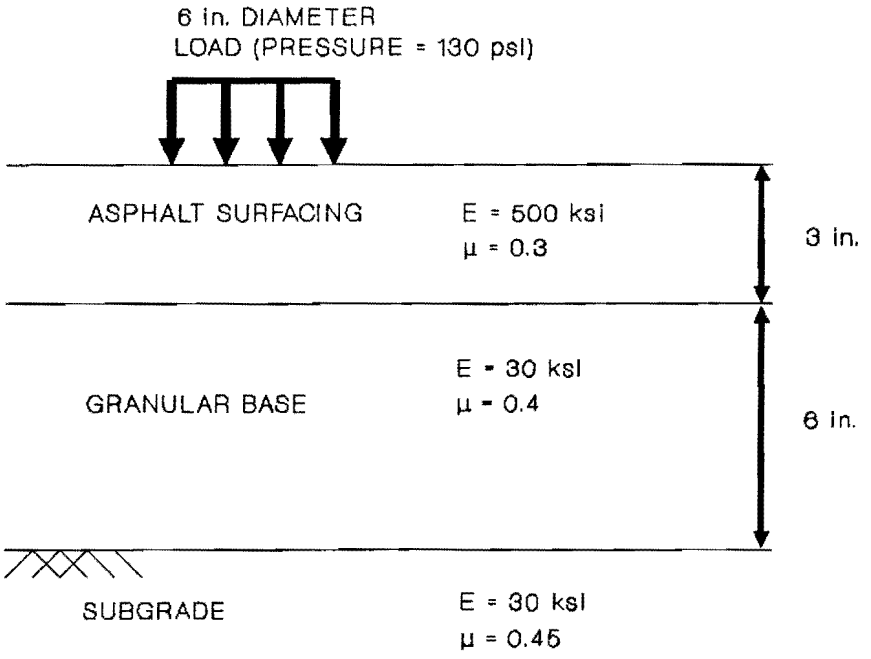

Figure A2. Pavement profile used in evaluating pavement response under superheavy trailer axle.

The total strain underneath the center of each wheel load was evaluated using the principle of superposition. The predicted strain, ε_{ac}, is observed to vary from 394 to 457 microstrains, while ε_{sg} ranges from -831 to -1028 microstrains. Herein, positive strains denote tension while negative strains denote compression.

An evaluation was made to determine if fewer tires may be used to model pavement response under the superheavy-trailer axle. Since the configuration shown in Figure A1 consists of three tire groups of four tires each, pavement response was evaluated assuming only four tires (i.e., tires 1 through 4 in Figure A1). In this instance, the maximum horizontal strain, ε_{ac}, at the bottom of the asphalt was found to be 453 microstrains, while the maximum vertical strain, ε_{sg}, at the top of the subgrade was computed to be -1038 microstrains. These values compare very favorably with the corresponding maxima determined using all twelve wheel loads, with the differences being less than 1 percent of the computed maximum strains under all twelve tires. These results indicate that, with respect to ε_{ac} and ε_{sg}, the superheavy trailer axle can be reasonably represented by a set of four tires.

In addition to ε_{ac} and ε_{sg}, the vertical displacements at the top of the base, Δ_b, at the top of the subgrade, $(\Delta_{sg})_o$, and at a depth of 1 ft. (0.305 m) into the subgrade, $(\Delta_{sg})_1$, were evaluated using the BISAR computer program. Total displacements due to the combined action of the twelve different wheel loads are plotted in Figure A5. The range of the predicted displacements at the top of the base is 34 to 47 mils. (0.86 to 1.19 mm) At the top of the subgrade, the predicted displacements vary from 30 to 43 mils. (0.76 to 1.09 mm), while at 1 ft. (0.305 m) into the subgrade, the predicted displacements range from 23 to 34 mils (0.58 to 0.86 mm). As expected, the displacements are highest at the middle of the axle, and the magnitudes diminish with depth into the pavement.

A similar analysis was made to determine if, on the basis of predicted vertical displacements, the given axle can also be reasonably modeled using only four tires. For this case, however, the results significantly underestimated those obtained for the reference condition. The predicted maximum displacement at the top of the base was 35 mils. (0.898 mm). At the top of the subgrade, it was 31 mils. (0.79 mm), while at a depth of 1 ft. into the subgrade, the predicted displacement was 22 mils. (0.56 mm).

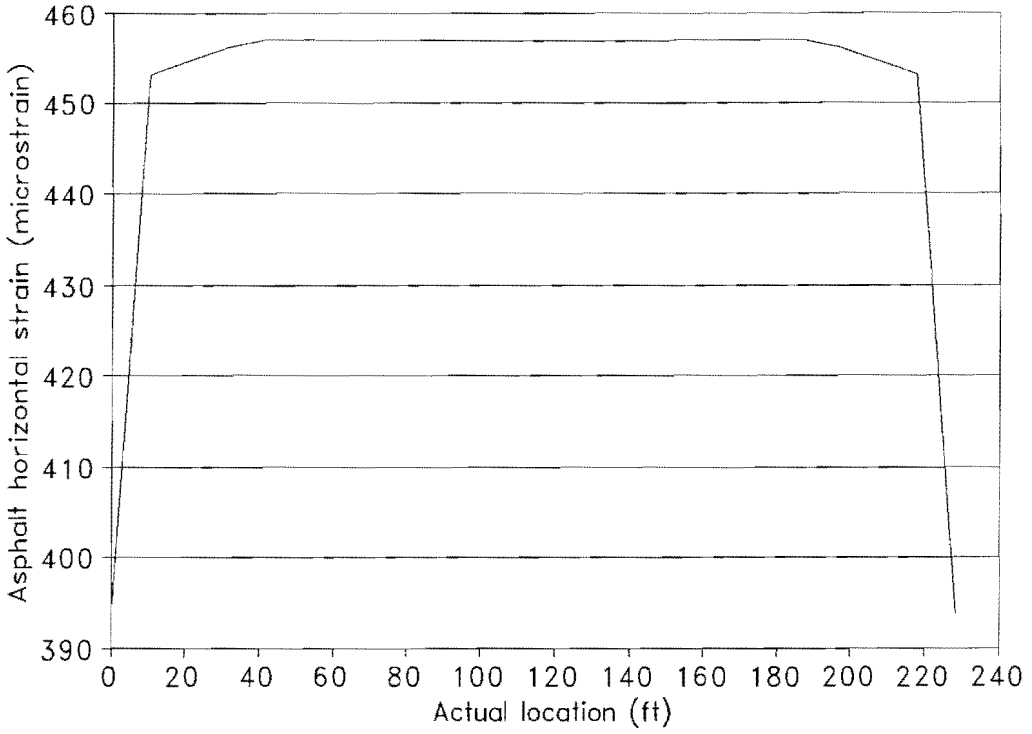

Figure A3. Predicted asphalt horizontal strains under superheavy trailer axle (1 ft.= 0.30 m).

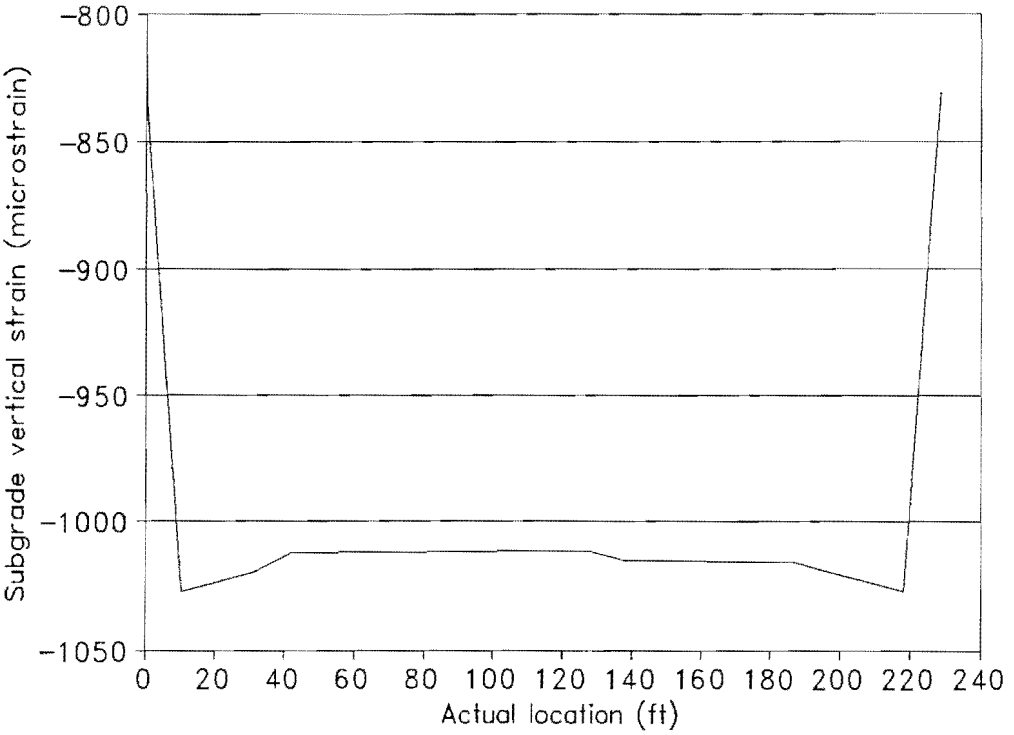

Figure A4. Predicted subgrade vertical strains under superheavy trailer axle (1 ft.= 0.30 m).

These differences are 26, 28, and 35 percent, respectively, of the corresponding maximum displacements calculated under the reference condition. These results indicate that the influence of a given wheel load spans a greater distance when viewed with respect to predicted vertical displacement as opposed to predicted horizontal asphalt strain, ε_{ac}, or vertical subgrade strain, ε_{sg}.

EVALUATION OF PAVEMENT RESPONSE FOR DIFFERENT PAVEMENT SYSTEMS AND LOADS

In view of the results presented previously, it becomes important to evaluate how predicted pavement response varies with distance from a given wheel load. This should provide guidance on how to model the multiple wheels of a superheavy vehicle when predicting pavement response using the method of superposition. For this evaluation, the following cases, covering a wide range in field conditions, were considered:

1) a weak pavement subjected to a heavy wheel load,
2) a weak pavement subjected to a light wheel load,
3) a strong pavement subjected to a heavy wheel load, and
4) a strong pavement subjected to a light wheel load.

The three-layer pavement system shown in Figure A6 was used in the analysis. Values of layer thicknesses and moduli assumed for the different cases are given in Table A1.

Table A1. Pavement Layer Moduli and Thicknesses Assumed for Weak and Strong Pavements

	Weak Pavement	Strong Pavement
E_1 (ksi)	250	1000
E_2 (ksi)	15	60
E_3 (ksi)	5	20
h_1 (inches)	2	6
h_2 (inches)	4	12

Note: 1 ksi = 6900 kPa

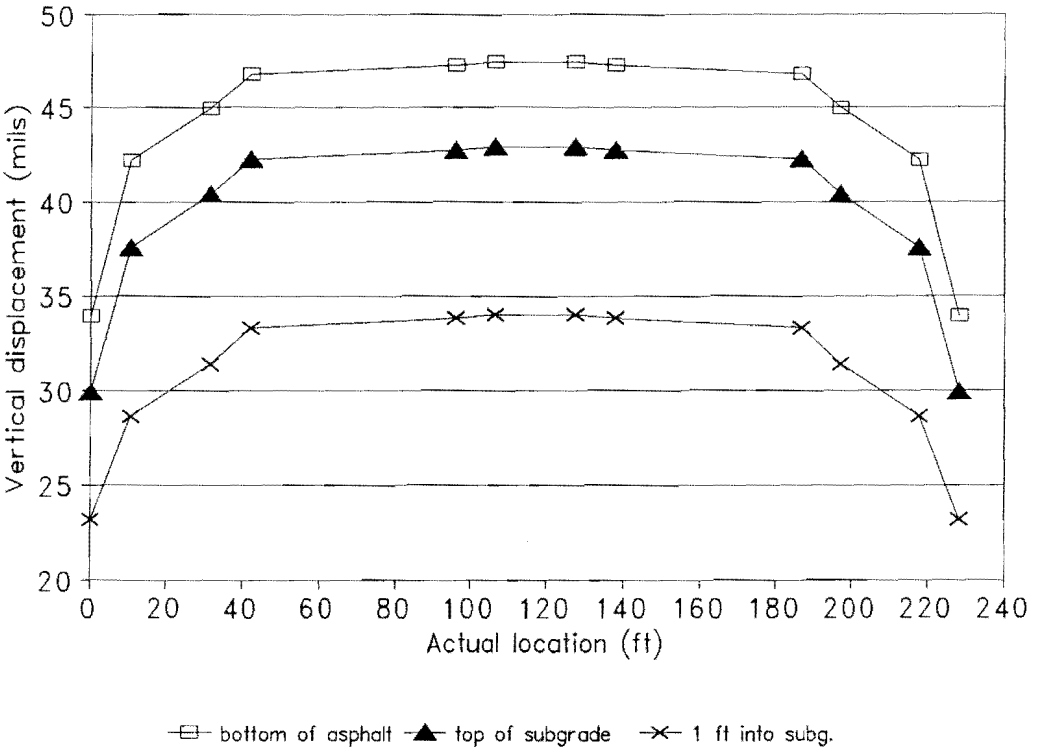

Figure A5. Predicted displacements under superheavy trailer axle (1 ft.= 0.30 m, 1 mil = 25.4 μm).

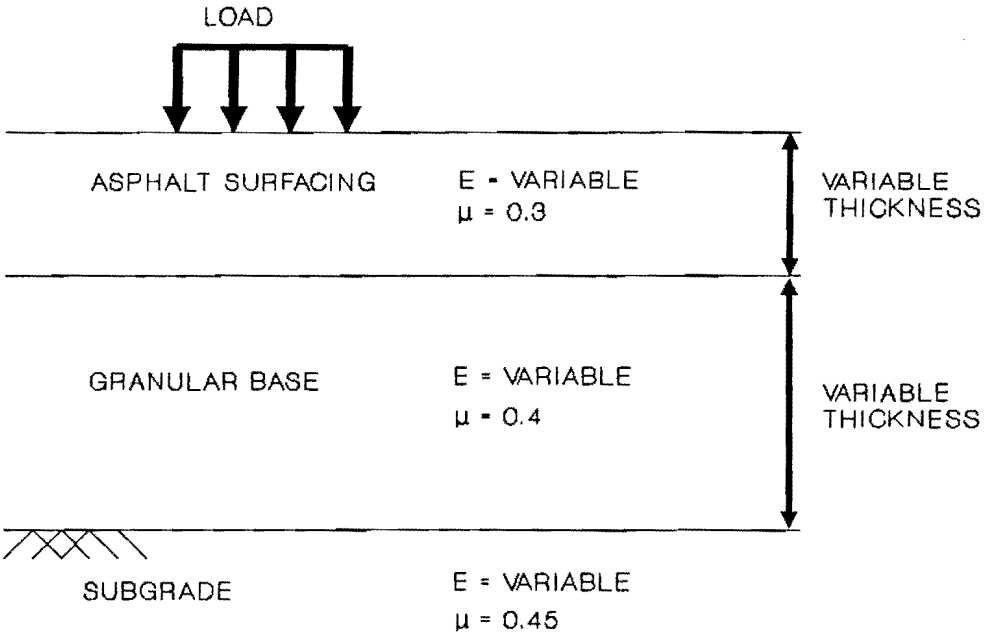

Figure A6. Pavement profile used in evaluation of pavement response for different pavement systems and loads.

It is noted that the strong pavement has more structure, i.e., it has thicker and stiffer layers than those used to characterize the weak pavement. A light wheel load of 5 kips. (22.2 kN), and a heavy wheel load of 15 kips. (66.7 kN) were used, which cover the range of expected superheavy tire loads. The tire pressure assumed was 120 psi (828 kPa).

For each case considered, the horizontal strain, ε_{ac}, at the bottom of the asphalt, and the vertical strain, ε_{sg}, at the top of the subgrade, were evaluated at various offsets from the given wheel load. Figures A7 to A14 show results from the analysis. For a given wheel load, lower strains are predicted for the strong pavement. However, for this same pavement, the predicted strains also diminish more slowly with distance from the wheel load, i.e, the zone of influence is larger. In general, for the weak pavement the predicted strains diminish to less than 2 percent of the corresponding maximum values at a distance of 2 ft. (0.61 m) from the given wheel load. In contrast, for the strong pavement, the corresponding distance is 4 ft. (1.22 m). These results indicate that, for the purpose of calculating the strains ε_{ac} and ε_{sg} at a given point to evaluate potential pavement damage, a greater number of loads may have to be modeled when the pavement has more structure. In such a case, the influence of a given wheel load spans a greater distance, and care must be taken to keep the errors in the calculation of pavement strains using the superposition principle within acceptable limits.

It is of interest to examine why the influence of a given wheel load extends a greater distance for the case of a strong pavement. A plausible reason is that the strong pavement is characterized by thicker layers, which means that the points of evaluation for ε_{ac} and ε_{sg} are deeper than the corresponding points for the weak pavement. Since the area of influence of a surface load gets larger with depth into the pavement, this may help explain the results obtained.

In order to test this hypothesis, pavement response was evaluated for the case of a strong pavement subjected to a heavy wheel load but with layer thicknesses reduced to those of the weak pavement in accordance with Table A1. Figures A15 and A16 show, respectively, the predicted asphalt and subgrade strains from this analysis. The predicted strains diminish with distance from the given wheel load at a rate very much like that

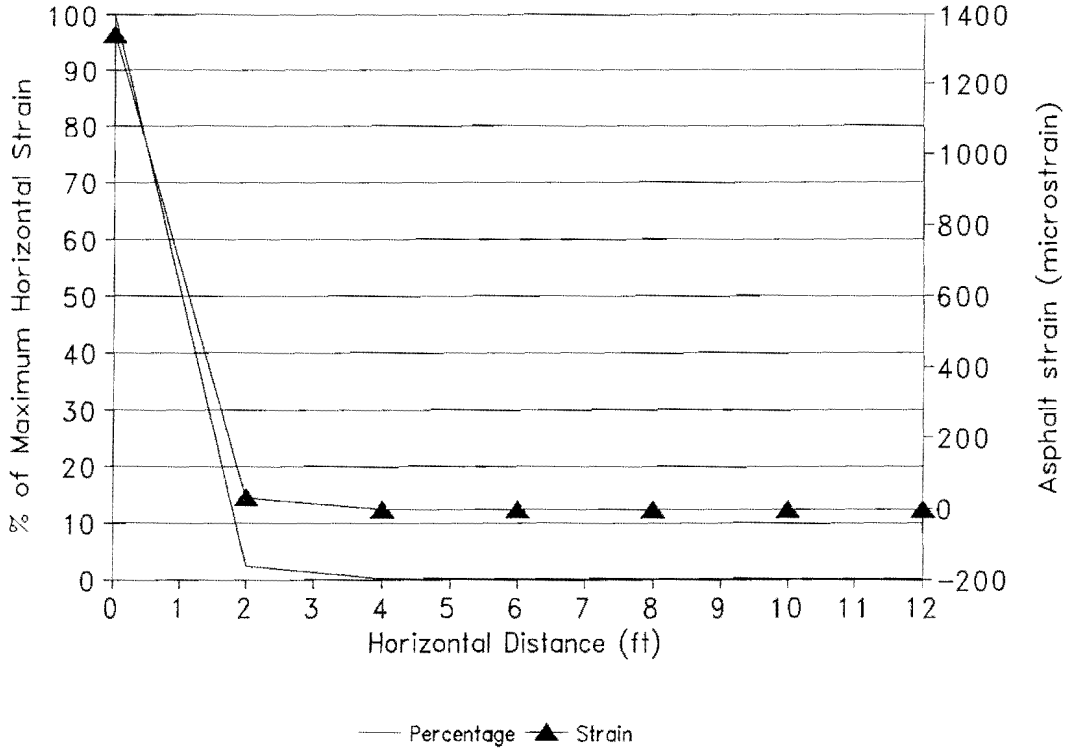

Figure A7. Predicted asphalt horizontal strains (weak pavement under heavy wheel load) (1 ft. = 0.30 m).

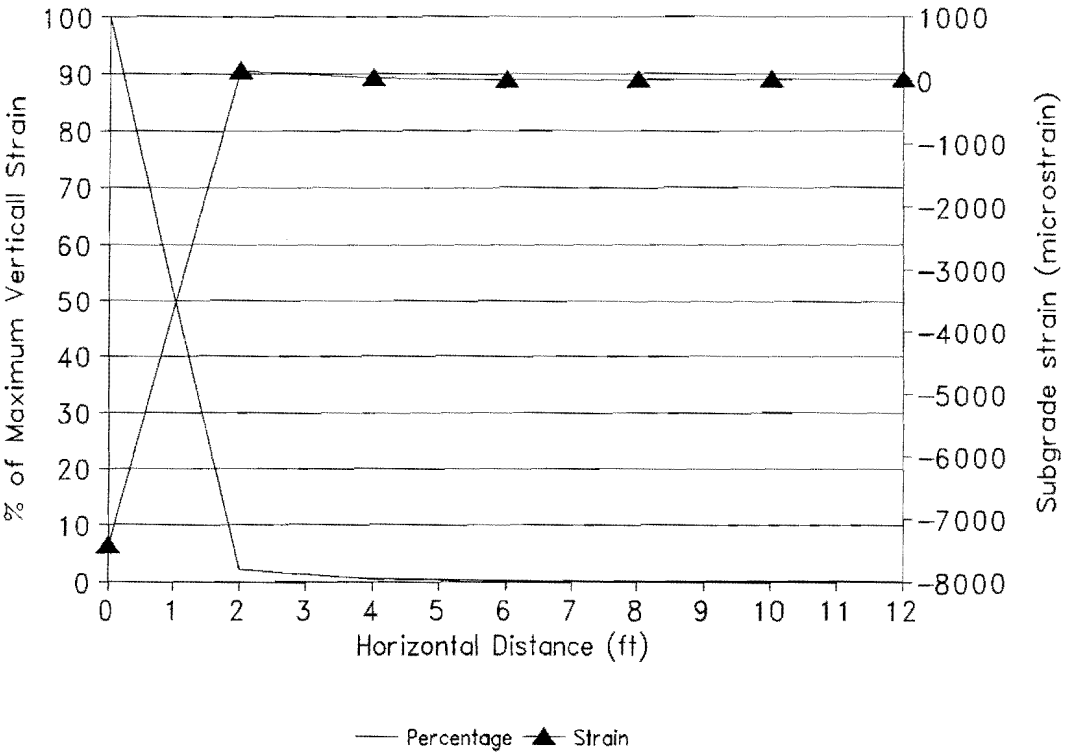

Figure A8. Predicted subgrade vertical strains (weak pavement under heavy load) (1 ft.= 0.30 m).

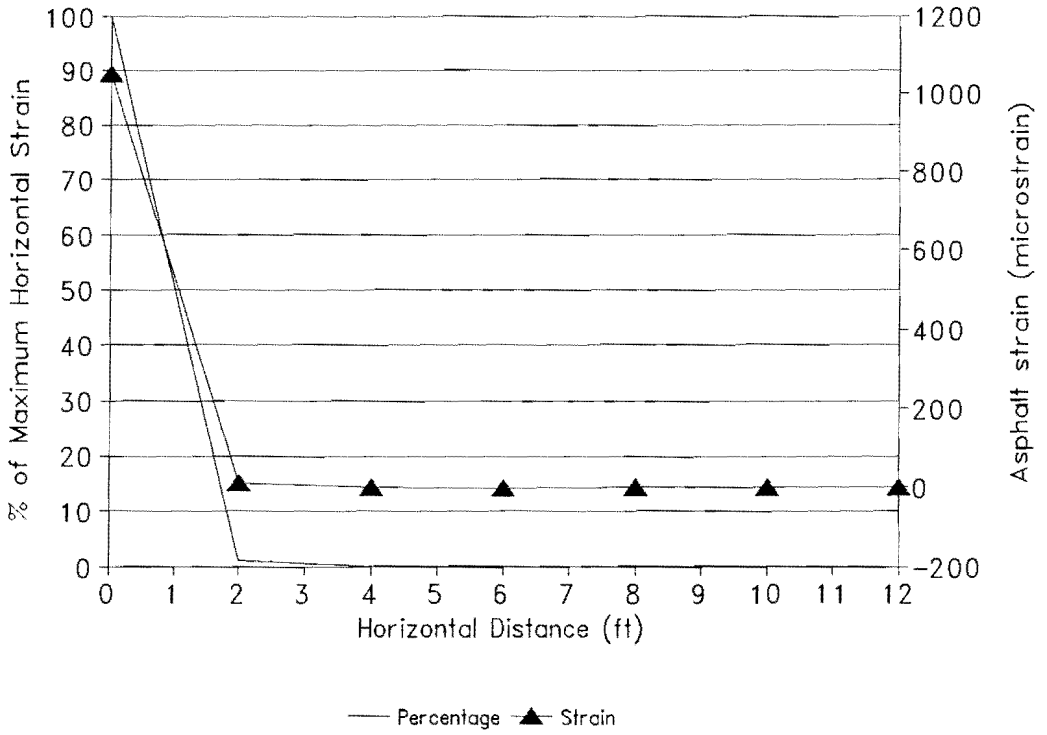

Figure A9. Predicted asphalt horizontal strains (weak pavement under light wheel load) (1 ft.= 0.30 m).

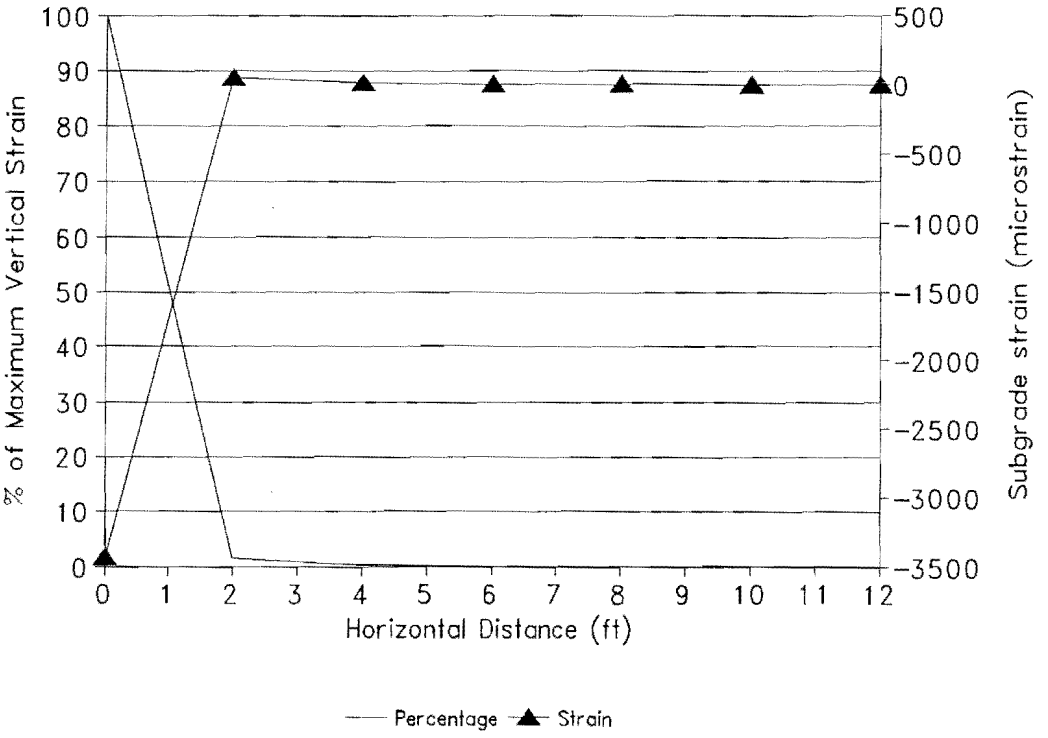

Figure A10. Predicted subgrade vertical strains (weak pavement under light wheel load) (1 ft.= 0.30 m).

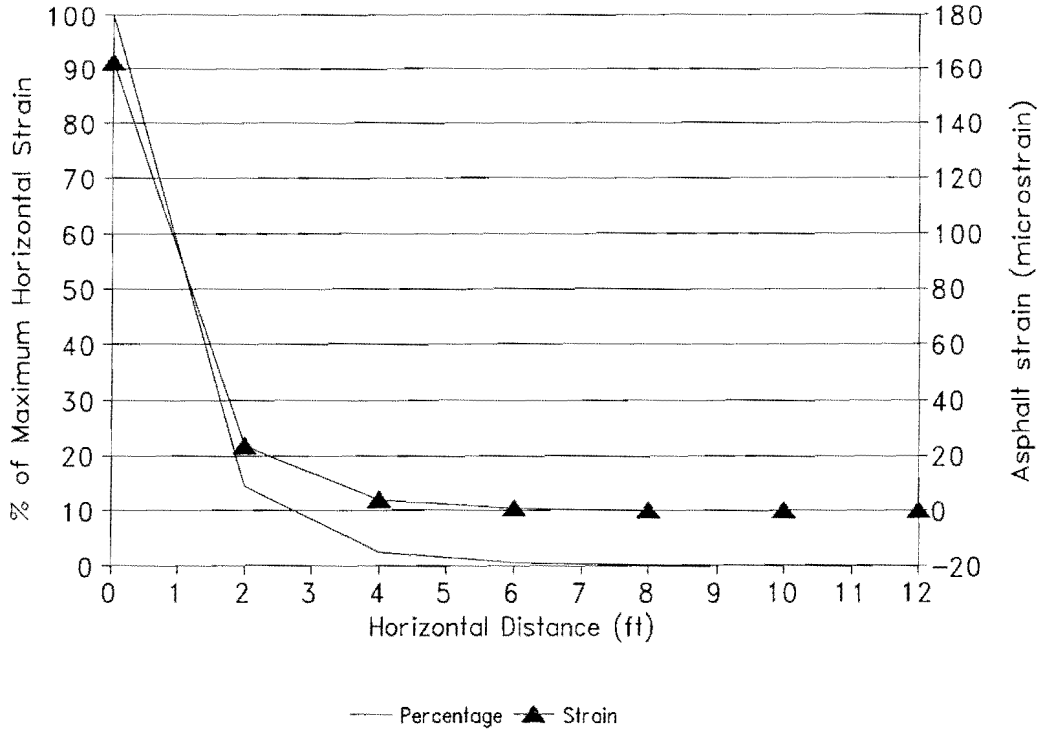

Figure A11. Predicted asphalt horizontal strains (strong pavement under heavy wheel load) (1 ft.= 0.30 m).

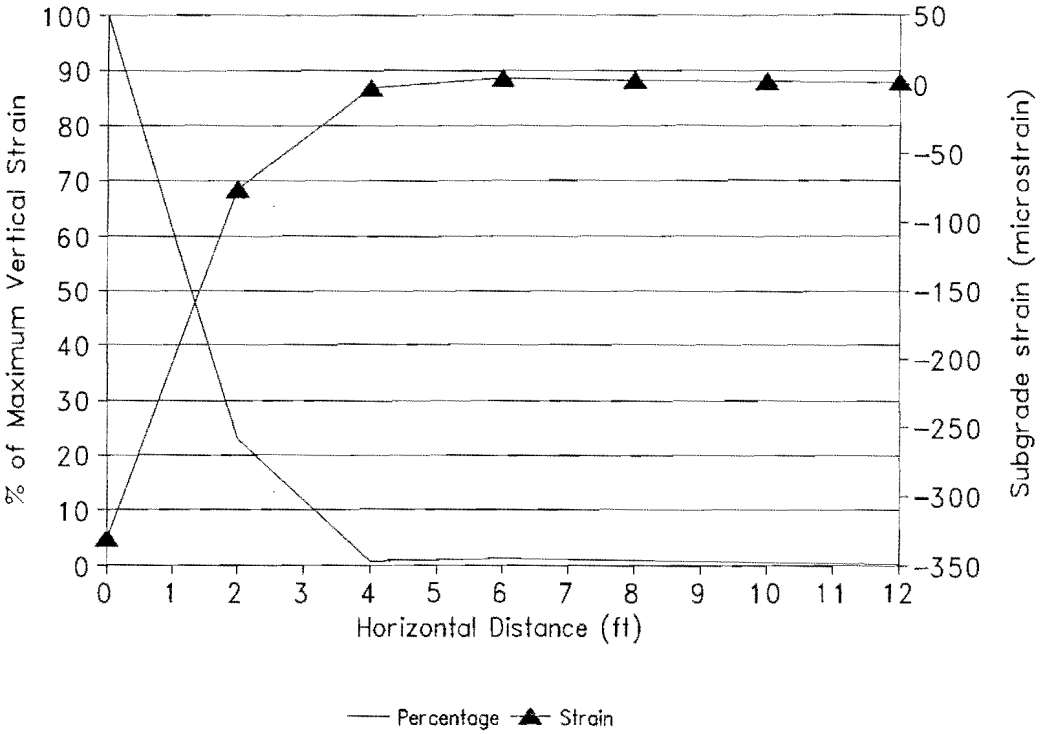

Figure A12. Predicted subgrade vertical strains (strong pavement under heavy wheel load) (1 ft.= 0.30 m).

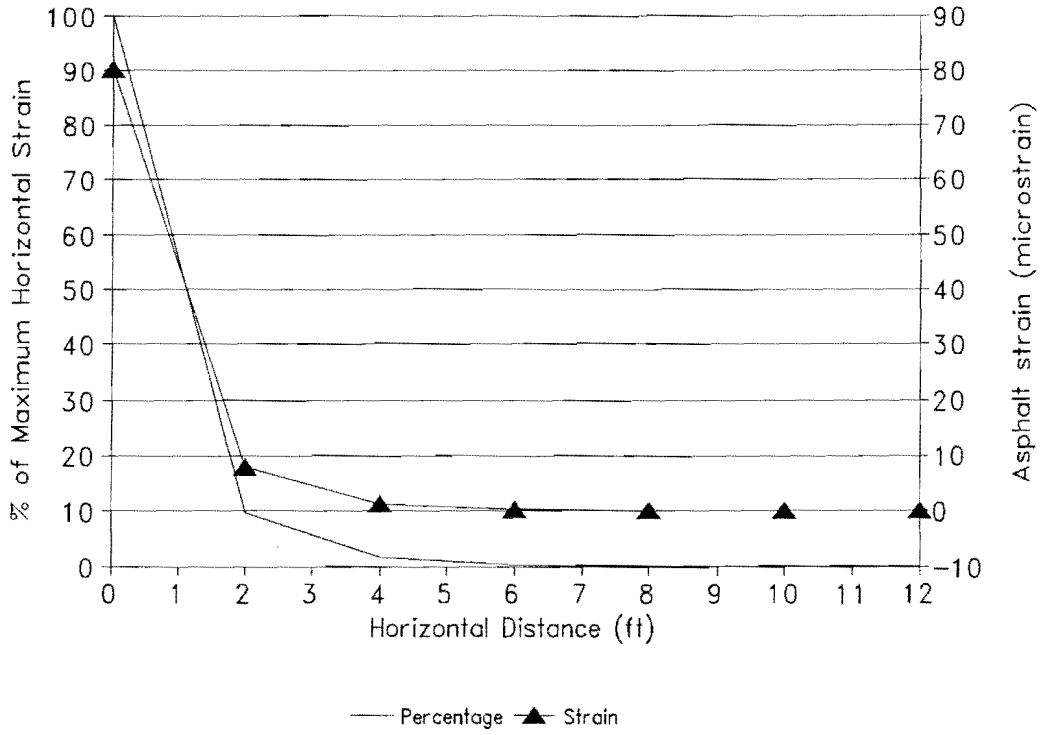

Figure A13. Predicted asphalt horizontal strains (strong pavement under light wheel load) (1 ft.= 0.30 m).

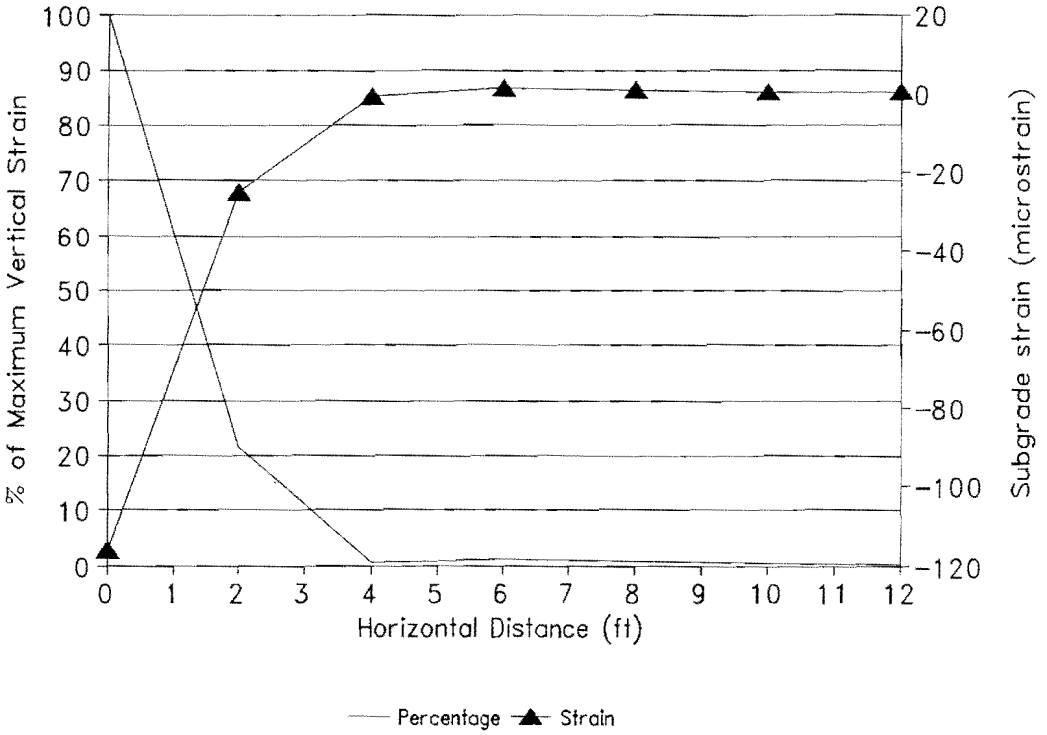

Figure A14. Predicted subgrade vertical strains (strong pavement under light wheel load) (1 ft.= 0.30 m).

observed for the case of a weak pavement. The strains diminish to less than 2 percent of the corresponding maximum values underneath the load at a distance of about 2 ft. (0.61m). This finding is consistent with the hypothesis given previously and indicates that, on the basis of the critical pavement response parameters examined, the extent of influence of a given surface load is affected most significantly by pavement thickness. The thicker the pavement, the deeper the points of evaluation for the critical strains, and thus, the greater the zone of influence of a given wheel load.

In addition to the strains ε_{ac} and ε_{sg}, the vertical deflections at the top of the base, Δ_b, the top of the subgrade, $(\Delta_{sg})_o$, and 1 ft. (0.30 m) into the subgrade, $(\Delta_{sg})_1$ were evaluated. The purpose of this analysis was to establish how to model pavement deflections under multiple-wheel loads for the purpose of analyzing the data from Multi-Depth Deflectometers taken during actual superheavy load moves. Figures A17 through A19 show the predicted displacements for the case of a weak pavement subjected to a heavy wheel load.

The following observations are made from these figures:

1) the predicted vertical displacements at the top of the base reduce to 5 percent of the maximum value at a distance of approximately 9 ft. (2.74 m) from the center of the given wheel load;
2) at the top of the subgrade, the calculated displacements reduce to 5 percent of the maximum value at a distance of about 11 ft. (3.35 m) from the center of the wheel load; and,
3) at a depth of 1 ft. (0.30 m) from the top of the subgrade, the calculated displacement 12 ft. (3.66 m) from the center of the wheel load is approximately 8 percent of the maximum value underneath the load.

The above observations are again consistent with the fact that the area of influence of a given wheel load increases with depth into the pavement. At a depth of 1 ft. (0.30 m) into the subgrade, for instance, further calculations at farther offsets from the load revealed that the predicted displacements diminish to 5 percent of the maximum value at a distance of approximately 19 ft. (5.79 m) from the given wheel load.

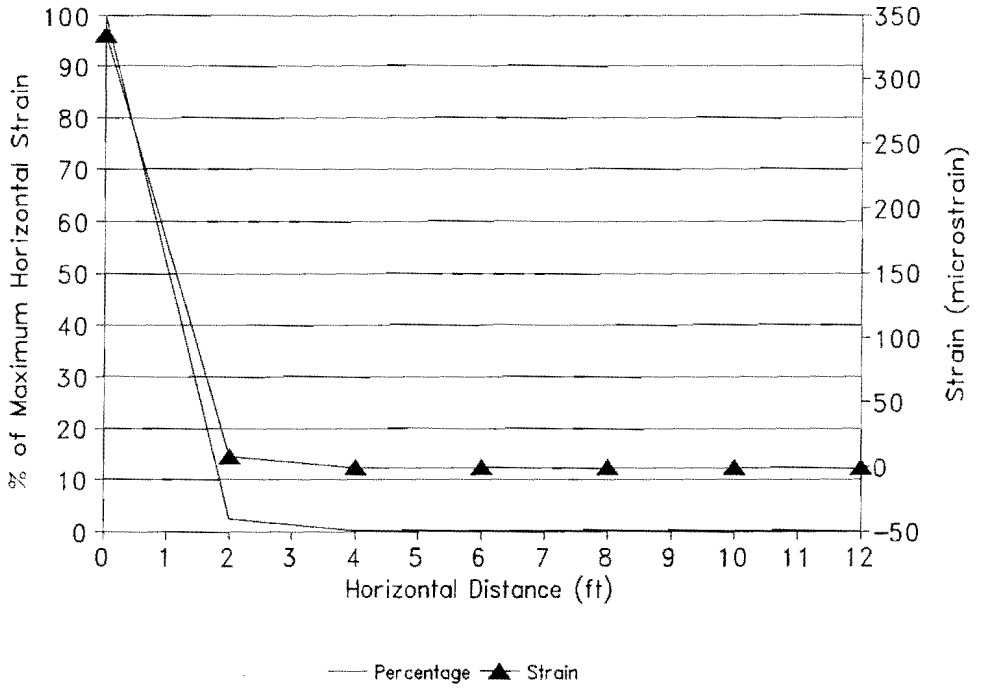

Figure A15. Predicted asphalt horizontal strains (strong pavement under heavy wheel load but with thicknesses reduced to those of weak pavement) (1 ft.= 0.30 m).

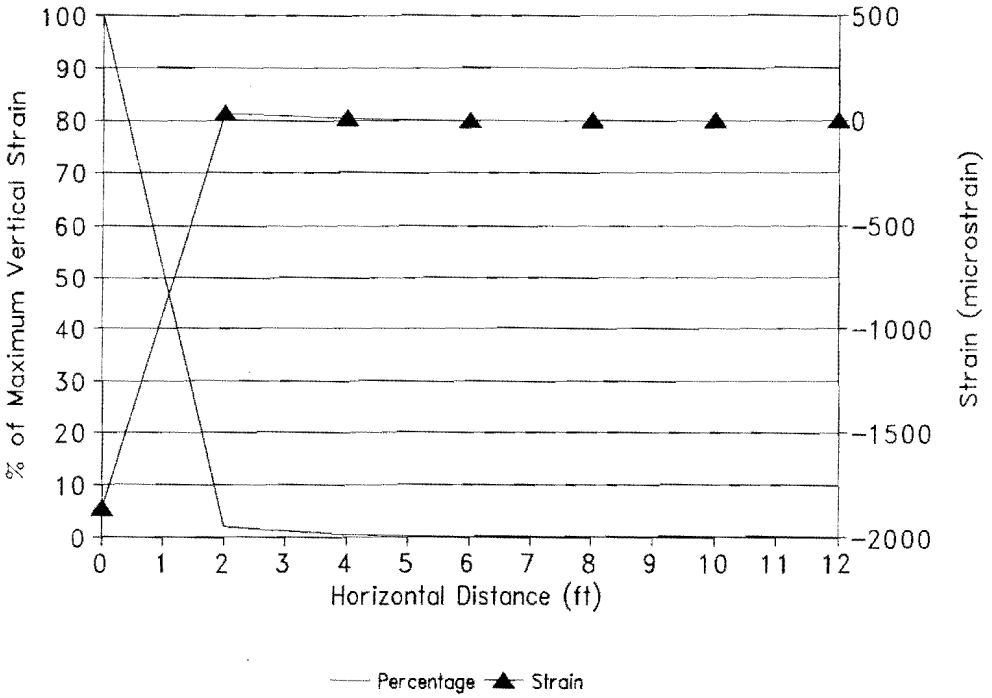

Figure A16. Predicted subgrade vertical strains (strong pavement under heavy wheel load but with thicknesses reduced to those of weak pavement) (1 ft.= 0.30 m).

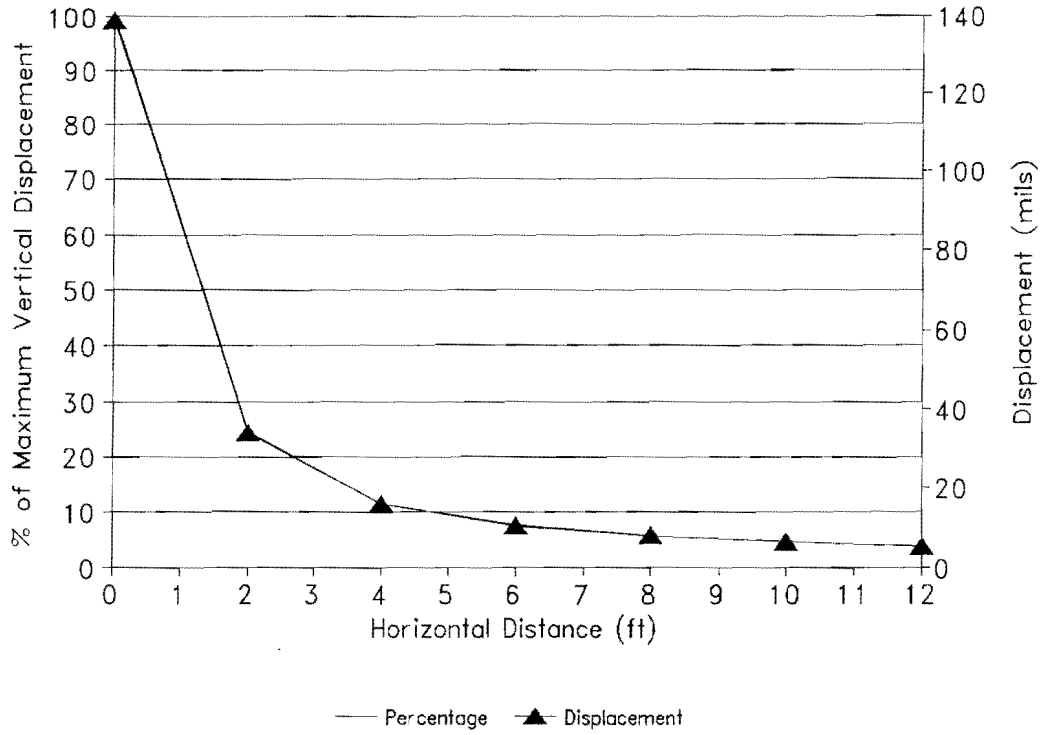

Figure A17. Predicted vertical displacements at top of base (weak pavement under heavy wheel load) (1 ft.= 0.30 m, 1 mil = 25.4 μm).

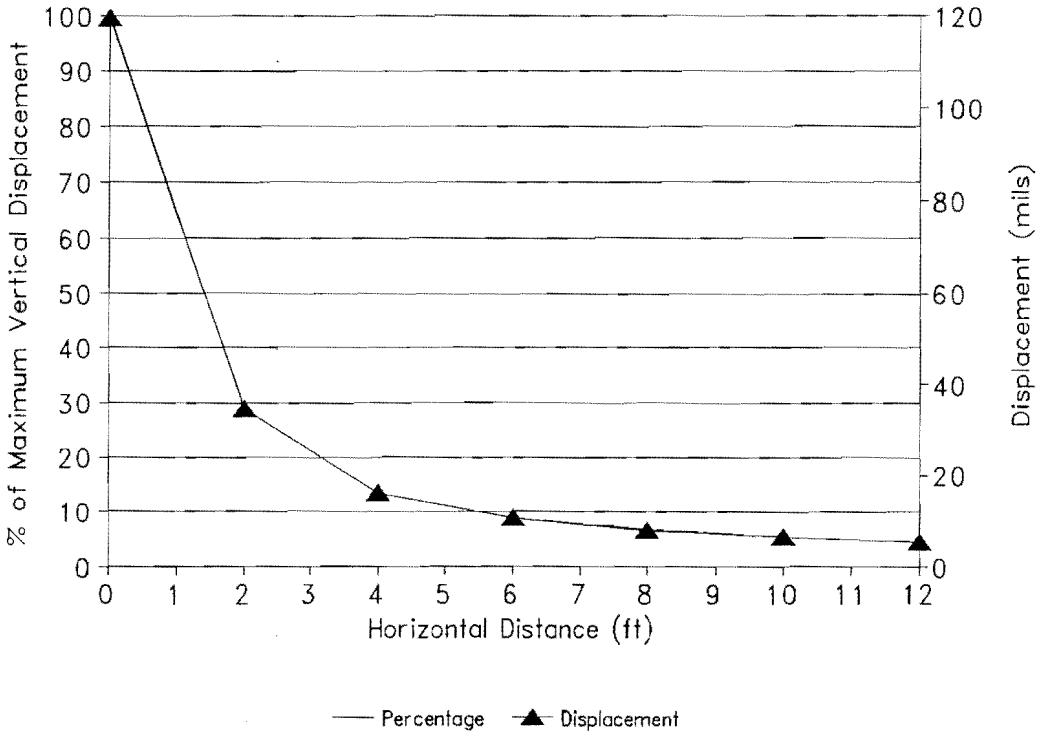

Figure A18. Predicted vertical displacements at top of subgrade (weak pavement under heavy wheel load)
(1 ft.= 0.30 m, 1 mil = 25.4 μm).

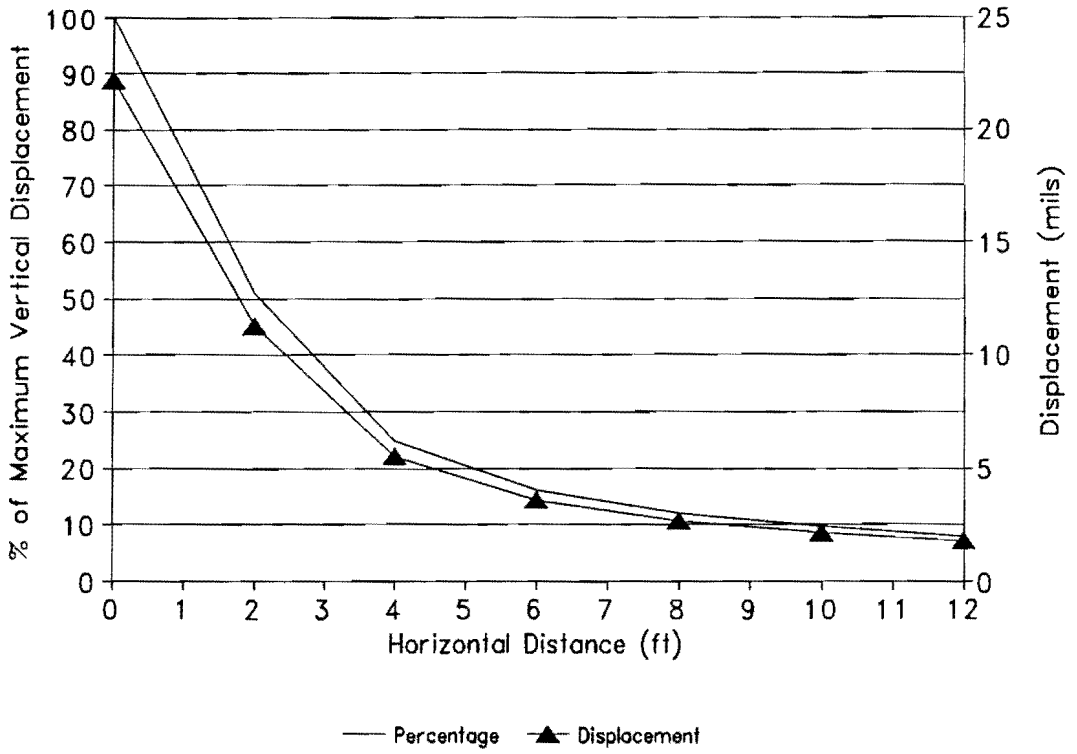

Figure A19. Predicted vertical displacements at a depth of 1 foot into subgrade (weak pavement under heavy wheel load) (1 ft. = 0.30 m, 1 mil = 25.4 μm).

A similar trend was observed for the case of a strong pavement subjected to a heavy wheel load. However, in this particular instance, the zone of influence is greater than for the previous case. This is reflected in Figures A20 through A22, from which the following observations are made:

1) at the top of the base layer, the calculated displacement 12 ft. (3.66 m) from the center of the given wheel load is approximately 9 percent of the maximum value underneath the load;
2) at the top of the subgrade, the same displacement is approximately 12 percent of the corresponding maximum; and
3) at a depth of 1 ft. (0.30 m) into the subgrade, the same displacement is about 16 percent of the maximum value underneath the load.

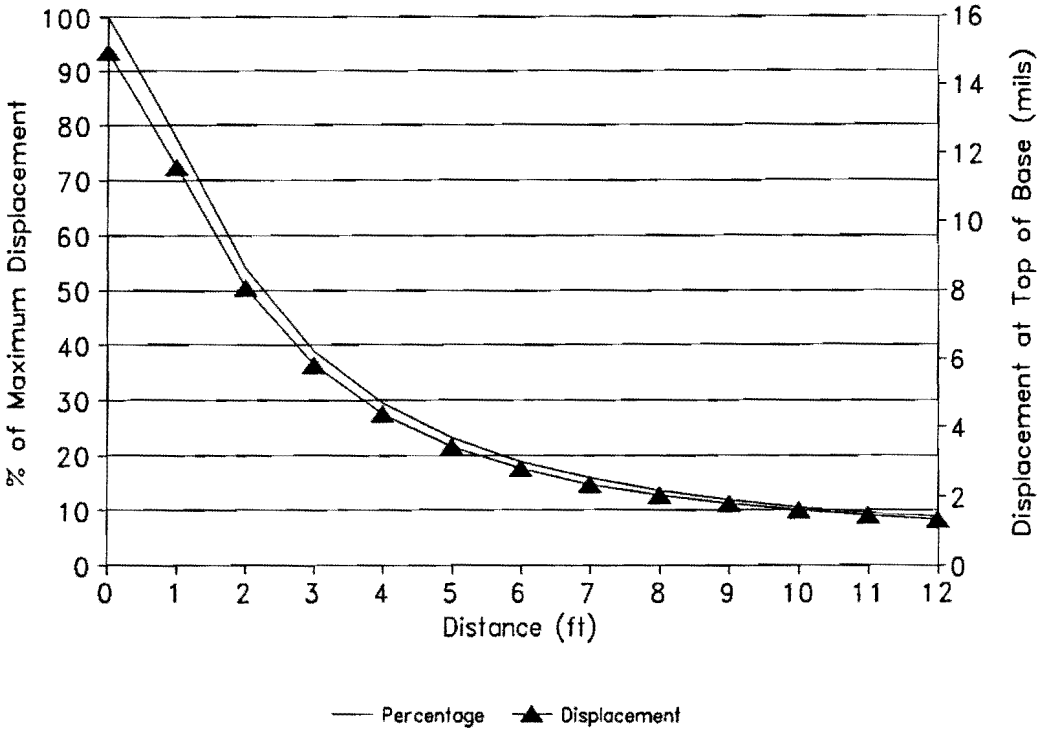

Figure A20. Predicted vertical displacements at top of base (strong pavement under heavy wheel load) (1 ft.= 0.30 m, 1 mil = 25.4 μm).

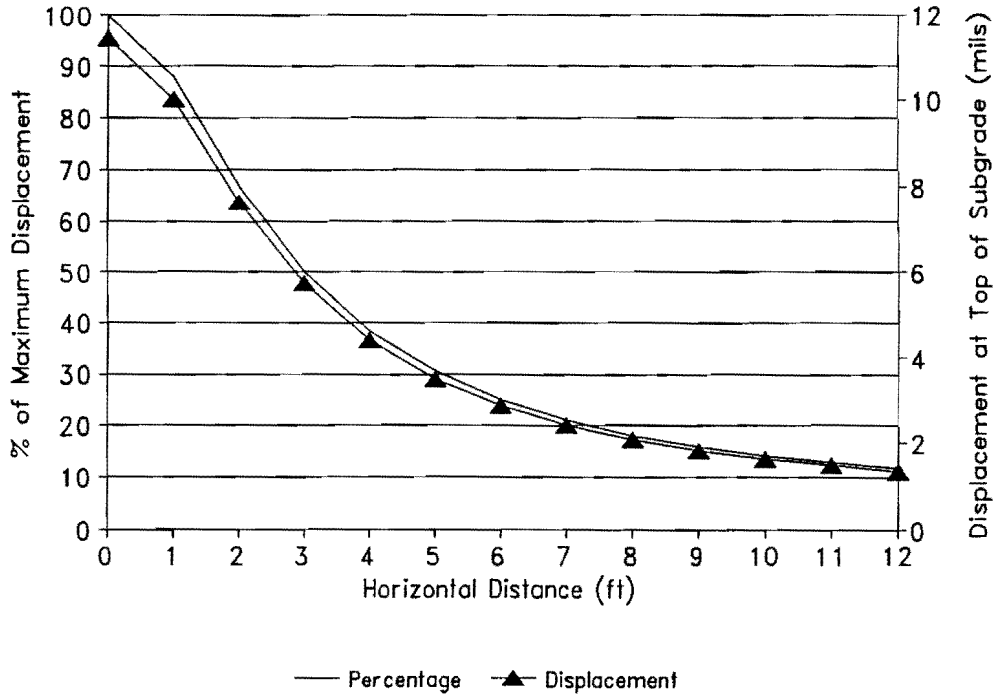

Figure A21. Predicted vertical displacements at top of subgrade (strong pavement under heavy wheel load) (1 ft.=0.30 m,1 mil= 25.4 μm).

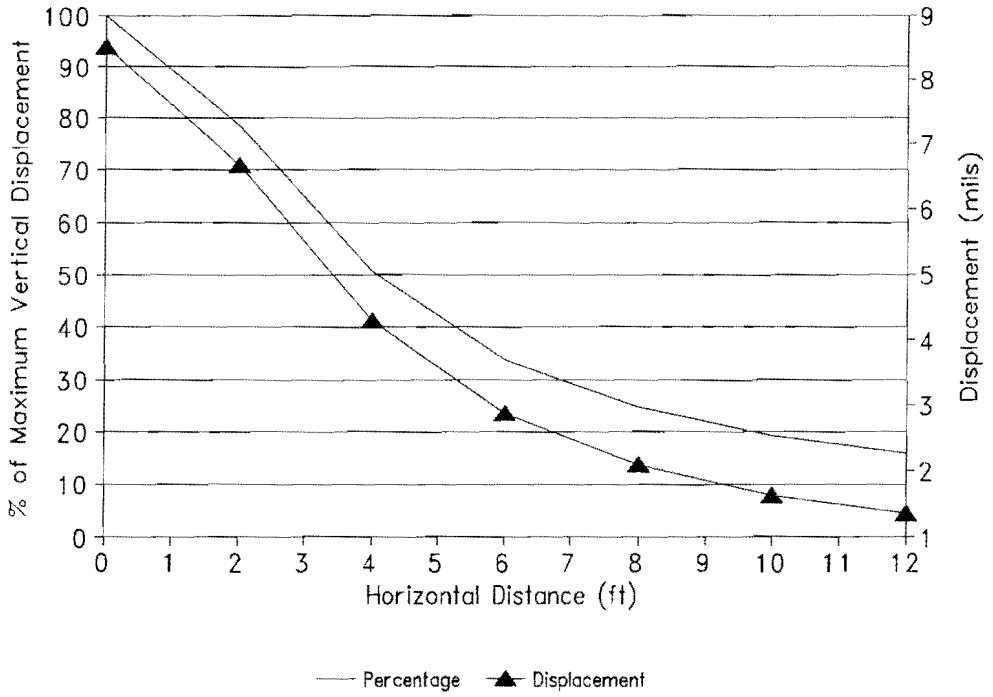

Figure A22. Predicted vertical displacements at a depth of 1 foot from top of subgrade (strong pavement under heavy wheel load) (1 ft.= 0.30 m, 1 mil = 25.4 μm).

The larger zone of influence for the strong pavement is again attributed to the fact that the points of evaluation are located deeper because of the thicker pavement layers. It was found that when the layer thicknesses are reduced, while maintaining the stiffnesses at the levels characteristic of the strong pavement, the results obtained are very similar to those presented for the case of the weak pavement.

Some further analyses were made to establish the effects of a rigid layer underlying the subgrade on the variation of predicted strains and displacements with distance from a given wheel load. The significant influence of a rigid layer on pavement deflections has been noted by several researchers. Physically, this layer may be bedrock located at a certain depth within the pavement or an apparent rigid layer by which the increase in stiffness with depth into the subgrade is modeled. This occurs due to the stress-sensitive nature of most subgrade materials, i.e., the stiffness of the material is dependent on the stress state. In particular, granular materials such as sands are known

to get stiffer with increase in confining pressure (caused by the increase in the overburden as depth increases). Consequently, it becomes important to consider the effects of a rigid layer underlying the subgrade. For this purpose, a re-evaluation of pavement response was conducted for the case of a weak and a strong pavement subjected to a heavy wheel load. In this analysis, a shallow rigid layer was introduced at a depth of 4 ft. (1.22 m) from the top of the subgrade, and the strains ε_{ac} and ε_{sg}, and displacements, Δ_b, $(\Delta_{sg})_o$, and $(\Delta_{sg})_l$ were calculated.

From an examination of the predictions generated, it was found that, with respect to the critical strains, ε_{ac} and ε_{sg}, the presence of a rigid layer underlying the subgrade had negligible influence on the variation of the predicted strains with distance from the given wheel load. Figures A23 through A26 show that the trends in the variation of ε_{ac} and ε_{sg} for the case of a semi-infinite subgrade are very similar to those obtained when a rigid layer underlying the subgrade is introduced.

However, with respect to displacements, the results do show the significant influence of a rigid layer on the predicted variation of displacements with distance from a given wheel load. Figures A27 through A32 show the predicted displacements for the cases considered. In general, the displacements are smaller under the presence of a rigid layer and attenuate more rapidly with distance from the wheel load. For the case of a weak pavement subjected to a heavy wheel load, the displacements diminish to 1 percent of the maximum value underneath the load at a lateral offset of approximately 4 ft. (1.22 m). For the strong pavement, the offset is larger, at approximately 6 ft. (1.83 m), but this is again explained by the fact that the points of evaluation for this particular case are deeper because of the thicker pavement layers used.

SUMMARY OF FINDINGS

The problem of predicting the potential pavement damage due to superheavy loads will necessarily require the evaluation of pavement response under the multiple wheels of the transport vehicle. At any given point within the pavement, the magnitudes of the displacements, strains, and stresses are influenced by the loads surrounding that point; the loads at closer proximity have larger contributions to the total pavement response at the

given point than the loads farther away. Consequently, when predicting pavement response at a given point, it may not be necessary to model all the wheels of a superheavy transport vehicle since the influence of a particular load diminishes with distance from the given point. To determine the number of loads to include in the evaluation, it is necessary to evaluate how predicted pavement response varies with distance from a given wheel load. With this information, guidelines for demarcating an influence zone around a given point can be established. All wheel loads within the zone will thus be included in the evaluation of pavement response. Such was the purpose of the current investigation.

From the study conducted, the following important findings are noted.

1) The size of the influence zone is dependent on the specific pavement response parameter(s) of interest. In general, under the same set of conditions, predicted displacements attenuated much more slowly with distance from the given wheel load than did the predicted strains. This means that if one were interested in calculating ε_{ac} or ε_{sg} (to evaluate the potential pavement damage based on fatigue cracking or pavement rutting), the number of wheel loads to be considered in the calculations will be fewer than if displacements were the parameters of concern.
2) The deeper the points of evaluation for the critical pavement response parameters, the larger the size of the influence zone required. Thus, for thick pavements, a larger influence zone is necessary than for thin pavements since the point of evaluation for a given pavement response parameter (e.g., ε_{ac}, ε_{sg}, Δ_b) is deeper. This is attributed primarily to the increase in the area of influence of a given surface load with depth into the pavement.
3) The presence of a rigid layer underlying the subgrade has a significant influence on the predicted variation of vertical displacements with distance from a given wheel load. In general, the displacements are smaller when a rigid layer is present, and they attenuate more rapidly with distance from the given wheel load than if the subgrade is semi-infinite. Consequently, the required size of the influence zone will be smaller under the presence of a rigid layer. This finding

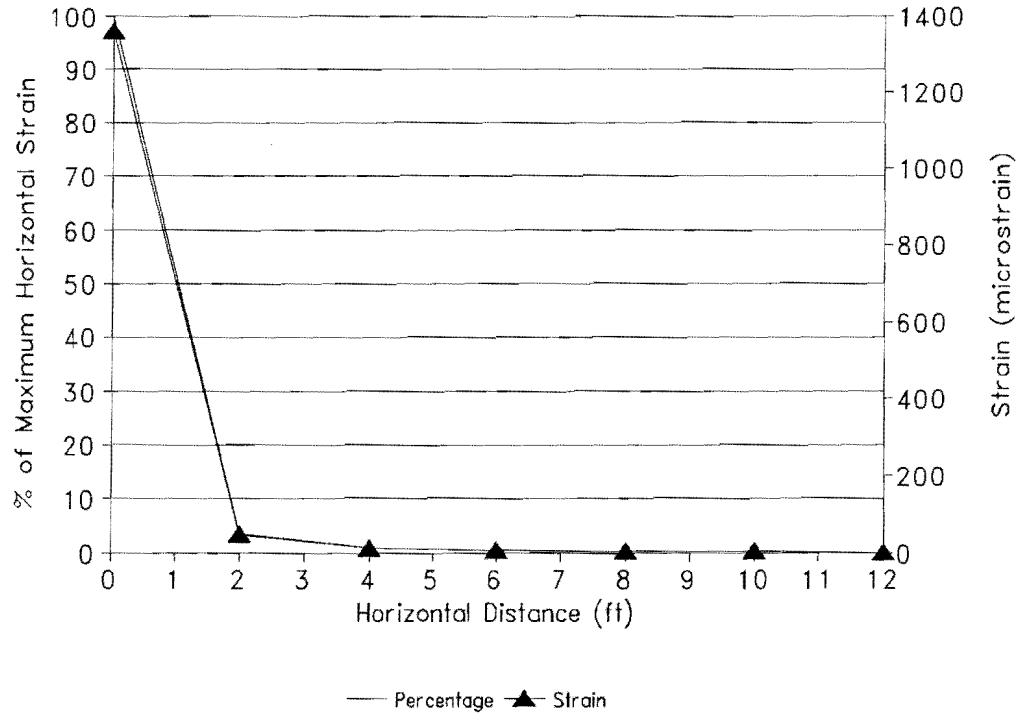

Figure A23. Predicted asphalt horizontal strains (weak pavement under heavy wheel load but with rigid bottom) (1 ft.= 0.30 m).

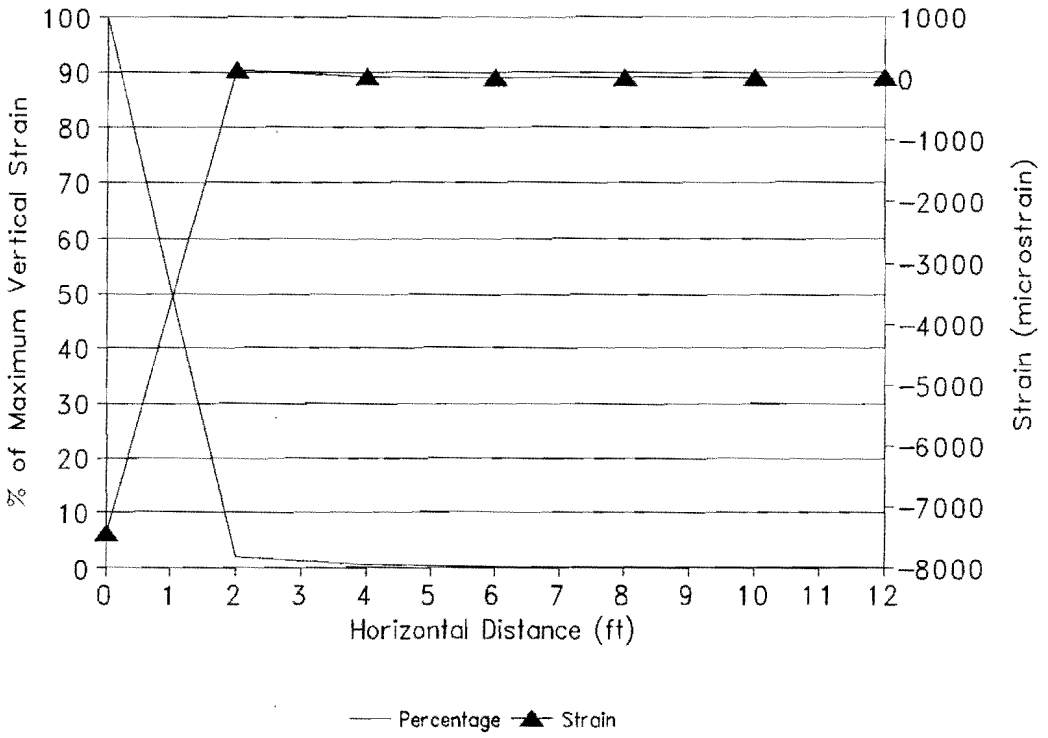

Figure A24. Predicted subgrade vertical strains (weak pavement under heavy wheel load but with rigid bottom) (1 ft.= 0.30 m).

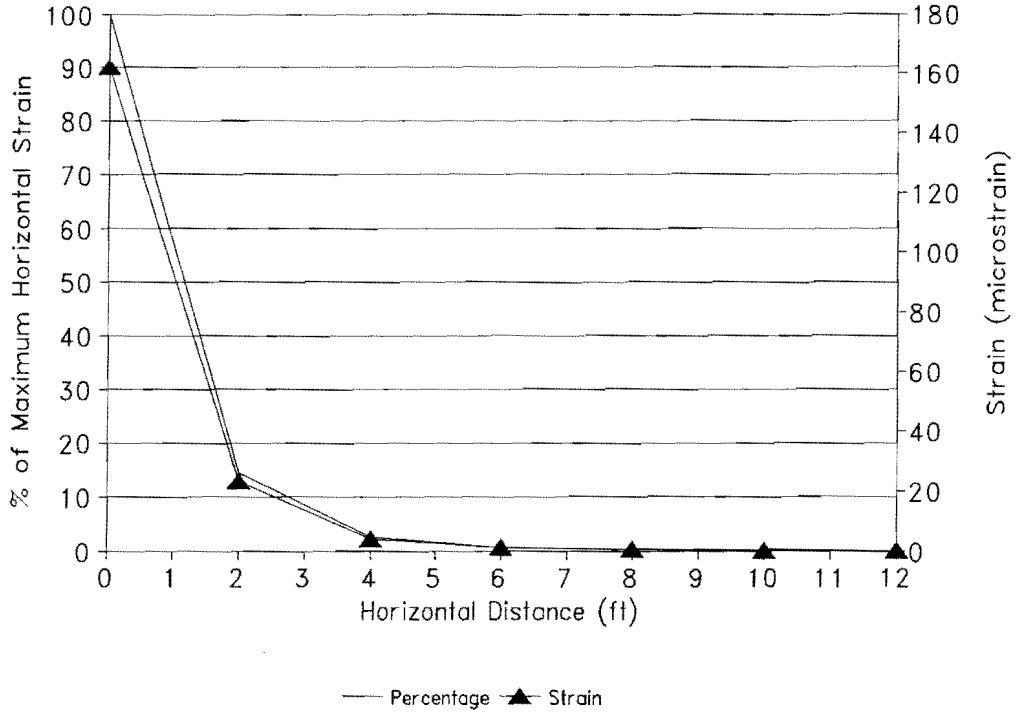

Figure A25. Predicted asphalt horizontal strains (strong pavement under heavy wheel load but with rigid bottom) (1 ft.= 0.30 m).

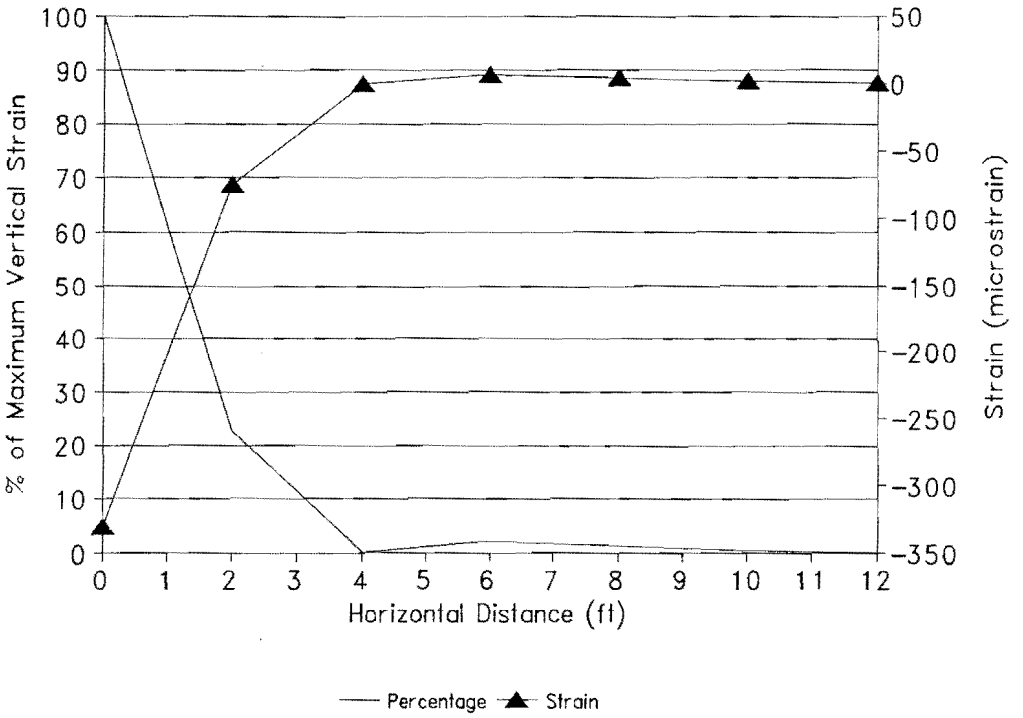

Figure A26. Predicted subgrade vertical strains (strong pavement under heavy wheel load but with rigid bottom) (1 ft.= 0.30 m).

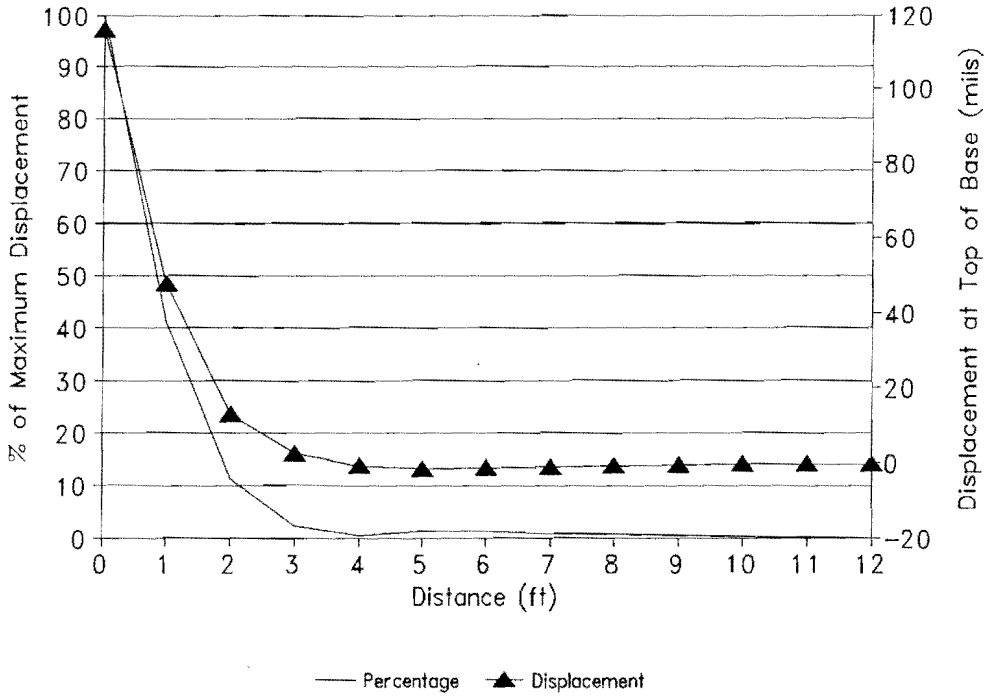

Figure A27. Predicted vertical displacements at top of base (weak pavement under heavy wheel load but with rigid bottom) (1 ft.= 0.30 m, 1 mil = 25.4 μm).

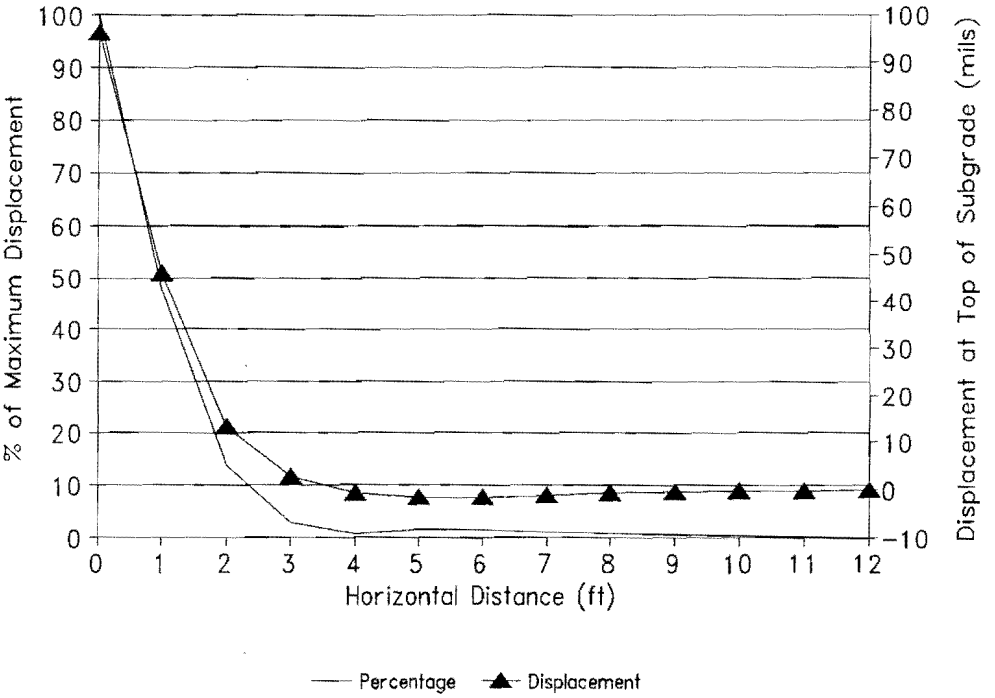

Figure A28. Predicted vertical displacements at top of subgrade (weak pavement under heavy wheel load but with rigid bottom) (1 ft.= 0.30 m, 1 mil = 25.4 μm).

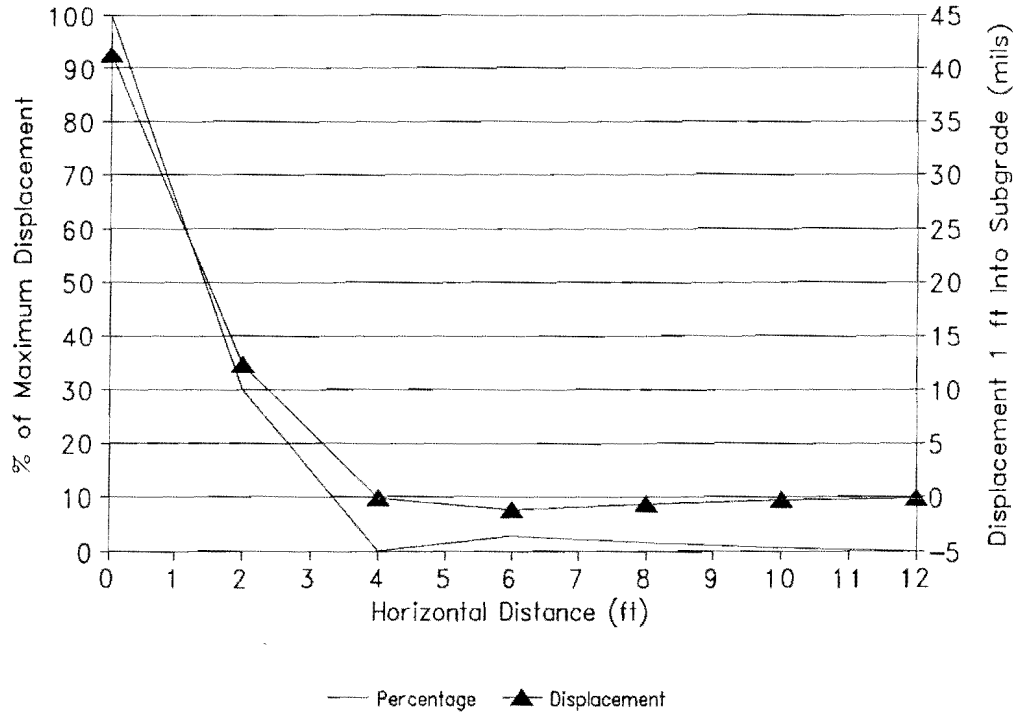

Figure A29. Predicted vertical displacements at a depth of 1 ft. from top of subgrade (weak pavement under heavy wheel load but with rigid bottom) (1 ft.= 0.30 m, 1 mil = 25.4 μm).

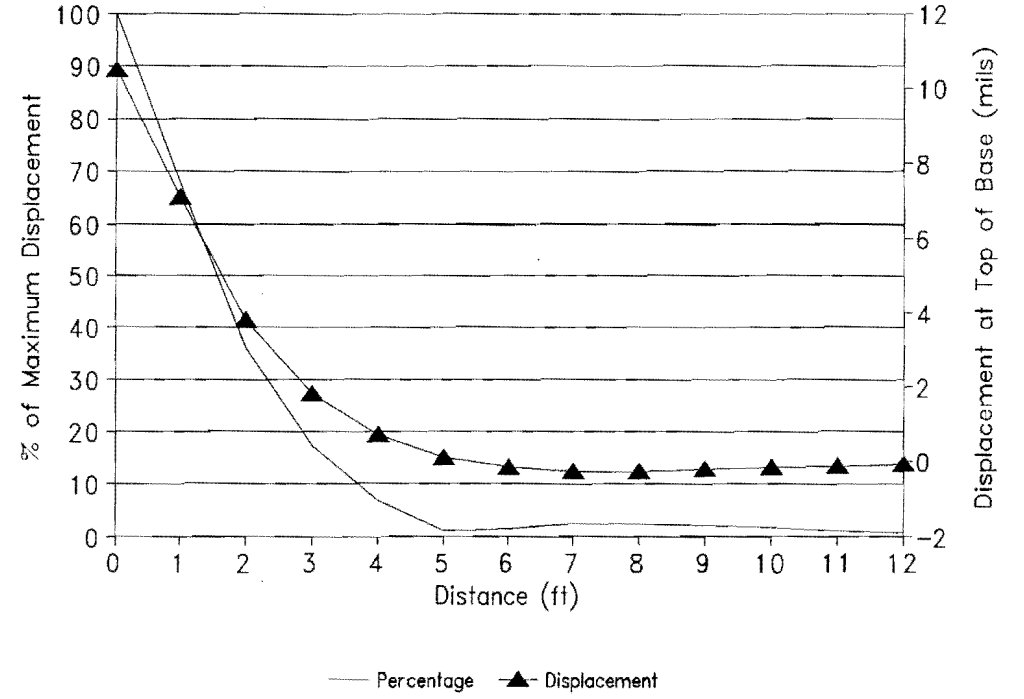

Figure A30. Predicted vertical displacements at top of base (strong pavement under heavy wheel load but with rigid bottom) (1 ft.= 0.30 m,1 mil = 25.4 μm).

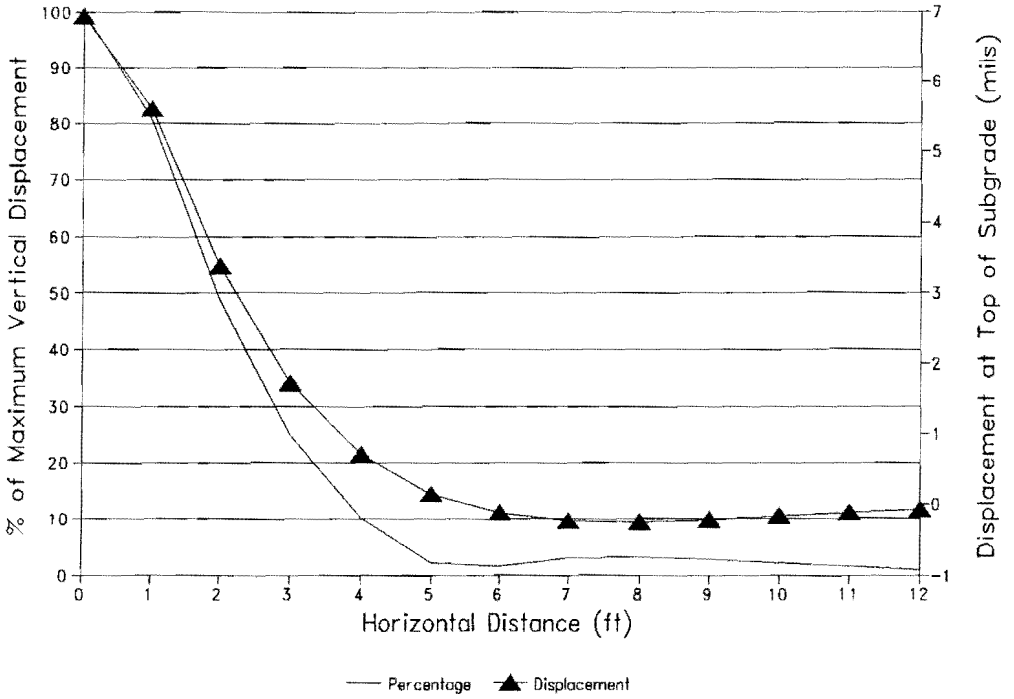

Figure A31. Predicted vertical displacements at top of subgrade (strong pavement under heavy wheel load but with rigid bottom) (1 ft.= 0.30 m, 1 mil = 25.4 μm).

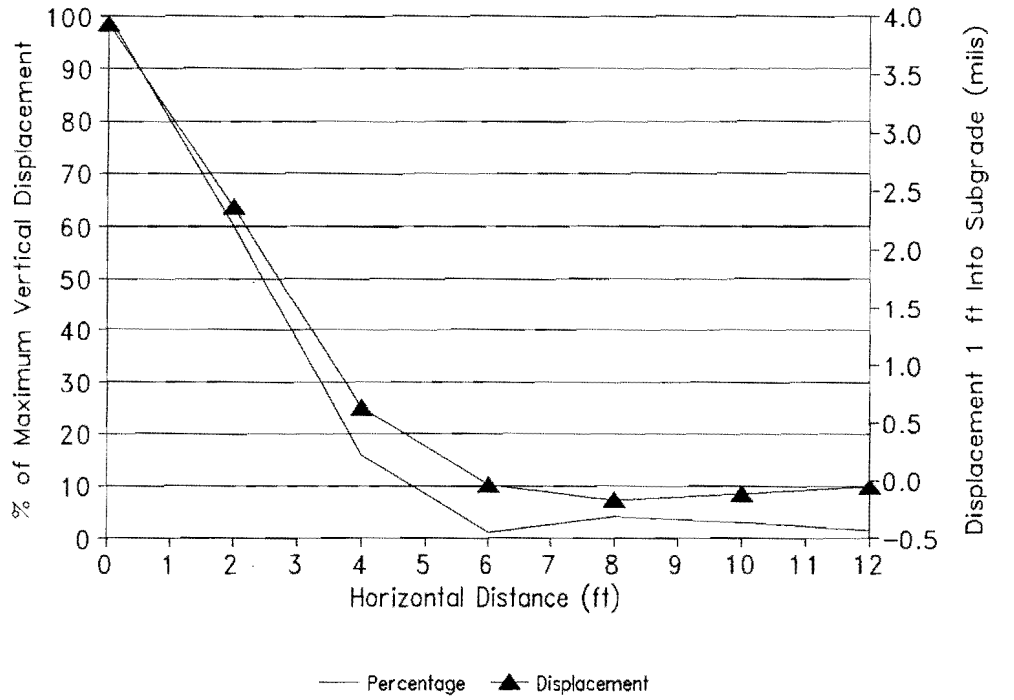

Figure A32. Predicted vertical displacements at a depth of 1 foot from top of subgrade (strong pavement under heavy wheel load but with rigid bottom) (1 ft.= 0.30 m, 1 mil = 25.4 μm).

points out the importance of considering the stratification of the subgrade when evaluating pavement deflections. The rigid layer may be bedrock, or an apparent rigid layer brought about by the increase in stiffness with depth into the subgrade.

4) With respect to the strains ϵ_{ac} and ϵ_{sg}, the presence of a rigid layer has negligible influence on the variation of the predicted strains with distance from a given wheel load.

5) The effect of stiffer layers is to reduce the predicted strains and displacements. However, when normalized with respect to the maximum predicted value underneath the load, layer stiffness has negligible effect on the extent of influence of a given wheel load.

In addition to the preceding, the following specific results may be used as guidelines in deciding the radius of the influence zone for evaluating pavement response at a selected point due to multiple wheel loads.

1) With respect to the strains ϵ_{ac} and ϵ_{sg}, the radius of the influence zone varied from 2 ft. (0.61 m) for the thin pavement to 4 ft. (1.22 m) for the thick pavement. The thick pavement considered herein had asphalt and base thicknesses, respectively, of 6 and 12 in. (150 and 300 mm) Since the area of influence of a given wheel load increases with depth into the pavement, radii greater than 4 ft. (1.22 m) may have to be used for thicker pavements.

2) With respect to displacements, the size of the influence zone will depend on the location of the point of evaluation and whether or not a rigid layer underlies the subgrade. If the subgrade is semi-infinite, the size of the influence zone for evaluating displacements at a given point can be large. For the cases considered herein, the extent of influence of a given wheel load was found to range from 9 to 19 ft. (2.74 to 5.79 m) for the thin (weak) pavement, and from 21 to 36 ft. (6.40 to 10.79 m) for the thick (strong) pavement. These numbers are based on the distance at which the predicted displacement diminishes to 5 percent of the maximum value underneath the given load. The lower limit of the given range is associated with the predicted displacements at the top of the base layer, while the upper limit is associated with the

predicted displacements at a depth of 1 ft. (0.30 m) into the subgrade.

3) If a rigid layer such as a shallow bedrock underlies the subgrade, or when the material stiffness increases with depth, the required size of the influence zone for evaluating pavement displacements is significantly reduced. For the cases considered herein, the radius of the influence zone varied from 4 ft. (1.22 m) for the thin pavement to 6 ft. (1.83 m) for the thick pavement, with an assumed rigid layer at a depth of 4 ft. (1.22 m) into the subgrade. The size of the required influence zone will logically increase as the rigid layer gets deeper, and with increasing depth, will tend to approach the magnitudes given previously for the case of a semi-infinite subgrade.